INFORMATION TO USERS

This manuscript has been reproduced from the microfilm master. UMI films the text directly from the original or copy submitted. Thus, some thesis and dissertation copies are in typewriter face, while others may be from any type of computer printer.

The quality of this reproduction is dependent upon the quality of the copy submitted. Broken or indistinct print, colored or poor quality illustrations and photographs, print bleedthrough, substandard margins, and improper alignment can adversely affect reproduction.

In the unlikely event that the author did not send UMI a complete manuscript and there are missing pages, these will be noted. Also, if unauthorized copyright material had to be removed, a note will indicate the deletion.

Oversize materials (e.g., maps, drawings, charts) are reproduced by sectioning the original, beginning at the upper left-hand corner and continuing from left to right in equal sections with small overlaps. Each original is also photographed in one exposure and is included in reduced form at the back of the book.

Photographs included in the original manuscript have been reproduced xerographically in this copy. Higher quality 6" x 9" black and white photographic prints are available for any photographs or illustrations appearing in this copy for an additional charge. Contact UMI directly to order.

UMI

A Bell & Howell Information Company
300 North Zeeb Road, Ann Arbor MI 48106-1346 USA
313/761-4700 800/521-0600

Single Overload Fatigue Crack Growth Retardation -An Implementation of Plasticity Induced Closure

by

Ghulam Ashraf-Ul-Harmain Kirmani
B. E., Regional Engineering College, University of Kashmir, 1985
M. Tech., Indian Institute of Technology, New Delhi, India, 1990

A Thesis Submitted in Partial Fulfillment of the
Requirements for the Degree of
DOCTOR OF PHILOSOPHY
in the
Department of Mechanical Engineering.

We accept this thesis as conforming
to the required standard

Dr. D. W. Provan, Supervisor (Dept. of Mechanical Engineering)

Dr. B. Tabarrok, Member (Dept. Mechanical Engineering)

Dr. N. Djilali, Member (Dept. Mechanical Engineering)

Dr. F. El-Guibaly, Member (Dept. Electrical Engineering)

Dr. G. Glinka, External Examiner (University of Waterloo)

Supervisor: Dr. James W. Provan

Abstract

Fatigue life prediction following overloads is required in such applications as. aerospace. automobile. and pressure vessels industries for damage tolerant design. Modelling of life prediction in fatigue is complicated by a host of variables which includes loading history. The characteristic features which result as *a posteriori* evidence of the loading history include overload plasticity zone. crack closure with a special trend with respect to crack length. spike-dip in fatigue crack growth rate and retardation in fatigue growth. This research focuses on life prediction of components subjected to variable magnitude single overloads. in a cyclic loading situation.

This thesis introduces the plasticity range interaction. and closure effects for variable magnitude single overload problems. A simple model is presented which captures these characteristic features following overloads. A detailed study on the crack-tip plasticity is conducted to identify the dimensions of the plasticity zone.

A new approach is presented which is useful in obtaining suppression factor for fatigue growth retardation. This factor is required in fatigue crack growth models to account for retardation effect following overloads. The model for fatigue crack growth is tested for constant amplitude loads. A detailed study is presented on fatigue crack closure based constant amplitude calculations. Two different approaches to fatigue growth calculations are presented. An assessment of the errors that occur in assumed-crack extension method is also presented. Several examples have shown a good agreement between experimental and theoretical results.

The study is extended to variable magnitude single overload problem for determination of fatigue growth calculations. Two different approaches have been adopted. one based on plasticity range interaction. and the other on closure. It has been shown

that the two approaches are equivalent. There is an excellent agreement between predictions and theory for fatigue life calculations and fatigue growth rate.

This research directly contributes to life prediction under single overloads without reliance on data fitting. It has tremendous potential for fatigue life prediction under programmed block loads, multiple overloads and finally for random loads, which can be investigated in further studies.

Examiners:

Dr. J. W. Provan, Supervisor (Dept. of Mechanical Engineering)

Dr. B. Tabarrok, Member (Dept. Mechanical Engineering)

Dr. N. Diilali, Member (Dept. Mechanical Engineering)

Dr. F. El-Guibaly, Member (Dept. Electrical Engineering)

Dr. G. Glinka, External Examiner (University of Waterloo)

Table of Contents

Abstract ii

Table of Contents iv

List of Tables vii

List of Figures viii

Nomenclature xi

Acknowledgements xv

Dedication xvi

1 INTRODUCTION 1
- 1.1 Background 1
- 1.2 Application of LEFM to Fatigue 4
- 1.3 Fatigue Crack Closure 7
- 1.4 Load Interaction Effects on FCGR 7
- 1.5 Plasticity Zones 8
- 1.6 Thesis Objectives 9
- 1.7 Thesis Layout 9

2 CRACK-TIP PLASTICITY 11
- 2.1 Introduction 11
- 2.2 The Fracture Mechanics View of the Plastic Zone 12
- 2.3 Two Parameter Characterization of Crack-tip Stresses 20
- 2.4 Experimental Investigations 21
- 2.5 Numerical Models 23
- 2.6 Crack-Tip Cyclic Stresses and Strains 24
- 2.7 An Approach to the Estimation of the Plasticity Zone 27

2.7.1 Characterization of Plastic Zone Size 27
2.7.2 Nondimensional Form of the Equations 29
2.7.3 Computational Results 29
2.8 Implications of Crack-tip Plasticity on FCGR Predictions 39

3 FATIGUE CRACK CLOSURE 42
3.1 Closure Concept and Experimental Evidence 42
3.2 An Explanation of Closure and its Effect 44
3.3 Closure Mechanisms 46
3.4 Crack-tip Shielding 49
3.5 Mechanisitic Aspects of Crack Closure 50
3.5.1 Microcrack Closure 51
3.5.2 Plasticity Induced Closure 52
3.6 Crack Closure Analysis 56
3.6.1 Plasticity-Induced Closure Models 58
3.6.2 Analytical Approaches 58
3.6.3 Numerical Approaches 60
3.7 Experimental Difficulties 61

4 CONSTANT AMPLITUDE LOADING 64
4.1 Introduction 64
4.2 Fatigue Crack Growth under CAL 66
4.3 The Assumptions for CAL 66
4.4 The Fatigue Crack Growth Characterization 67
4.5 Fatigue Crack Growth Calculations 70
4.6 Plasticity in Wake and Opening Loads under CAL 70
4.7 Opening Loads under PSS and PSN 73
4.8 FCG Calculations - Examples 75
4.8.1 Example - I 75
4.9 Further Examples 78
4.9.1 Example - II 79
4.9.2 Example - III 79
4.9.3 Example - IV 84
4.9.4 Example - V 84
4.10 Discussion about CAL 86

5 SINGLE PEAK OVERLOADS 92
5.1 Introduction 92
5.2 Wheeler's Approach and its Impact 93
5.3 Other Approaches and Some Experimental Works 97

5.4 Generations of Retardation Models 100
5.5 Need for Model under SOL 102
5.6 Modelling 105
5.6.1 Opening Loads 105
5.6.2 Plasticity in the Wake 106
5.7 Crack Growth Calculations 107
5.8 Plasticity Range Interaction (PRI) Model 108
5.8.1 Load Retardation Range Concept (LRR) 108
5.8.2 Evaluation of Exponent m_w 112
5.9 Concept of Opening Load Decomposition: 113
5.10 Results 114
5.11 An Interpretation of Results Based on Opening Load Decomposition . 119
5.12 Discussion 125

6 CONCLUSIONS **130**
6.1 General Conclusions 130
6.2 Recommendations for Future Work 132

References **134**

A Additional Plasticity Zones **145**

B Details of Some Crack Closure Mechanisms **151**
B.1 Oxide-Induced Closure Models 151
B.2 Asperity-Induced Closure Models 154

List of Tables

2.1 Some examples of plastic zone correction factor. 19
2.2 The shape ratio β obtained from various investigations. 23
2.3 Some values of β obtained in this investigation. 34

3.1 Some basic differences between microcracks and macrocracks [64]. . . 50
3.2 Some basic differences between short cracks. 51

4.1 A comparison of N_f with Rolfe and Barsom [5]. 76
4.2 A tabular comparison with Rolfe and Barsom [5]. 76
4.3 Cases used in investigation. 87
4.4 Errors for $\Delta\sigma = 276.0\ MPa$. 89
4.5 Errors for $\Delta\sigma = 414.0\ MPa$. 90
4.6 Errors for $a_0 = 3.8\ mm$. 90
4.7 Errors for $a_0 = 15.2\ mm$. 91

5.1 Variation in values of n_0 and n_{0i}. 112
5.2 N_f, N_D and N_T values for various values of OLR. 128
5.3 Crack opening stress obtained by Yisheng and Schijve from three different methods [107]. 128
5.4 N_D and N_f values for various values of m_w during calibration with experimental work of Kumar [89], for an $OLR = 2.5$. 129

B.1 Oxide thickness, d, and crack-tip-opening displacement, CTOD [60]. . 152
B.2 The predicted opening loads, P^1 from eqn(B.3) and P^2 from eqn(B.4) compared with the observed opening loads P^3 [60]. 157

List of Figures

1.1 Tensile test of wire by Leonardo da Vinci 5

2.1 A possible mechanism of fracture [15]. 13
2.2 Various modes of loading. 15
2.3 The process zone and HRR zone in plasticity affected region. 16
2.4 Thickness effect on plasticity zone size. 18
2.5 Schematic showing the effect of Poisson's ratio on FCGR. 26
2.6 Comparison of plasticity zones for various Poisson's ratio, ν, under PSN. 31
2.7 Comparison of plasticity zones for various Poisson's ratio, ν, PSS included. 32
2.8 Plasticity zones for various values of Poisson's ratio ν, a 3D representation. 33
2.9 Comparison of plasticity zones for various load ratios, ε, under PSN. . 35
2.10 Comparison of plasticity zones for various load ratios, ε, under PSS. . 36
2.11 Plasticity zones for various values of load ratio ε, a 3D representation. 37
2.12 The effect of angular coordinate θ, on shape ratio β, for Mises yield criteria. 38
2.13 The effect of angular coordinate θ, on shape ratio β, for Tresca yield criteria. 39
2.14 The effect of Poisson's Ratio $\nu < 0.49$ on shape ratio β. 41
2.15 The effect of Poisson's Ratio $\nu > 0.49$ on shape ratio β minute detail. 41

3.1 Experimental evidence of post overload crack closure. This is a micrograph of crack-path profile taken at the center thickness of the specimen after application of 100 % overload. Note the closure in region B [79]. 43
3.2 A possible representation of fatigue crack closure [60]. 45
3.3 Fatigue crack closure mechanisms [1,60,61,62,63]. 48
3.4 Development of plastic zone. 53
3.5 Plasticity induced crack closure. 54
3.6 Shear lip formation in fatigue [64]. 57

3.7 Types of closure. 62

4.1 Regimes of fatigue crack growth. 68
4.2 Crack opening load map for PSN. 72
4.3 Crack opening load map for PSS. 72
4.4 The CAL result on Rolfe and Barsom's data [5]. 77
4.5 Crack length versus N and ΔK versus FCGR for various stress range. 77
4.6 Crack length for various initial lengths of crack. 78
4.7 The CAL result on Farhangdoost's data [85]. 79
4.8 The CAL result on Zhang's data [86]. 80
4.9 The CAL result on Zhang's data for crack length [86]. 80
4.10 The CAL result on Zhang's data for R ratios [86]. 82
4.11 The CAL result on Zhang's data on effective stress [86]. 82
4.12 The effect of α on life of component [86]. 83
4.13 Some comparisons on Zhang's data [86]. 83
4.14 A comparison with experimental work of Kumar [88]. 85
4.15 Number of cycles to failure versus crack length for CAL on Kumar's data [89]. The hollow rounds represent experimental data and firm line is the predicted values. 85
4.16 Error for various crack extensions for an a_0. 86
4.17 Error for various values of crack extension for various values of $\Delta\sigma$. . 88
4.18 Error for various initial values of crack length a_0. 88

5.1 da/dN versus ΔK by Goel and Satish from an experimental perspective. Notice the sharp triangular dip in da/dN [93]. 94
5.2 da/dN versus ΔK by Bolotin and Lebedev from a different theoretical approach than the current work. (1) Regular loading (2) Single overloading and (3) Two overloadings. Notice the absence of sharp triangular dip in da/dN for overload situations (2) and (3) [99]. . . . 96
5.3 Experimental evidence of plasticity induced crack closure. Notice closure over a considerable crack length following overload. this is indicated by marker "A". A pronounced crack-tip opening displacement at the eve of application of overload is conspicuous [79]. 99
5.4 Schematic showing events after an overload application. 103
5.5 Plastic range interaction. 110
5.6 Comparison for SOL with experimental work of Kumar [89]. The solid lines represent the predicted values based on current model of plasticity affected ranges for each OLR. 115
5.7 The load pattern for comparison with work of Kumar [89]. 116

5.8 FCGR variation w.r.t. stress intensity factor range. The connected hollow rounds represent experimental work [89] and the solid line is the prediction of the model. 118
5.9 FCGR variation w.r.t. stress intensity factor range for $OLR = 2.25$. The connected dotted line represent experimental work [89] and the solid line is the prediction of the model. 119
5.10 FCGR variation w.r.t. stress intensity factor range for $OLR = 2.15$. The dashed line represents experimental work [89] and the solid line is the prediction of the model. 120
5.11 FCGR variation w.r.t. stress intensity factor range for $OLR = 2.0$. The connected '+' line represent experimental work [89] and the solid line is the prediction of the model. 121
5.12 Second component of opening loads P_{OP2}. 122
5.13 Fatigue crack length versus number of cycles. The hollow rounds represent experimental work of Yisheng and Schijve [107], solid line is the prediction of the model. 123
5.14 The decomposition of opening stresses, a comparison with experimental work of Yisheng and Schijve [107]. 124
5.15 Example of calibration for various values of n_0. The hollow rounds represent experimental values for an $OLR = 2.5$, Kumar [89]. 126
5.16 n_{0i} versus OLR. 127
5.17 Exponent m_w versus OLR. 128

A.1 The plasticity zones obtained on Mises yield criteria. 146
A.2 The plasticity zones obtained on Tresca yield criteria. 147
A.3 The plasticity zones obtained on Mises yield criteria, PSS included. . 148
A.4 The plasticity zones obtained on Tresca yield criteria, PSS included. . 149
A.5 The plasticity cone obtained on Tresca yield criteria. 150

B.1 Different dimensions that are used for calculation of K_R due to a rigid wedge of constant thickness d located at distance $2l$ behind the crack-tip for steel. 153
B.2 Single-asperity crack closure model. 156

Nomenclature

A_{0i}	Newman's coefficients $\{i = 0, 1, 2, 3\}$
a	crack length for C(T) specimen
a_{eff}	effective crack length
a_0	initial physical length of the crack
a_f	final length of the crack
a_o	physical length of the crack
ASTM	American Society for Testing and Materials
B & H Model	Budiansky and Hutchinson's model
b	width of the asperity
C	Paris constant
CAL	constant amplitude loading
CCT	central cracked tension specimen
CMOD	crack mouth opening displacement
COD	crack opening displacement
CTOD	crack tip opening displacement
$C(T)$	compact tension specimen
C_0	distance between the crack-tip to asperity
$C_1(n)$	material constant
c_1	empirical constant
c_2	empirical constant
d	oxide thickness
da	the extension in the length of the crack
da/dN	fatigue crack growth rate
$(\frac{da}{dN})^{SOL}$	FCGR under SOL
$(\frac{da}{dN})^{CAL}$	FCGR under CAL
E-399	PSN fracture toughness of metallic materials ASTM
E	Young's modulus of elasticity
E'	elastic modulus in PSN
ECL	effective crack length

Exp	experimental
F_R	retardation factor
FCG	fatigue crack growth
FCGR	fatigue crack growth rate
FEM	finite element method
$f_{ij}(\theta)$	functions of θ
G	elastic constant
HRR	Hutchinson Rosengren Rice
H_P	$R_f\Big\vert_{\theta=90}$
K	stress intensity factor
K_{max}	maximum stress intensity factor in general
K_{min}	minimum stress intensity factor in general
K^s_{max}	stress intensity factor associated with r^s_f
K^{CAL}_{cl}	closure stress intensity factor under CAL
K_{cl}	closure stress intensity factor in general
K_c	fracture toughness of material
K^{CAL}_{max}	maximum stress intensity factor under CAL
K^{SOL}_{max}	maximum stress intensity factor for SOL
K^{CAL}_{min}	minimum stress intensity factor under CAL
K_{open}	opening stress intensity factor in general
K^{CAL}_{open}	opening stress intensity factor under CAL
$(K^*_{open})_i$	second component of opening stress intensity factor
K^{SOL}_{open}	opening stress intensity factor following SOL
K_R	stress intensity factor for oxide induced crack closure
L	height of the asperity
l	half the distance between crak-tip and oxide-wedge
LEFM	linear elastic fracture mechanics
LRR	load retardation range
L & G Model	Llorca and Gálvez model
m	Paris constant
m_w	Wheeler's exponent
n	hardening exponent
n_0	a constant for determination of m_w
n_{0i}	other possible constants for determination of m_w
N	number of cycles
N_c	current number of cycles
N_f	number of cycles to failure
N_p	previously obtained number of cycles
N_R	reference number of cycles
OLR	over load ratio

ONERA	Office National d'Etudes et de Recherches Aerospatiales
P	load
PCN	plastic constraint
PRI	plasticity range interaction
PSN	plane strain
PSS	plane stress
P^{CAL}	CAL block load in a SOL
P^{SOL}	overload in a SOL
P_{cl}	closure load
P_{max}	maximum value of load
RICC	rigid insert crack closure
P_{min}	minimum value of load
P_{open}	opening load
P_{OP1}	opening load for CAL block prior to overload in SOL
P_{OP2}	second component of opening load
q	elapsed number of cycles in general
r_e	elastic region which engulfs the plastic zone
r_f	forward plasticity affected range
r_f^{CAL}	plasticity affected range due to CAL block in SOL
r_f^{SOL}	plasticity affected range due to Overload in SOL
r_f^s	difference between r_f^{SOL} and Δa
r_y	plastic zone size correction
r_p	plasticity affected region
r, θ	polar coordinates centered at the crack-tip
R	stress ratio, $\frac{\sigma_{min}}{\sigma_{max}}$
R_P	$R_f\Big\vert_{\theta=0}$
R_f	nondimensional plasticity range
RL	random loading
s	scaling parameter for plasticity zones
SEM	scanning electron microscopy
SOL	single overloads
SSY	small scale yielding
T_{ii}	T-stress
t	thickness of specimen
U	$U = \frac{\Delta K_{eff}}{\Delta K}$
u_I	mode-I CTOD
u_{II}	mode-II CTOD
VAL	variable amplitude loading
x	ratio of u_{II} to u_I
Y	geometry factor
Y_{cc}	geometry factor for central crack type specimen
Y_{ct}	geometry factor for edge crack type or C(T) specimen

Greek Symbols

α_j	plastic constraint coefficient
α	plastic constraint factor
β	shape ratio, H_P to R_P
γ	ratio of height to width of saw tooth asperity
γ_{0i}	arbitrary constants for evaluation of m_w
γ_{11}	$\frac{K}{2\sqrt{2\pi}\sigma_{ys}\varepsilon}$
ϵ_z	z-component of strain
Δa	extension in crack length
ΔK	$K_{max}^{CAL} - K_{min}^{CAL}$, also, stress intensity factor range in general
ΔK_{eff}	K_{max}^{CAL}-K_{open}^{CAL}, also, effective stress intensity factor range in general
$(\Delta K_{eff})_i$	effective stress intensity factor range for a given cycle i
ΔK_{th}	threshold value of stress intensity range
ΔP_{eff}	effective load
$\Delta\sigma$	stress range, $\sigma_{max}^{CAL} - \sigma_{min}^{CAL}$
η	factor for PSS/PSN situation
ε	ratio of applied stress to the yield strength
ϕ_g	grain diameter
λ	plastic zone correction factor
$\lambda(n)$	$\frac{C_1(n)}{4\pi}$
ν	Poisson's ratio
ρ	crack-tip blunting
σ_i	principal stresses {i = 1, 2, 3 }
σ_{max}	maximum value of stress in general
σ_{min}	minimum value of stress in general
σ_{max}^{CAL}	maximum value of stress for CAL
σ_{max}^{OL}	maximum value of stress for SOL
σ_{min}^{CAL}	minimum value of stress for CAL
σ_{OP}	total opening stress in SOL
$\sigma_{ij}(r, \theta)$	stress component
σ_{ys}	yield strength of the material
σ_z	z-component of stress
σ_0	flow stress
σ_∞	stress applied in mode-I type of loading
σ_ρ	stress due to crack-tip blunting
ψ	a dimensionless ratio
$\tau_{r\theta}$	shear stress

Acknowledgements

It is my pleasure to thank my wonderful supervisor Dr. James W. Provan. for his help and guidance during the course of this research. It is a rare opportunity for me to express my very deep appreciation for his superb supervision.

I would also like to thank Dr. Bez Tabarrok for his help during my programme as a graduate student. It is his magnetic personality which attracted many of us from far off countries to The Department of Mechanical Engineering. University of Victoria. I would like to acknowledge his unconditional cooperation and assistance.

It is my privilege to thank other members of the supervisory committee Dr. Ned Djilali and Dr. Guibaly for their assistance.

I take this opportunity to thank Interlibrary Loans Office. for their tremendous help in getting hold of many papers. Thanks are also extended to Mr. Nik of Physics Department for colour pictures.

The financial support through University of Victoria Fellowship is gratefully acknowledged.

Lastly I would like to thank my friend Dr. Shafei Zeidan for his nice advises. I would also like to thank many other friends. too long a list to carve a space in thesis.

Dedicated to my wonderful Parents
and people of Kashmir Valley

Chapter 1

INTRODUCTION

1.1 Background

Many engineering applications involve components subjected to cyclic loads. The prediction of the life for such components is one of the important areas of research at present. Problems pertaining to cyclic loading fall under the discipline of *the fatigue of materials*. The word fatigue has roots in the Latin expression *fatīgāre* which means *to tire*. However, in scientific and engineering literature the expression *fatigue of materials* refers to changes in properties associated with the application of cyclic loads. The credit for coining the term fatigue in connection with metal failure goes to Poncelet, although the first study of fatigue of a metal was reported by a German mining engineer W. A. J. Albert around 1829 [1] who performed repeated load proof tests on mine hoist chains made of iron. In 1948, N. Shute, an aircraft engineer [2], made a statement which, although inaccurate, even today colours the wider public's notion of fatigue: "Fatigue may be described as a disease of metal. When metals are subjected to an alternating load, after a great many reversals the whole character of the metal may alter, and this change may happen very suddenly.

An aluminum alloy which has stood up quite well to many thousands of hours in flight may suddenly become crystalline and break under quite small forces, with most unpleasant consequences to the aeroplane."

A detailed definition of fatigue is reported in *General Principles for Fatigue Testing of Metals (1964)* by the International Organization for Standardization (in Geneva) [1]. The definition of fatigue as given in this report *applies to changes in properties which can occur in metallic material due to repeated application of stresses or strains, although this term applies specially to those changes which lead to cracking failure.*

The replacement of wooden parts of machines with cast and wrought iron may have caused many unrecognised fatigue failures [3] [1]. It was as a result of serious failures, associated with railways, bridges and aeroplanes leading to loss of human life and massive damages, that serious research efforts were diverted towards the study of fatigue. For example, in 1842 one railway accident resulted in the loss of 1500-1800 lives near Versailles, France [2]. Another noteworthy failure was that of the Boston molasses tank which failed in January 1919 while it contained 2,300,000 gallons of molasses. Twelve people were drowned in molasses or died of injuries. Houses were damaged and a big portion of the Boston Elevated Railway Structure was knocked over [5] [3]. A major impetus to the study of fatigue occurred as a result

[1] Hertzberg in his book [4] gives details of the crack that developed in Liberty Bell in 1835, it was in use from 1778. A new bell was cast in 1846 the crack again developed. *Cracked* Liberty Bell has become symbol of American independence.

[2] The Times of London May 11, 1842.

[3] Several structures have survived the test of time. In this pursuance, whether ancient people had notions of fatigue author came across a book *Building Construction Before Mechanization, by John Fitchen, MIT Press, Fifth printing, 1994.* Thus on pp. 75-76, John Fitchen remarks, 'Probably because metal was not formerly a major structural material, and perhaps because at least buildings of historic importance are being preserved and cared for today, we lack records of whether or not fatigue has been a significant problem in buildings of previous centuries.' The author noted in some similar reference that six of the seven wonders of the world used ceramic material except the Colossus of Rhodes which used Bronze.

of two consecutive catastrophic failures, over the Mediterranean, of Comet aircraft in the 1950's [4]. The cause of the failure was found to be cracks that developed near the fastener holes of remarkably square cabin windows. Despite continuous research directed to the problems related to fatigue, several disastrous accidents have occurred more recently, *e.g.*, the 1985 crash of Japan Airlines 747 jumbo-jet.

Fatigue research based on fracture and the deformation of materials, *e.g.*, the nineteenth century Wöhler's empirical investigation of stress range/life relationships and the concepts of fatigue limit, is now well established [3]. In 1903 Ewing and Humfrey (as cited in [3]), published a study pertaining to cyclically stressed iron samples, showing photomicrographs which indicated progressive development of slip bands on the surfaces of samples, the slip bands finally culminating in the form of cracks. Thus, a qualitative understanding of the slow growth of microscopic flaws has been documented. It is also worth noting that fatigue of materials has emerged as an interdisciplanary area of research which encompasses such diverse disciplines as materials science, mechanical, civil and aerospace engineering, biomechanics, mathematics and physics [5].

As a result of this research activity, the fatigue life of structural components may be considered as a combination of elapsed cycles required to initiate a crack and to propagate it to its critical size. Thus, it is composed of: 1) fatigue crack initiation, 2) fatigue crack propagation, and 3) fracture. The fracture stage represents the final stage.

---

[4]Later Comets were grounded and the story of the Comet jets was screened in 1951 in the film *No Highway in Heaven*, with Marlene Dietrich and James Stewart.

[5]The author came across an interesting paper pertaining to the use of waveguides for the detection and online monitoring of surface cracks. This relatively new successful technique belongs to the discipline of electrical and electronics engineering (in fact paper appeared in one of the IEEE publications) involves use of microwaves. The reference is *Detecting stress and fatigue cracks, by C. Huber and R. Zoughi, IEEE Potentials, pp. 20-24, October/November 1996.*

Cracks are both beneficial and detrimental. Beneficial, because life is associated with cracks. From butterflies (they hatch from *cracked* cocoons) to birds (as they *crack* egg shells): all make use of the positive side of cracks [6]. However, the detrimental side [7] of cracks is equally important. Many catastrophic disasters in the air and at sea, and accidents occuring globally have their roots in cracks. Furthermore, cracks represent a potential threat to humans. Therefore it is necessary to study problems pertaining to propagating cracks so that fatigue crack growth can be controlled.

1.2 Application of LEFM to Fatigue

The first recorded experimental work on fracture was performed by Leonardo da Vinci (1452-1519), as cited by Timoshenko [7]. In his note "Testing the Strength of Iron Wires of Various Lengths" he gives a sketch similar to Figure 1.1 and makes the following remark: "The object of this test is to find the load an iron wire can carry. Attach an iron wire 2 braccia (approximately 1.3 m) long to something that will firmly support it, then attach a basket or any similar container to the wire and feed into the basket some fine sand through a small hole placed at the end of a hopper. A spring is fixed so that it will close the hole as soon as the wire breaks. The basket is not

[6] Calligrapher's nibs and ink-pen-nibs are intentionally cracked for easy and adequate flow of ink.

[7] It is well known that the ideal strength (theoretical strength, calculated on the basis of attracting forces binding two atoms) in a crystalline solid is much greater than the actual strength (experimental). This anamalous behavior was explained by academician A. F. Ioffe (in 1920) through a simple experiment on sodium chloride crystal. Ioffe as cited in Parton [6] determined experimentally strength (actual strength) of sodium chloride crystal, which is much less (by tens of hundreds of times) than theoretical strength (ideal strength). Then the crystal was immersed in hot water to dissolve the surface layer, and strength was measured again. This time strength was about 2000 MN/m^2, i.e., it had reached a value only two times lower than predicted by theory. According to Parton [6], conclusion was obvious: "having lost its surface layer, the crystal also lost the numerous 'wounds' accumulated on its surface during its long history, i.e., of scratches, cracks and other small defects. It became obvious that it is these defects that reduce the actual strength of the crystal."

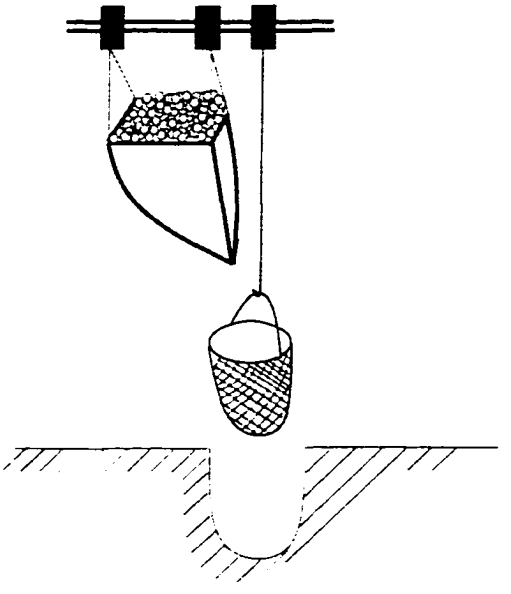

Figure 1.1: Tensile test of wire by Leonardo da Vinci

upset while falling, since it falls through a very small distance. The weight of sand and the location of the fracture of the wire is recorded. The test is repeated several times to check the results. Then a wire of one-half the previous length is tested and additional weight it carries is recorded; then a wire of one-fourth length is tested and so forth, noting each time ultimate strength and the location of the fracture."

Fatigue problems are broadly treated under the discipline of *fracture mechanics* (for comprehensive details see *e.g.*, [8]). Fracture mechanics deals with the behavior of materials in the presence of cracks under given loading conditions. Most of the fatigue data has been modelled on the fracture mechanics parameter K, the stress intensity factor, which is sometimes referred to as the crack driving force. In the 1960s, Paris and his co-workers [9] failed to find receptive audiences for their ideas of applying

fracture mechanics principles to fatigue crack growth. Although several experimental and theoretical arguments were provided for this novel approach, it appears that design engineers were not ready to abandon their faith in the S-N curves [8].

Based on energy concepts the quantitative modelling of brittle fracture began through the work of Griffith [10] in 1921. However, these ideas could not be directly used to characterize the failures in metallic materials. Irwin [11, 12] showed that the stress singularity ahead of the crack can be expressed in terms of a scalar quantity known as the stress intensity factor K. Some more details in this regard are provided by Provan [10] [9]. In Linear Elastic Fracture Mechanics (LEFM), the state of stress and displacement is defined on the basis of K in the neighborhood of the crack-tip region. In LEFM the stress intensity factor range determined from the remote loading conditions together with the geometry of the cracked component characterizes the crack growth without requiring detailed information regarding the mechanisms of fatigue fracture. The crack extension can be restrained either through the enhancement of the inherent toughness of materials, *e.g.*, microstructural modifications or by decreasing the stress intensity factor.

---

[8] The resistence to this new approach was so phenomenal that Paris and his co-workers were unable to find a peer-reviewed technical journal that was willing to publish their manuscript. Thus most widely referred to paper in fatigue (for past 30 years or so) appeared in University of Washington periodical entitled *The Trend in Engineering*.

[9] In his Foreword to *Fracture and Fatigue Control in Structures by Rolfe and Barsom [5]*, George Irwin remarked that "In his well-known text on 'Mathematical Theory of Elasticity', Love inserted brief discussions of several topics of engineering importance for which linear elastic treatment appeared inadequate. One of these topics was rupture. Love noted that various safety factors, ranging from 6 to 12 and based upon ultimate tensile strength, were in common use. He commented that 'the conditions of rupture are but vaguely understood.' " George Irwin noted that it was still applicable in terms of engineering practice in 1946.

1.3 Fatigue Crack Closure

The crack driving force may be locally reduced through mechanical, microstructural, and environmental factors. This process, also known as *extrinsic toughening*, causes what is known as *crack tip shielding*. These arguments were put forth in 1968 when it was discovered by Elber [13] that fatigue cracks may remain closed for a significant portion of the fatigue loading cycle due to elastic constraints acting on the plastically stretched material in the crack wake. The local crack driving force (stress intensity factor) is significantly affected and this plays a crucial role in the process of fatigue crack growth and arrest. Research conducted in the area of fatigue crack closure is from both qualitative and quantitative points of view. There are several models based on analytical and numerical treatments.

The phenomenon of crack closure is very complicated and a large number of variables enters into the calculations. In the past three decades there has been a considerable amount of research pertaining to the quantitative evaluation of closure. The contribution of several factors which influence the crack closure stress intensity level, including specimen size and geometry, load spectrum, material properties and environment, etc., has not been fully investigated.

1.4 Load Interaction Effects on FCGR

The phenomena of load interaction effects caused under variable amplitude loading (VAL) is important in life prediction models with regard to establishing fatigue crack growth rate (FCGR) estimates. It is necessary to know the behavior of a material under the influence of a single overload (SOL) to obtain the information regarding the load interaction effects. In the present investigation a problem pertaining to single

overloads with variable magnitude overloads is presented.

After more than 30 years of research pronounced ambiguities exist concerning the prediction of the life of components under single overloads. The introduction of a reduction of the crack driving force on the basis of crack closure has received attention and many researchers have incorporated this effect into fatigue crack growth models. However, the crack closure loads are difficult to determine even under constant amplitude loading (CAL) and it is an on-going standardisation effort within the ASTM Committee E08 [14].

1.5 Plasticity Zones

The formation of plasticity zones at the crack-tip and the interaction of an overload plastic zone with the current plastic zones is another possible way to account for impeding effect of overloads on fatigue crack growth rates. But very limited research has been conducted to identify the dimensions of the plasticity zone. The widely used crack-tip plasticity model by Dugdale is based on an assumption that the plasticity zone is of vanishingly small height, which is contrary to various experimental findings and clearly reveals that plasticity affected height is larger than the plasticity affected range. Also, the information pertaining to constant amplitude loading for the determination of closure loads can be incorporated in the life prediction models of single overloads, with the load interaction effect, accounted for, by using the retardation factor obtained on the basis of plasticity affected ranges. Further, information pertaining to the closure loads, for overload situations is reported in the recent literature on the basis of experimental methods or extensive finite element (FEM) models. Therefore, there is a need to obtain expressions for closure loads under single overloads from analytical considerations.

1.6 Thesis Objectives

With this background, the following thesis topics evolved. The objectives of this thesis, may be summarized as follows.

- The introduction of a novel approach that reveals the effect of various parameters on crack-tip plasticity.
- The incorporation of a cycle-by-cycle approach to establishing fatigue crack growth rates based on the effective stress intensity factor range. Further, to account for errors in the assumed crack-extension approach.
- The modelling of FCGR under single overloads based on fatigue crack closure and a retardation factor obtained on the basis of plasticity affected ranges.
- The decomposition of the crack closure stress intensity factor into two components:
  - the closure stress intensity factor that results under CAL.
  - the closure stress intensity factor that exists until the crack-tip is in the overload zone and vanishes outside the overload zone.
- The verification of these issues by comparison with experimental results obtained from various sources.

1.7 Thesis Layout

In pursuance of these objectives, this thesis is organized in the following manner.

Chapter 2 presents fatigue crack-tip plasticity. A detailed literature review is also presented.

Chapter 3 presents a discussion of the crack closure concept, mechanisms, followed by a survey of some models.

Chapter 4 details fatigue crack growth under constant amplitude loading. The closure phenomenon is incorporated, two different approaches are presented for FCGR and several examples are taken and thorough comparisons made with experimental results obtained from other sources.

Chapter 5 is devoted to the modelling of FCGRs under variable magnitude, single overloads. The Chapter begins with a thorough literature review, utilises the work of Chapters 2, 3, and 4, and finally ends with a verification based upon the experimental work of others.

Chapter 6 concludes this thesis with emphasis on material covered in Chapters 2, 4, and 5.

The thesis also contains appropriate appendices.

Chapter 2

CRACK-TIP PLASTICITY

2.1 Introduction

Fatigue crack initiation and growth under cyclic loading conditions is integrally associated with and is primarily controlled by, the plastic zones that result from the applied stresses that exist both in the vicinity of a propagating crack and in its wake or flanks of the adjoining surfaces. For example, the fatigue characteristics of a cracked specimen or component under a single overload (SOL) or variable amplitude loading (VAL) situation are significantly influenced by these plastic zones. This beneficial effect of the overloads is well known. In modelling of the fatigue crack growth rate (FCGR) this is accounted for by incorporation of suppression factors which involve careful estimation of plasticity effects. In some models the suppression is introduced through crack closure loads which are also dependent on the plasticity in the wake of an advancing crack.

Prediction of the fatigue characteristics of structural components subjected to either SOL or VAL requires an estimation of plastically affected regions ahead of

the crack-tip. One of the most widely used plasticity models in fatigue is Dugdale's yield strip model. In this model the plastically affected zone is assumed to be of vanishingly small height which is contradictory to various experimental and numerical investigations on crack-tip plasticity. Therefore, to obtain an estimate of the plastic yielding ahead of the crack-tip, this thesis first presents a novel procedure of obtaining plastic zone sizes and shapes. Williams' equations in a nondimensional form are used to obtain the principal stresses, while Tresca and von Mises yield criteria have been employed to obtain the plastic zone size under both plane strain (PSN) and plane stress (PSS) conditions. Several parameters which effect the extent of the plastic zone are thereby identified and their corresponding influence on the shapes and sizes of these zones are presented.

2.2 The Fracture Mechanics View of the Plastic Zone

According to linear elastic fracture mechanics (LEFM), a $\frac{1}{\sqrt{r}}$ stress singularity exists at the tip of an elastic crack, where r is the distance from the crack-tip. Metals, however, have a plastic yield stress which implies that there is always a region around the crack-tip where plastic deformation occurs, inferring that the stress singularity does not in fact exist. This plasticity affected region is known as the plastic zone whose size can be estimated either in PSN, or PSS conditions. As indicated in Figure 2.1, the crack-tip blunts and sharpens during a loading cycle, Broek [15]. Even closer to the actual crack-tip, the stress field must return to zero since the boundary conditions are such that a portion of the tip forms a part of the free surfaces of the crack. The distribution of plastic deformation around a crack-tip has been the subject of many investigations. These include experimental, numerical and analytical procedures with

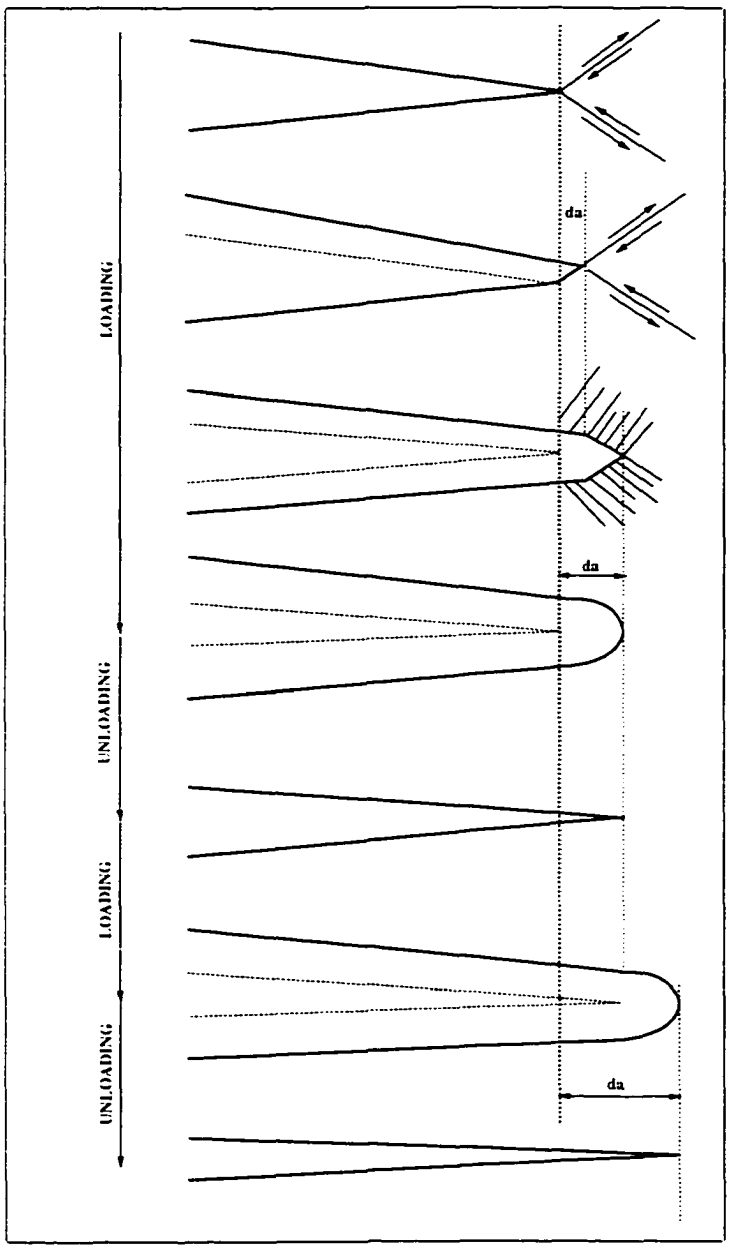

Figure 2.1: A possible mechanism of fracture [15].

the earliest work on the deformation near the crack-tip being performed by Westergaard [16], using complex variables. Under small scale yielding approximations, it is assumed that the actual shape of the local region affected by plasticity may be characterized by a circle of radius r_p. The formula for the calculation of the dimension of the crack-tip plastic zone size r_p is given by, Rolfe and Barsom [5], and Hellen [17] as:

$$r_p = \alpha_J \left(\frac{K}{\sigma_{ys}} \right)^2 . \tag{2.1}$$

for a crack subjected to a uniform stress σ_∞ applied in a direction perpendicular to the crack plane for the Mode-I type of loading as shown in Figure 2.2. In eqn(2.1), K is the stress intensity factor, σ_{ys} is the yield strength of the material, and α_J is a dimensionless constant which may depend on Poisson's ratio ν (in the case of PSN), and strain hardening exponent n, but is independent of specimen geometry as well as applied load σ_∞. The above relation plays an important role in the discipline of fracture and fatigue and, as a result, the square of the ratio of stress intensity factor to the yield stress is known as the plastic constraint (PCN) and α_J, in this work is referred to as the plastic constraint coefficient.

As indicated in Figure 2.3 and in the case where the small scale yielding approximations apply, outside the plastic radius r_p a larger circle with radius r_e, being made as large as possible, is introduced. The region between the two circles is such that the material deformation behavior in this region can be characterized by a singular field or the K-dominant field due to Irwin [11, 18]. The small crack-tip yield zone is completely engulfed in the dominant singular field characterised by K, though various microprocesses occur in the immediate neighborhood of the crack-tip. Close to the crack-tip the damage is more intense and is likely to require, in principle, some explicit treatment. The region over which damage is important may be termed as the fracture process zone, as is suggested by Harlin and Willis [19]. The crack extends when the conditions inside the process zone reach a critical level so that, for example,

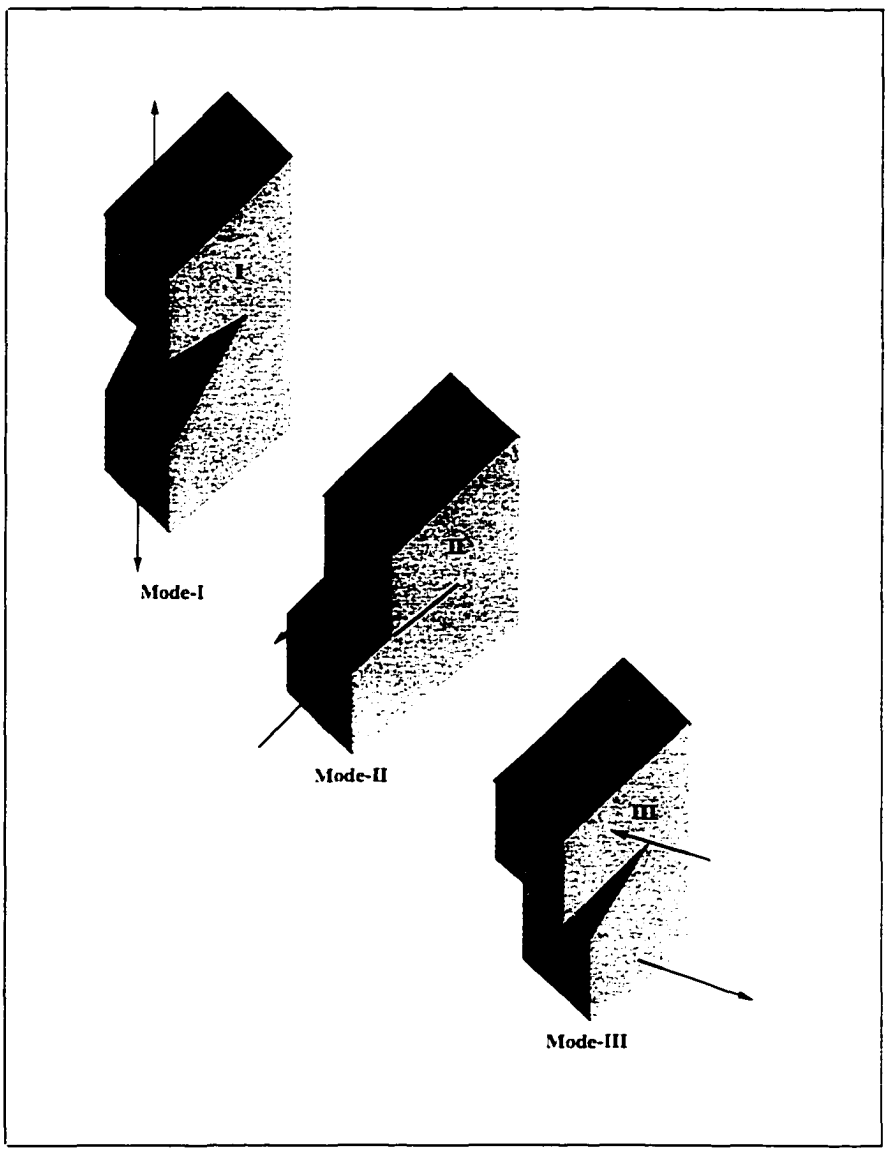

Figure 2.2: Various modes of loading.

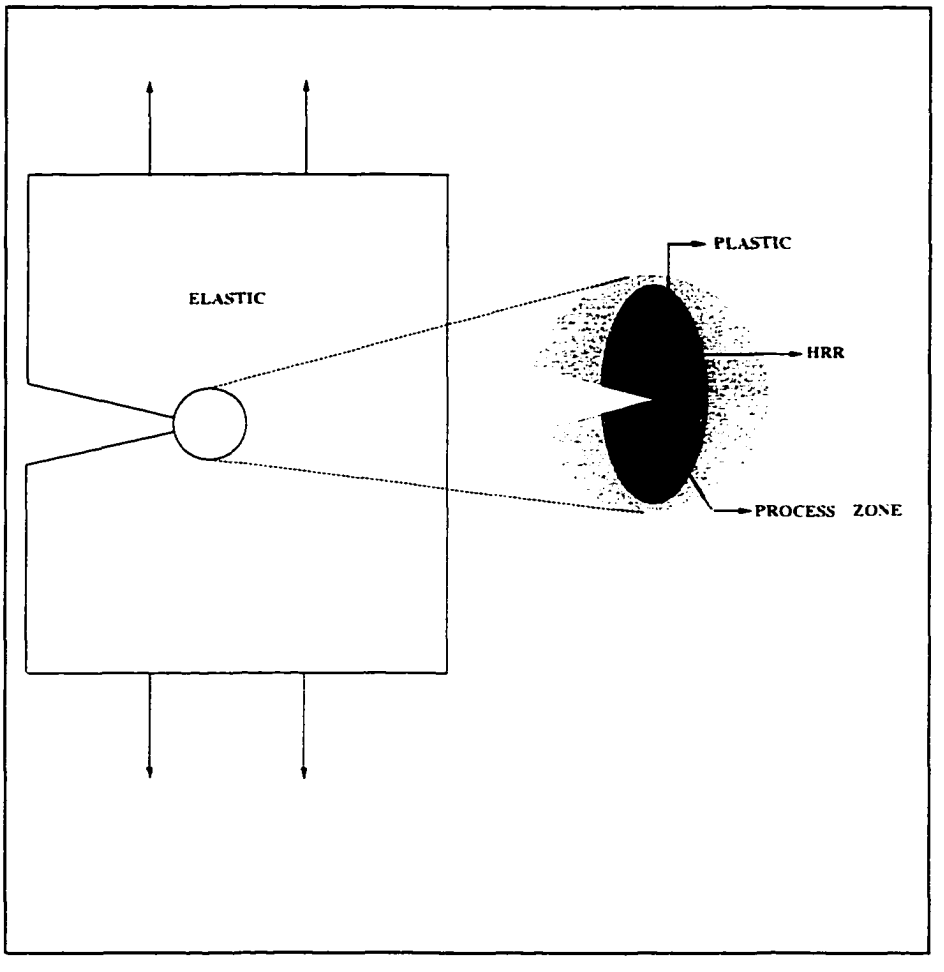

Figure 2.3: The process zone and HRR zone in plasticity affected region.

microcracks coalesce together or voids grow in size, perhaps by local necking. The events inside the process zone and the occurrences outside the process zone in the form of stresses and strains are very complicated. The process zone is confined to a small region, whose dimensions are characteristic of the material's microstructure surrounding the crack-tip. Crack extension is predicted when some combination of stresses and strains in the vicinity of the crack-tip reaches a critical level.

An estimation of the plastic zone size ahead of the crack in ductile solids was derived by Irwin [18]. Irwin used analytical solutions of Westegaard [16], to quantify the near-tip fields for the linear elastic crack in terms of stress intensity factor. In Mode-I the extent of the plasticity affected zones are:

$$r_p = \frac{1}{3\pi}\left(\frac{K}{\sigma_{ys}}\right)^2 \qquad \text{for PSN.} \tag{2.2}$$

$$r_p = \frac{1}{\pi}\left(\frac{K}{\sigma_{ys}}\right)^2 \qquad \text{for PSS.} \tag{2.3}$$

In general, the plasticity affected region is larger in PSS than in PSN. A schematic showing plasticity zones in PSS and PSN is given in Figure 2.4. Irwin [11], argued that plasticity makes cracks behave as if they were longer than their physical size. As a consequence and according to Hauf, Parks and Lee [20], the displacements related to work, conjugate to applied loading are larger and the stiffnesses are lower than in the elastic case. The size of the yield zone ahead of crack in Mode-I type of loading, for a thin plate of an elastic, perfectly plastic solid (subjected to PSS deformation) was estimated by Dugdale [21]. Like Irwin, Dugdale also considered an effective crack which is longer than the physical crack. The plastic region was envisioned as a narrow strip of near zero height, which extends a distance r_p ahead of the crack-tip. From this reason the plastic zone size is:

$$r_p = \frac{\pi}{8}\left(\frac{K}{\sigma_{ys}}\right)^2. \tag{2.4}$$

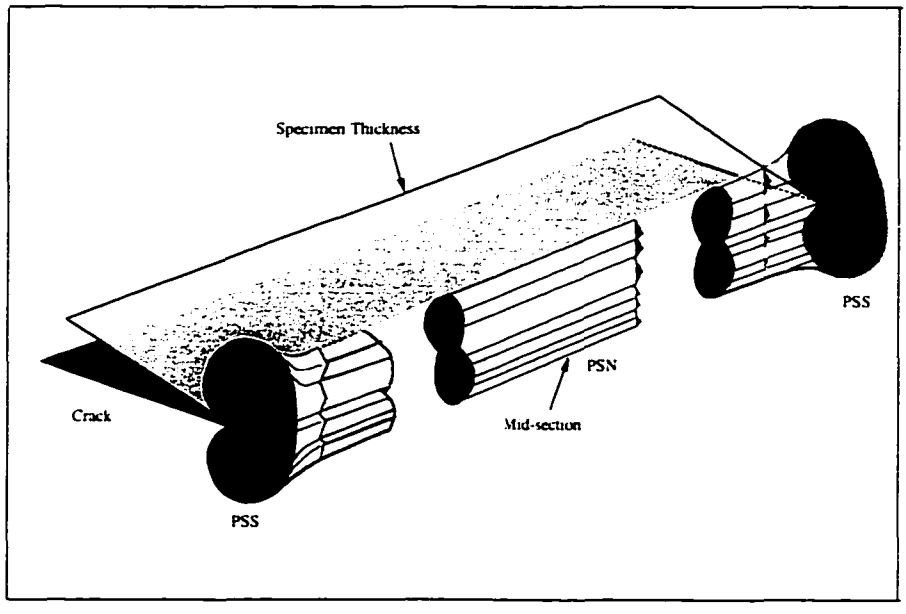

Figure 2.4: Thickness effect on plasticity zone size.

LEFM analyses become increasingly inaccurate as the inelastic region ahead of the crack-tip grows with increasing load magnitude. Therefore, the consideration of the effective crack length (ECL) is important if the effect of plasticity is to be taken into account. The expression for the ECL is:

$$a_{eff} = a_o + r_y, \quad \text{or} \quad a_{eff} = a_o + \lambda \left(\frac{K}{\sigma_{ys}}\right)^2. \tag{2.5}$$

where a_o is the physical crack length and r_y is the plastic zone size correction. The parameter λ is the plastic zone correction factor. Commonly used values for r_y and λ are cited in [22], while some values of a_{eff}, λ, and plastic zone correction factors are presented in Table 2.1.

Serial Number	Effective Crack length	Plastic zone correction factor	Researcher(s)
1	$a_o + PCN/2\pi$	$1/2\pi$ (for PSS)	Irwin [11]
2	$a_o + PCN/6\pi$	$1/6\pi$ (for PSN)	Irwin [11]
3	$a_o + PCN * \pi/16$	$\pi/16$	Dugdale [21] [21]
4	$a_o + PCN * \pi/24$	$\pi/24$ (for PSS) (Perfectly plastic)	Edmunds and Willis [25]
5	$a_o + PCN * .019$	.019 (for PSN)	Edmunds and Willis [25]
6	$a_0 + PCN * .025$	.025 (for PSN)	Sham [26]

Table 2.1: Some examples of plastic zone correction factor.

In nonlinear fracture mechanics an elastoplastic stress analysis is performed. The detailed fracture process occurs in a region in which the stresses and strains have a well defined form, given by the elastoplastic singularity (the HRR singularity of Hutchinson [23], Rice and Rosengren [24]) for the power-law plastic behavior. Edmunds and Willis [25] obtained an expression for the plastic zone correction in the form :

$$r_y = 2C_1(n)\gamma_{11}^2\varepsilon^2, \quad \text{where } \gamma_{11} = \frac{K}{2\sqrt{2\pi}\sigma_{ys}\varepsilon}. \tag{2.6}$$

$\varepsilon = \frac{1}{s}(\sigma_\infty/\sigma_{ys})$, s is a scaling parameter. $C_1(n)$ is a material constant which depends on the hardening exponent n and is determined from the far field expansion of the elastic-plastic solution. The plastic zone correction factor λ is a function of hardening exponent n. The expression for $\lambda(n)$ is:

$$\lambda(n) = \frac{C_1(n)}{4\pi}. \tag{2.7}$$

For the Dugdale yielding model and a perfectly plastic material Edmunds and Willis [25] give the plastic zone correction as:

$$r_y = \frac{\pi}{24}\left(\frac{K}{\sigma_{ys}}\right)^2. \tag{2.8}$$

A material satisfying the von Mises yield criteria in conjunction with non-hardening PSN conditions [25], gives a value for $\lambda = 0.019$, which is considerably smaller than conventional PSN values. Sham [26] obtained a similar value for PSN plastic zone size correction factor $\lambda = .025$, for a non-hardening material by using some modifications suggested by Hilton and Hutchinson [27].

2.3 Two Parameter Characterization of Crack-tip Stresses

Larsson and Carlsson [28] reported PSN elastic-plastic finite element analyses of test specimen geometries. It was found that significant discrepancies exist in comparison with boundary layer solutions, even within the range of loads permitted by the ASTM Standard Test Method for Plane Strain Fracture Toughness of Metallic Materials (E-399). At the maximum permitted load levels, the computed plastic zone sizes for center-cracked and double edge cracked specimen, for example, were greater than that of the boundary layer solutions by 50% and 25%, respectively.

The plastic zone sizes for various cases would have coincided had the elastic-plastic crack-tip state been determined by K alone. It was shown by Larsson and Carlsson that the differences observed in the size of plastic zones of various specimens are due to differences in the T-stress, the second term of Williams [29] eigen-expansion of

near crack-tip elastic stress field, *i.e.*:

$$\begin{bmatrix} \sigma_{xx}(r,\theta) & \sigma_{xy}(r,\theta) \\ \sigma_{yx}(r,\theta) & \sigma_{yy}(r,\theta) \end{bmatrix} = \frac{K}{\sqrt{2\pi r}} \begin{bmatrix} f_{xx}(\theta) & f_{xy}(\theta) \\ f_{yx}(\theta) & f_{yy}(\theta) \end{bmatrix} + \begin{bmatrix} T_{xx} & 0 \\ 0 & 0 \end{bmatrix}. \tag{2.9}$$

The T-stress is not singular as $r \rightarrow 0$ but it can alter the elastic-plastic crack-tip stress state, thus modifying the crack-tip plastic zone [28, 30].

Rice [31] has shown with the help of a PSN model that the non-singular stress term, acting parallel to the crack-tip, has a less pronounced effect on such crack-tip parameters, such as the crack-tip opening displacement (CTOD). Recently, very extensive work has been conducted on two parameter characterizations of near-crack-tip fields [32, 33, 34].

2.4 Experimental Investigations

Several experimental works pertaining to crack-tip plasticity have been reported in the literature. The earliest isochromatic-fringe based experimental study involving stress distributions at the base of a crack was conducted by Hollister [35]. Later, Post [36] reported results pertaining to photoelastic observations of an edge crack. The shapes of fringe patterns were in agreement with the theoretical results provided by Williams [29]. A comprehensive investigation on the stresses for a rapidly moving crack was performed by Wells and Post [12]. Their results show a resemblance to the work of Irwin [12] and confirm the "butterfly" shape of the plasticity zone. An experimental work, conducted by Gerberich in (1964), and cited in [23], using the photoelastic coating method, obtained the plastic zones at the crack-tip for 2024-O-Aluminum and 6061-T6 Aluminum. The findings again confirm the butterfly shape of the plasticity affected zone ahead of the crack-tip.

Another technique known as the 'etch-pit technique' was used by Hahn and Rosenfield [37]. Under PSS conditions plastic zones were very diffusive while under PSN conditions a multiple series of hinge type zones were observed. In another investigation, conducted by Hahn, Sarrate and Rosenfield [38] the 'etch-pit technique' was used to obtain the experimental estimates of the plasticity affected zone. At high stress levels, when the zone size to beam height ratio reaches a value greater than 0.09 the zone begins to tilt backwards. The results of this experimental investigation are in agreement with Wilson's work [39], who has estimated enclave sizes and shapes for various specimens by applying the boundary collocation methods to Williams's [29] stress function. The principal disadvantage of this technique is that it is not suitable for other alloys. Another technique, known as 'electrolytic etching' is suitable for other materials.

Loye, Bathias, Retali and Devaux [40] used microhardness methods for the determination of plastic zone ahead of the crack, and presented a brief review of other experimental techniques. These include electron-channeling, X-ray diffraction, channeling contrast in scanning electron microscopy and stereographic techniques.

Experimental methods using strain gages to study the evolution of the cyclic plastic zone in the high strength aluminum alloy 2024-T351 were studied by Ranganathan, Jendoubi and Merah [41] using microstrain gages fixed to compact tension C(T) specimen surfaces on either side of the crack propagating line. They reported that as the stress ratio R increases the plasticity affected zone becomes smaller. Finally, a recrystallization technique was employed by Csizmazia and Czoboly [42] to study plastic zones in notched C(T) specimens of aluminum alloy. It was observed in this investigation that the plastic zone shapes obtained by this technique were different in extent from the calculations of [23, 24].

2.5 Numerical Models

Tuba [43] provided solutions to elastic-plastic plane problems using a finite difference scheme and relaxation method. The problem involved a rectangular bar with two symmetrically located edge cracks. The solution involved a non-homogeneous biharmonic equation, with the stresses prescribed on the boundary. This investigation provides the extent of the plastic region for various values of yield strength and fixed load and lends support to the butterfly shape of the plasticity affected region ahead of the crack-tip, similar to the one obtained on the basis of Irwin's solutions. Using these results one can determine the value of the shape ratio, β, the plasticity affected height to plasticity range. Such values are provided in the Table 2.2. The details

RESEARCHER(S)	SHAPE RATIO β	COMMENTS
Tuba [43]	2.75	For $\varepsilon = 0.66, s = 1$
Hutchinson [23]	1.834	For $n = 3$
Gerberich [23]	1.571	For 2024-O Aluminum
Rice and Rosengren [24]	6.2	For $n = 1.0.99$
Swedlow [44]	3.1	For $\varepsilon = 0.869, s = 1$
Ayres [45]	2.58	For $\varepsilon = 0.861, s = 1$

Table 2.2: The shape ratio β obtained from various investigations.

of stress and strain fields, associated with the plastic behavior of crack-tips, for a power hardening material, are provided by Hutchinson [23]. The plastic zone shape is similar to that given in [43]. The value of β as calculated on the basis of these results is 1.834.

The crack-tip strain singularities were investigated with the help of an energy line integral exhibiting path independence for all contours around the crack-tip in a

two-dimensional deformation field by Rice and Rosengren [24]. The solution involved a differential equation and fourth-order Runge-Kutta integration was used to obtain the location of the elastic/plastic boundary. The value of β obtained on the basis of this study is provided in Table 2.2.

The problem of an elasto-plastic cracked plate in tension for a hardening material was solved by Swedlow [44] using finite element methods. This study involved 348 constant-strain triangular elements with 200 nodes to represent the first quadrant of the plate. Furthermore, a finite difference procedure for the determination of stress and deformation in a three dimensional elastic-plastic solid with a slit was presented by Ayres [45]. The investigation uses relaxation methods in its solution methodology. The solid is assumed to be elastic, perfectly plastic material. The growth of the plastic zone near the tip for various tensile loads is presented. The shape of the plastic enclaves is similar to [23, 43, 44]. Based on this numerical investigation the value of β was computed as 2.58 for an applied load of .861 times yield strength.

2.6 Crack-Tip Cyclic Stresses and Strains

In FCGR calculations under SOL or VAL conditions, the stress intensity factor range ΔK and the overload plasticity affected zone size (essentially r_p) are the most crucial factors in flaw tolerant design. Fatigue crack growth was analysed as early as 1953 by Head [46]. Liu [47] found that the important stress parameter to correlate with fatigue crack growth is the stress range $\Delta\sigma$, rather than the maximum value of stress σ_{max}. One of the important milestones in the study of FCGR, is the application of stress intensity factor [9], where the maximum value of the stress intensity factor, K_{max}, was used to correlate the FCGR. Liu [48] indicated that the FCGR was proportional to $\Delta\sigma^2 a$ in a specimen with a central crack of length $2a$. For a wide plate $\Delta\sigma^2 a = \Delta K^2$.

This was the first work which correlated FCGR with ΔK. Subsequently, Paris and Erdogan [49], found that da/dN is proportional to ΔK^4. In the past 35 years, ΔK has been widely used to correlate FCGR.

The size of the plastic zone under cyclic loading is considerably smaller than the one observed under monotonic loading. The occurrence of reversed flow plasticity ahead of a fatigue crack has been reported in several earlier works [50, 51]. The reversed flow zone is embedded in the monotonic plastic zone. The size of the reversed plastic zone for a stationary crack is $\frac{1}{4}th$ the monotonic yield zone based on theoretical considerations. On the basis of the experimental investigation of [52], the cyclic yield zone size is $\frac{1}{5}th$ the non-cyclic yield zone. Subsequently, Jones [53] used the cyclic zone size of [52], which was obtained on the basis of experimental evidence, in the study on Titanium alloys subjected to single overloads.

It has been shown by Budiansky and Hutchinson [54], using Muskhelishvilli complex potentials, that for a propagating fatigue crack the reversed yield zone is 10% of the Dugdale monotonic yield zone size, which is much less than for a stationary crack, where a 25% value is used. Glinka [55] obtained an approximate relationship for the distance over which fatigue crack remains closed from various closure models including the closure model of Budiansky and Hutchinson [54]. For a stress ratio $R = 0$ ($R = \sigma_{min}/\sigma_{max}$, where σ_{min} and σ_{max} are the minimum and maximum values of stresses during a loading cycle), the distance over which crack remains closed was found to be approximately 0.015 of the reversed plastic zone, which is in agreement with the Budiansky and Hutchinson's [54] estimation. Details concerning the reversed flow plastic zone are given in the recent text by Suresh [1].

The FCGR is caused by crack-tip cyclic deformation. It has been shown by Liu [56], that the stress intensity range ΔK and the stress ratio R, characterize the cyclic strains and stresses at the crack-tip.

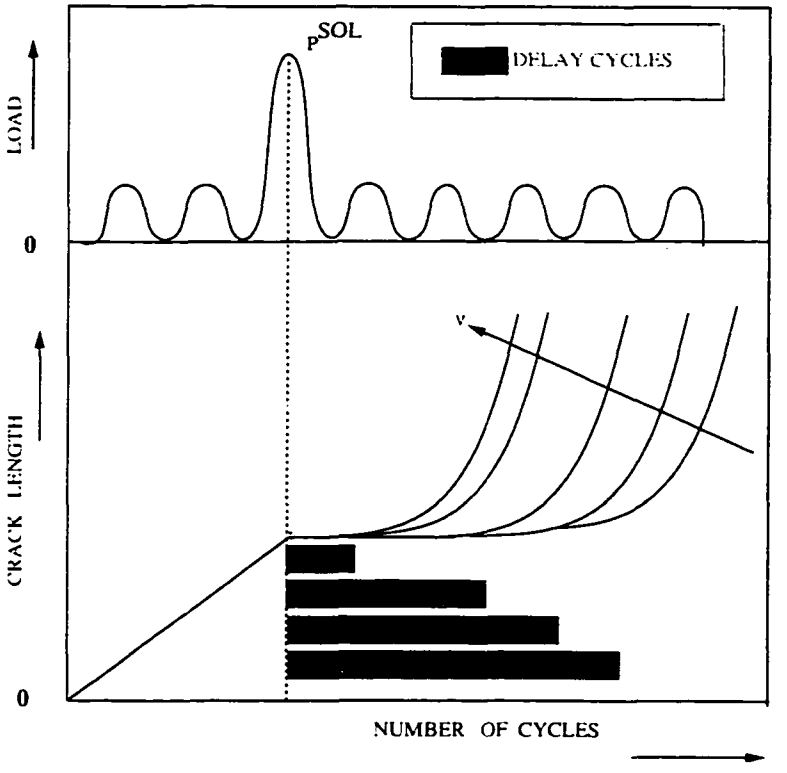

Figure 2.5: Schematic showing the effect of Poisson's ratio on FCGR.

Any estimation of the fatigue life of structural components requires an adequate description of the behavior of the fatigue crack growth rate following a rapid change in the loading condition. The most important of these load interaction effects is the retardation of the fatigue crack growth rate subsequent to an overload. The models by Dugdale and Irwin give an idea about the size of the plastic zone but not its shape. Since, it has been shown that the shape of the plasticity affected zone is very important for a good estimate of the life of structural components, it is important to incorporate it into FCGR models. As shown in Figure 2.5, the plasticity affected zones, and consequently their effect on the FCGR, are very sensitive to Poisson's ratio ν.

2.7 An Approach to the Estimation of the Plasticity Zone

2.7.1 Characterization of Plastic Zone Size

The models by Dugdale and Irwin give an idea of the size of the plastic zone but not its shape. The size, in general, is estimated on the basis of a circle of certain diameter obtained on the basis of reasonings given in the above models for crack-tip-plasticity. In these models the effect of the shape of the plasticity affected zones is not taken into account.

To obtain a better idea of the plastic zone shape, the components of stress in the radial and circumferential directions for a Mode-I type of loading were derived in this investigation via Williams' [29] study. With a modification to take into consideration crack-tip blunting, the resulting equations are:

$$\begin{bmatrix} \sigma_r \\ \sigma_\theta \\ \tau_{r\theta} \end{bmatrix} = \begin{bmatrix} \frac{1}{4}\frac{K}{\sqrt{2\pi r}}\left(5cos(\frac{\theta}{2}) - cos(\frac{3\theta}{2})\right) + T_{rr} + f(\rho, r, \theta) \\ \frac{1}{4}\frac{K}{\sqrt{2\pi r}}\left(3cos(\frac{\theta}{2}) + cos(\frac{3\theta}{2})\right) + f(\rho, r, \theta) \\ \frac{1}{4}\frac{K}{\sqrt{2\pi r}}\left(sin(\frac{\theta}{2}) + sin(\frac{3\theta}{2})\right) + f(\rho, r, \theta) \end{bmatrix}. \tag{2.10}$$

The first terms in eqns(2.10), represent the singular terms as $r \rightarrow 0$ and are therefore dominant near the crack-tip. The second term in eqn(2.10) arises from a consideration of higher power terms. This term is known as the T-stress, is not singular as $r \rightarrow 0$ but it can effect the elastic-plastic crack-tip stress state. The third terms arise as a contribution from crack-tip blunting and are not given in Williams'[29] work. The contribution of crack-tip blunting has been discussed in [5] and the contribution of this term is $\sigma_\rho = K/\sqrt{\pi\rho}$ for a sharp elliptic or hyperbolic notch with a crack-tip radius ρ. The above equations can now be used to obtain information regarding the principal stresses after the simplifying assumptions of negligible contributions of T_{rr}

and $f(\rho, r, \theta)$ are incorporated. Hence principal stresses, as derived from eqns(2.10), then become :

$$\begin{bmatrix} \sigma_1 \\ \sigma_2 \\ \sigma_3 \end{bmatrix} = \begin{bmatrix} \frac{K}{\sqrt{2\pi r}} cos\frac{\theta}{2}(1 + sin\frac{\theta}{2}) & \\ \frac{K}{\sqrt{2\pi r}} cos\frac{\theta}{2}(1 - sin\frac{\theta}{2}) & \\ \nu(\sigma_1 + \sigma_2) & \text{PSN} \\ 0 & \text{PSS} \end{bmatrix}. \tag{2.11}$$

which, in conjunction with the von Mises and Tresca yield criteria, give expressions for the plastic zone shape as follows:

von Mises:

$$r_p(\theta) = \begin{cases} \frac{K^2}{4\pi\sigma_{ys}^2}(\frac{3}{2}sin^2(\theta) + (1-2\nu)^2(1 + cos(\theta)) & \text{PSN.} \\ \frac{K^2}{4\pi\sigma_{ys}^2}(1 + \frac{3}{2}sin^2(\theta) + cos(\theta)) & \text{PSS.} \end{cases} \tag{2.12}$$

Tresca :

$$r_p(\theta) = \begin{cases} \frac{K^2}{2\pi\sigma_{ys}^2}cos^2(\frac{\theta}{2})(1 - 2\nu + sin(\frac{\theta}{2}))^2 & \text{PSN.} \\ \frac{K^2}{2\pi\sigma_{ys}^2}cos^2(\frac{\theta}{2})(1 + sin(\frac{\theta}{2}))^2 & \text{PSS.} \end{cases} \tag{2.13}$$

Some interesting observations can be drawn from these equations. From eqns(2.12 and 2.13) it may be seen that for $\theta = 0$, $r_f = r_p\Big|_{\theta=0}$, the plasticity affected range under PSN becomes:

$$r_f = \frac{K^2(1-2\nu)^2}{2\pi\sigma_{ys}^2} \qquad \text{PSN.} \tag{2.14}$$

and remains unaltered under both yield criteria. Similarly, for the PSS situation the corresponding relation is:

$$r_f = \frac{K^2}{2\pi\sigma_{ys}^2} \qquad \text{PSS.} \tag{2.15}$$

The plasticity affected zone at $\theta = 0$ is referred to as plasticity affected range in this work. The value of plasticity affected height is denoted by h_f for both PSS and PSN situations. The quantity $\alpha_j = (1-2\nu)^2/2\pi$ is the plastic constraint coefficient, and $\alpha = (1-2\nu)^{-2}$ is the plastic constaint factor based on the current model.

2.7.2 Nondimensional Form of the Equations

It is observed that the above equations are composed of several different factors, with K/σ_{ys} appearing in both eqns(2.12 and 2.13). The value of the stress intensity factor, K, for a plate with a crack is $K = \sigma_\infty \sqrt{\pi a} Y$, where $Y = f(a/W)$ is the geometric factor, a is the length of the crack and W is the width of the plate; for an infinite width plate $f(a/W) = 1$. Assuming infinite width conditions and incorporating load ratio ε as $\varepsilon = \frac{1}{s}(\sigma_\infty/\sigma_{ys})$ in the eqns(2.12 and 2.13), a nondimensionalization w.r.t. a, leads to the resulting equations:

von Mises:

$$R_f(\theta, \varepsilon, \nu) = \begin{cases} \frac{\varepsilon^2}{4}(\frac{3}{2}sin^2(\theta) + (1-2\nu)^2(1+cos(\theta)) & \text{PSN.} \\ \frac{\varepsilon^2}{4}(1 + \frac{3}{2}sin^2(\theta) + cos(\theta)) & \text{PSS.} \end{cases} \tag{2.16}$$

Tresca:

$$R_f(\theta, \varepsilon, \nu) = \begin{cases} \frac{\varepsilon^2}{2}cos^2(\frac{\theta}{2})(1-2\nu+sin(\frac{\theta}{2}))^2 & \text{PSN.} \\ \frac{\varepsilon^2}{2}cos^2(\frac{\theta}{2})(1+sin(\frac{\theta}{2}))^2 & \text{PSS.} \end{cases} \tag{2.17}$$

The expressions in eqns(2.16 and 2.17) are found to be functions of three factors, ε, ν, θ, *i.e.*, $R_f = f(\varepsilon, \theta)$ for PSS, and $R_f = f(\varepsilon, \nu, \theta)$ for PSN. Since the T_{rr} was neglected in the derivation of the eqns(2.16 and 2.17), the contribution of T_{rr} term does not appear in the final function. Also, the crack-tip radius and material hardening was considered negligibly small so their contribution is also absent. The nondimensional value of the plasticity affected range is denoted by, $R_P = R_f\Big|_{\theta=0}$ and nondimensional value of the plasticity affected height is $H_P = R_f\Big|_{\theta=90}$.

2.7.3 Computational Results

The results obtained on the basis of eqns(2.16 and 2.17) are now presented. The two different yield criteria, von Mises and Tresca are compared to examine their

effect on the plasticity affected regions formed at the crack-tip. Furthermore, the two parameters, Poisson's ratio ν and load ratio ε, are varied to reveal their corresponding effect on the plasticity affected regions. The shape ratios, β, for various Poisson's ratios, ν, are also been presented.

The effect of yield criteria

The von Mises zones as in Figure 2.6 are elongated and butterfly shaped, while the Tresca zones are slightly flattened and dumbbell shaped. Furthermore, it is observed in Figure 2.7, that the Tresca zones are larger in size for a PSS situation when compared with corresponding von Mises zones. However, this trend reverses under PSN as higher values of ν are approached. It is observed that the plastic zone ahead of the crack-tip is smaller in PSN conditions than in PSS. The plasticity affected range R_P remains unaltered under both yield criteria.

The shrinkage effect

It is seen from these results that increase in Poisson's ratio has a "shrinkage" effect on the plasticity zones in PSN situations under both the yield criteria: Figure 2.6 and Figure 2.7. Furthermore, the results obtained for various Poisson's ratios show that the extent of the plastic zone for PSN is highly sensitive to Poisson's ratio ν. The effect of Poisson's ratio ν on the plasticity affected zones is indicated in Figure 2.8, for a load ratio $\varepsilon = 1$, and the two yield criteria have been compared for values of ν between 0 to 0.5 . Some typical values of β are provided in Table 2.3.

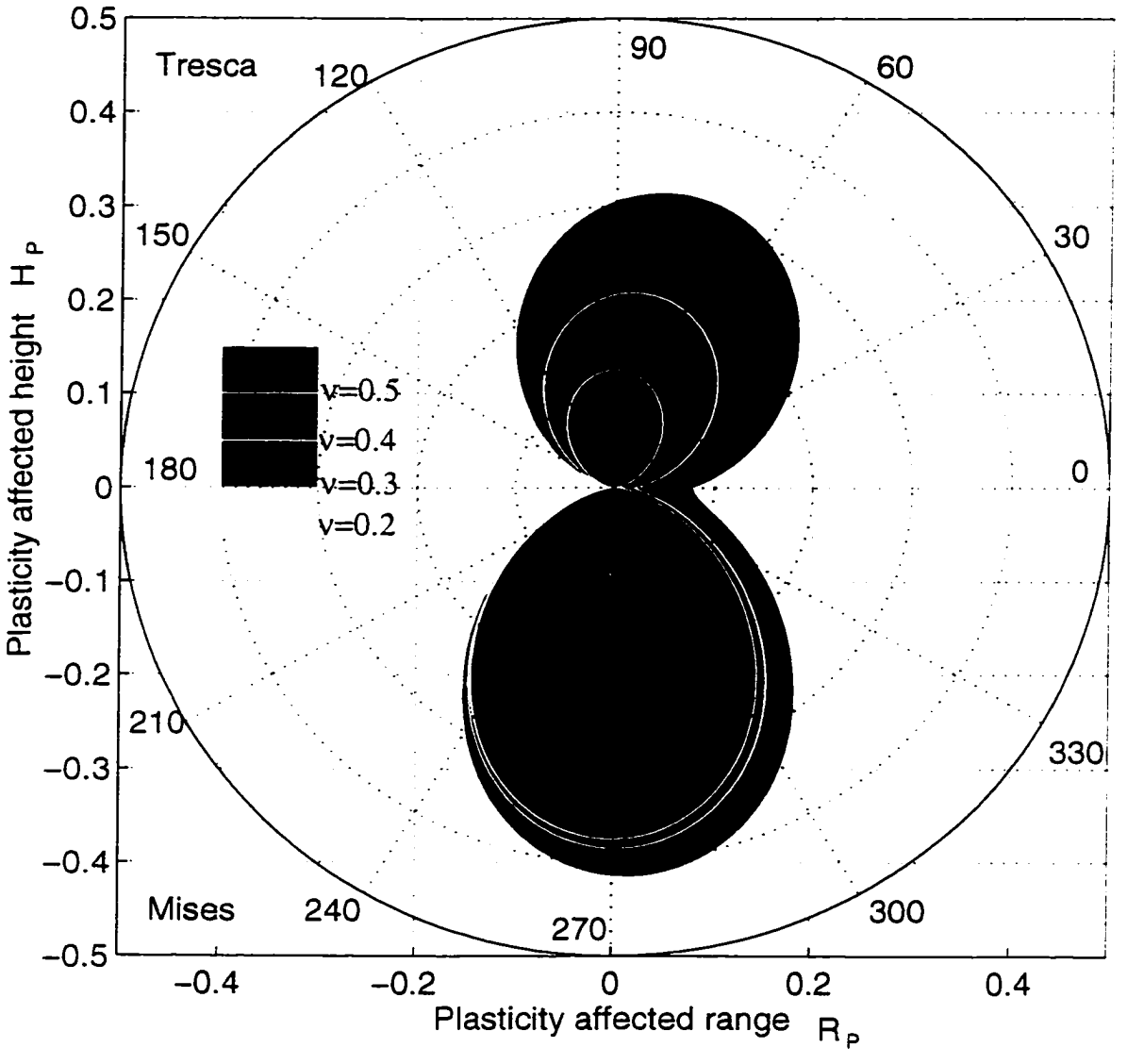

Figure 2.6: Comparison of plasticity zones for various Poisson's ratio, ν, under PSN.

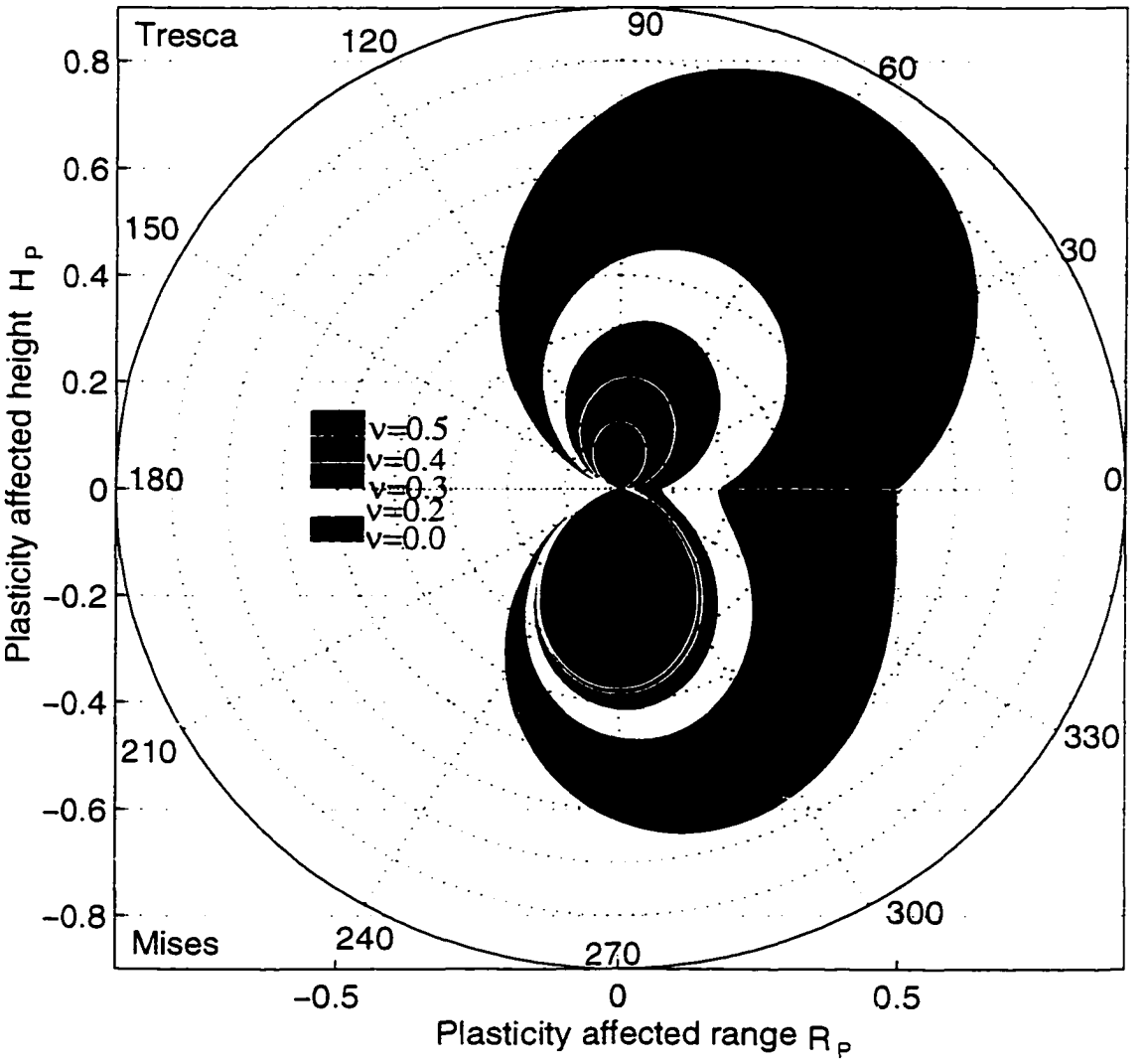

Figure 2.7: Comparison of plasticity zones for various Poisson's ratio, ν. PSS included.

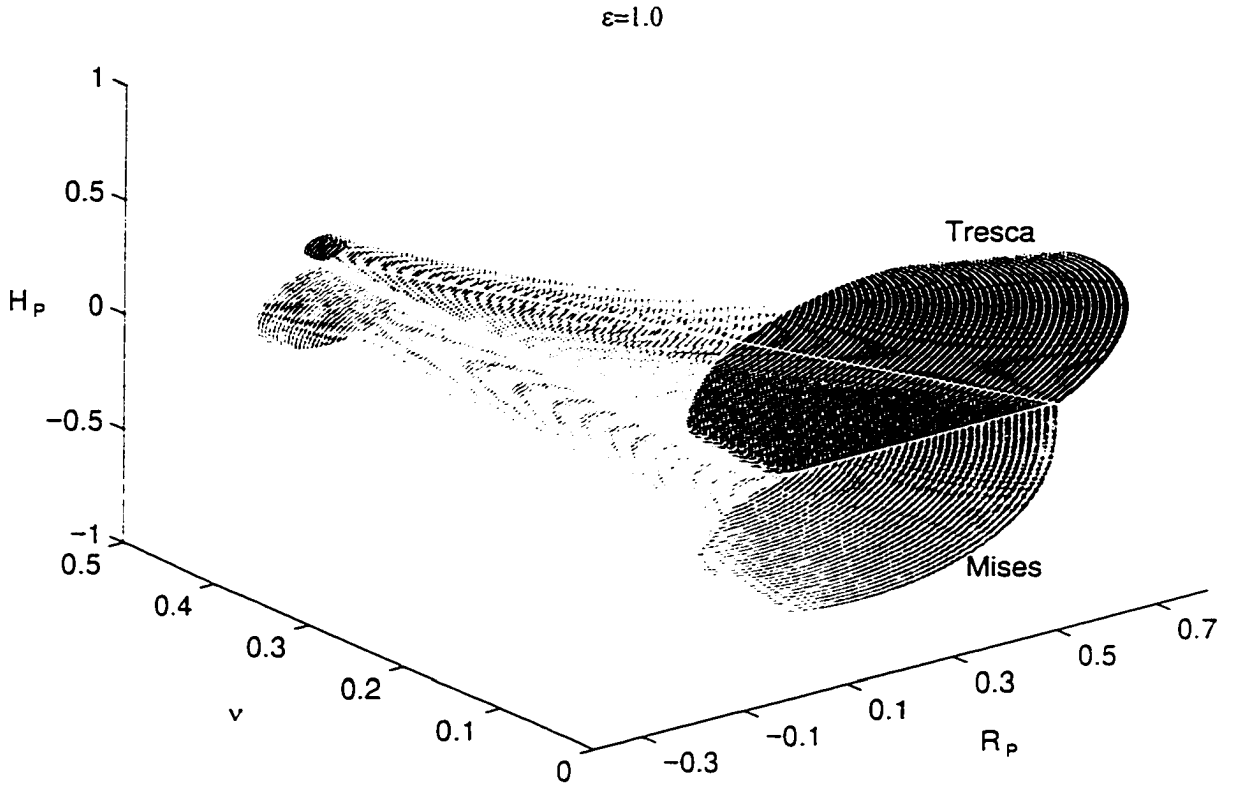

Figure 2.8: Plasticity zones for various values of Poisson's ratio ν, a 3D representation.

YIELD CRITERIA	PSS/PSN	POISSON'S RATIO ν	SHAPE RATIO β
von Mises	PSS	0.00	1.25
von Mises	PSN	0.30	5.18
von Mises	PSN	0.35	8.83
von Mises	PSN	0.40	19.25
Tresca	PSS	0.00	1.45
Tresca	PSN	0.30	3.90
Tresca	PSN	0.35	5.75
Tresca	PSN	0.40	8.10

Table 2.3: Some values of β obtained in this investigation.

The swelling effect

Another parameter (referred to as the load ratio in this study), ε, defined as the ratio of applied stress to the yield strength and its effect on plasticity zones is shown for PSN in Figure 2.8, Figure 2.9 and for PSS in Figure 2.10 and Figure 2.11, respectively. It is observed that an increase in ε has a swelling effect on the plasticity zones in general. In the PSN situation, as ε increases, von Mises zones become larger when compared with the corresponding Tresca zones. However, under PSS conditions Tresca zones are larger than the Mises zones for higher values of ε. The effect of the load ratio ε for a value of $\nu = 0.30$ on the plasticity affected zones is compared for the two yield criteria, and is provided in Figure 2.11.

The shape ratio

It is interesting to find the "shape ratio", β, defined as the plasticity affected height, H_P, relative to the plasticity affected range, R_P, the value of H_P being, in general, larger than the corresponding R_P. The values of β for various angular positions are

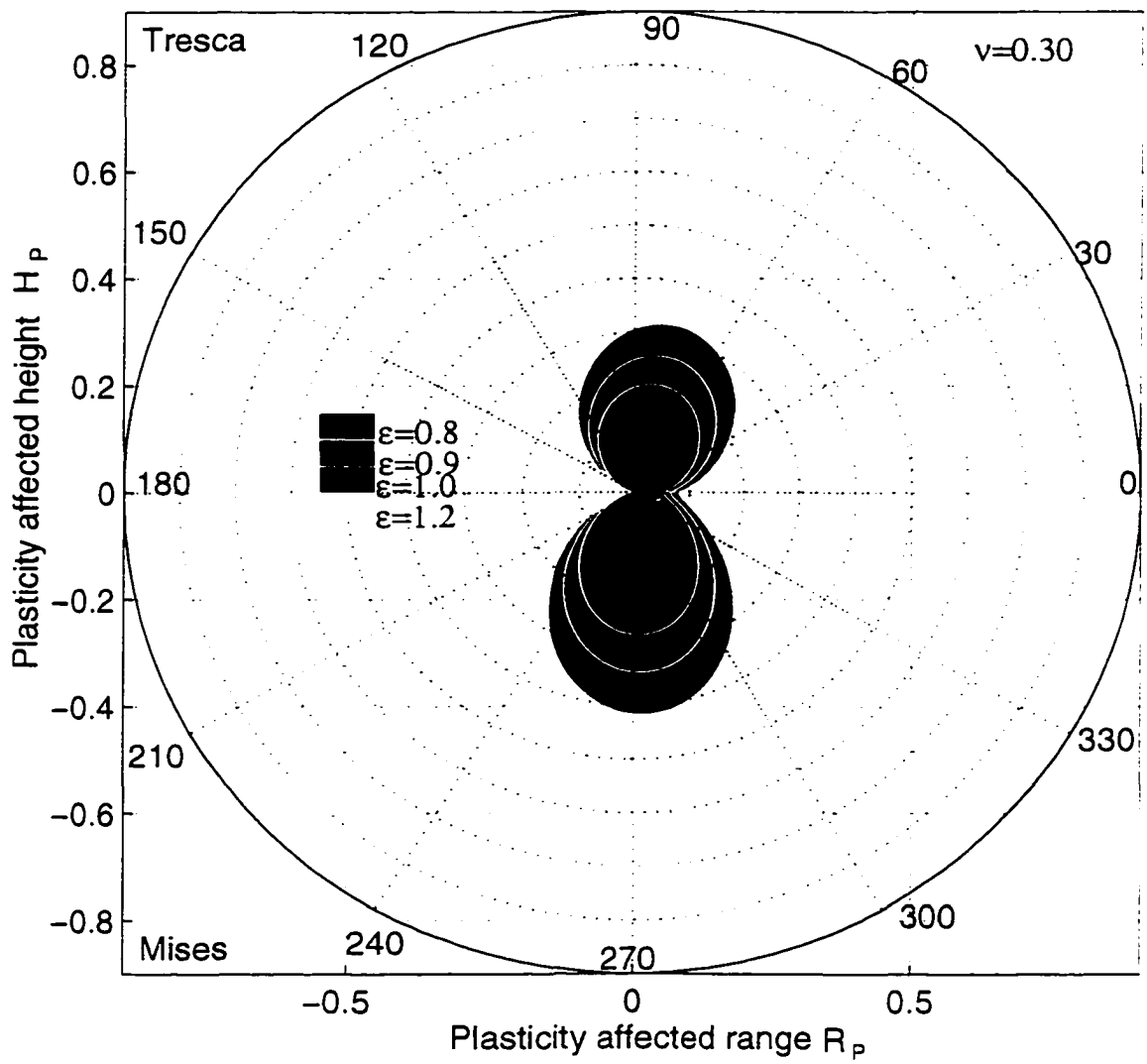

Figure 2.9: Comparison of plasticity zones for various load ratios, ε, under PSN.

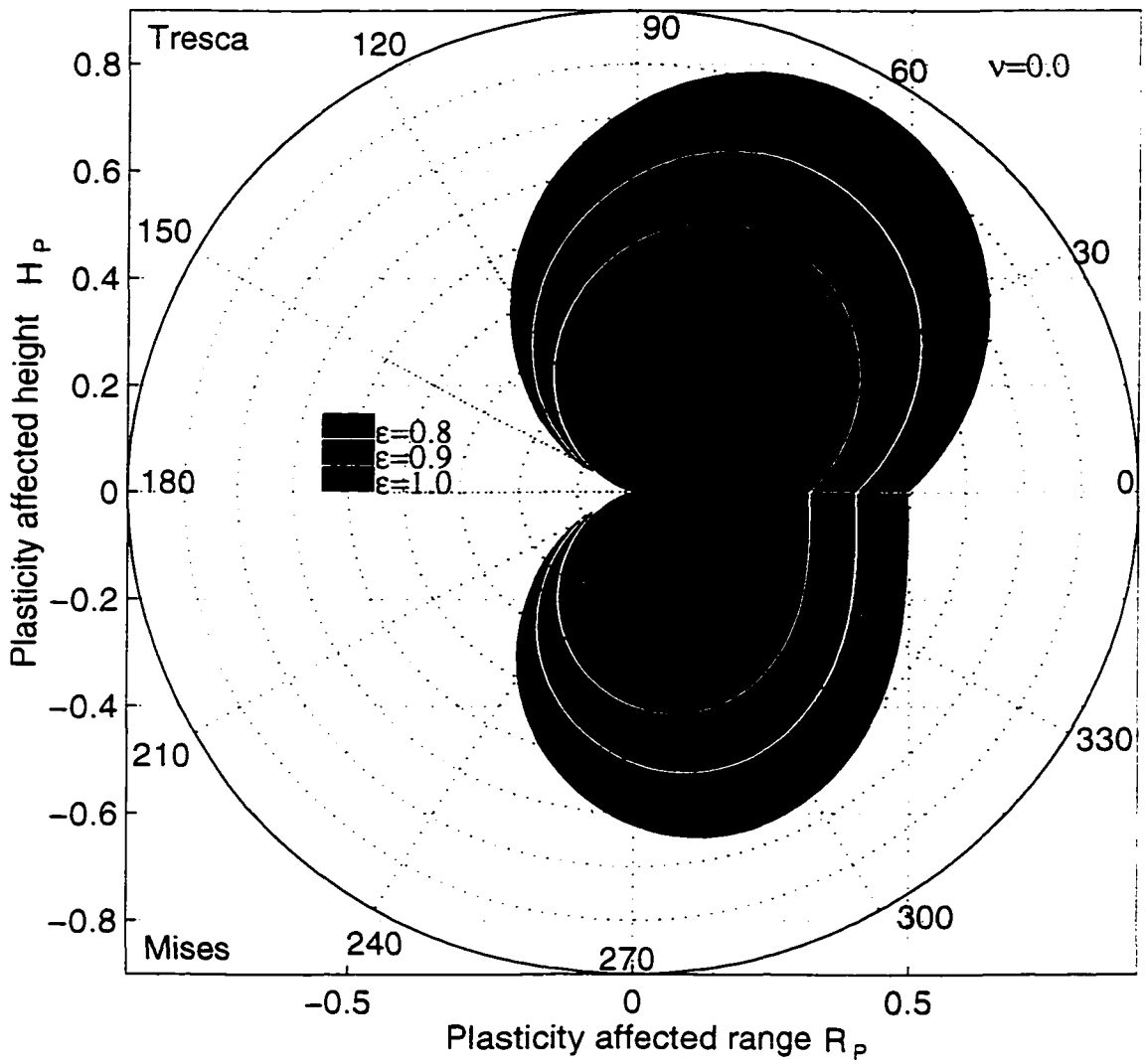

Figure 2.10: Comparison of plasticity zones for various load ratios, ε, under PSS.

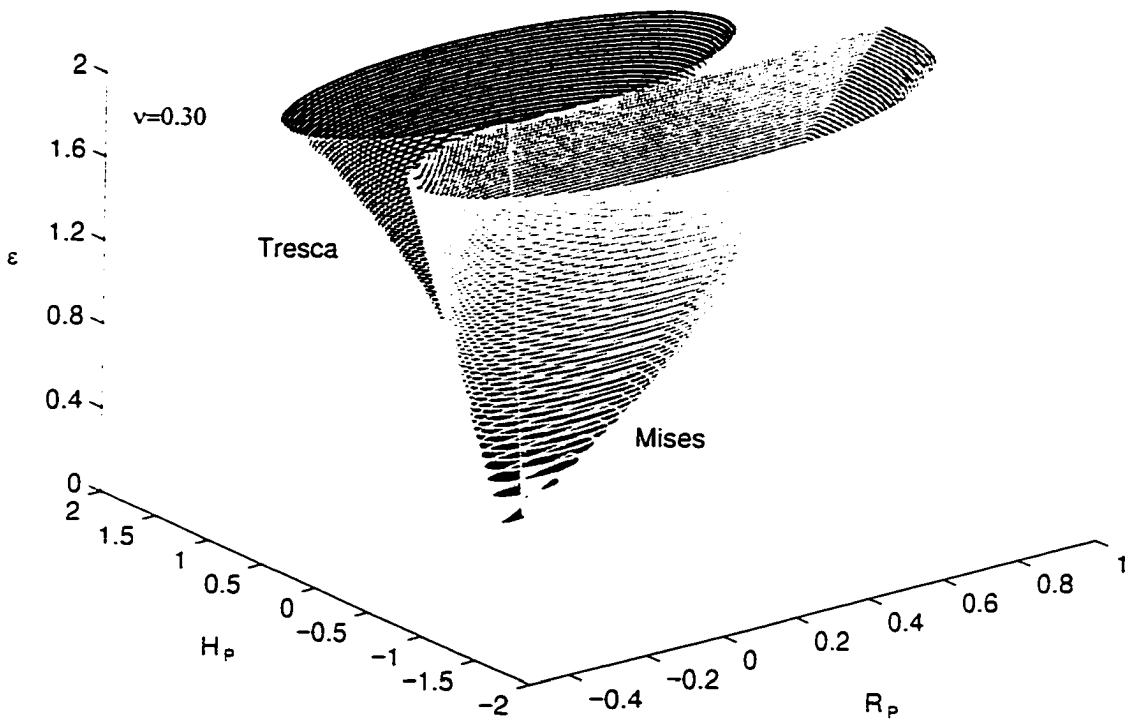

Figure 2.11: Plasticity zones for various values of load ratio ε, a 3D representation.

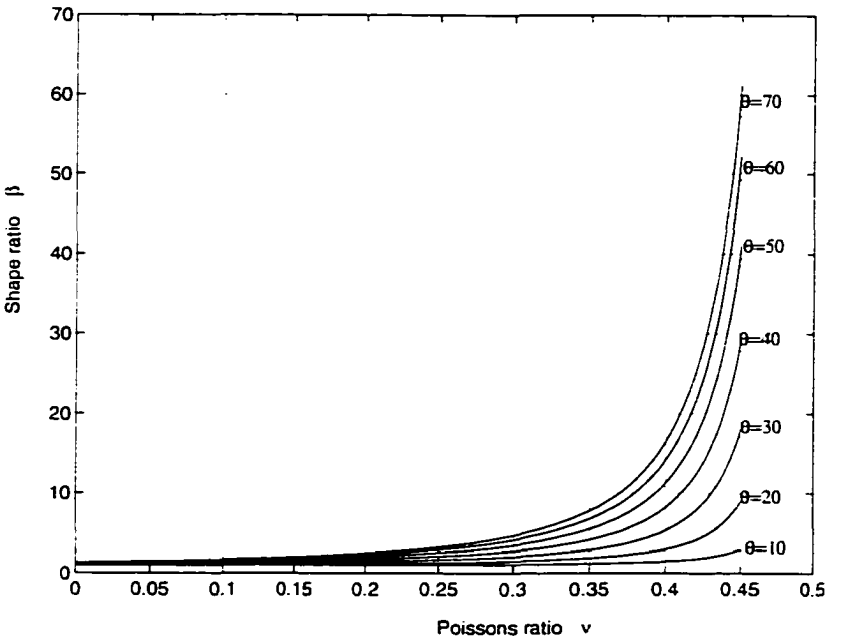

Figure 2.12: The effect of angular coordinate θ, on shape ratio β, for Mises yield criteria.

provided for the von Mises and Tresca yield criteria in Figure 2.12 and Figure 2.13, respectively. The values for β become a maximum at a value of θ approximately equal to 70 degrees. The values of β for the von Mises are very large compared with the corresponding values of Tresca for the higher Poisson's ratios ν. For ν values approaching 0.49, β reaches a value approximately 700 for Mises criteria, as shown in Figure 2.14, and for a value of $\nu = 0.499$ the value of β is approximately 2.7×10^4. An expansion of the graph for small values of β is presented in Figure 2.15. This implies that the plasticity affected range R_P becomes vanishingly small for high values of Poisson's ratio ν. For a material like rubber under PSN condition it indicates that the delay cycles (the number of cycles exhausted in the plastic zone under overload) essentially reduces to 0 for Mode-I type of loading. Some additional zones of plasticity are provided in Appendix A.

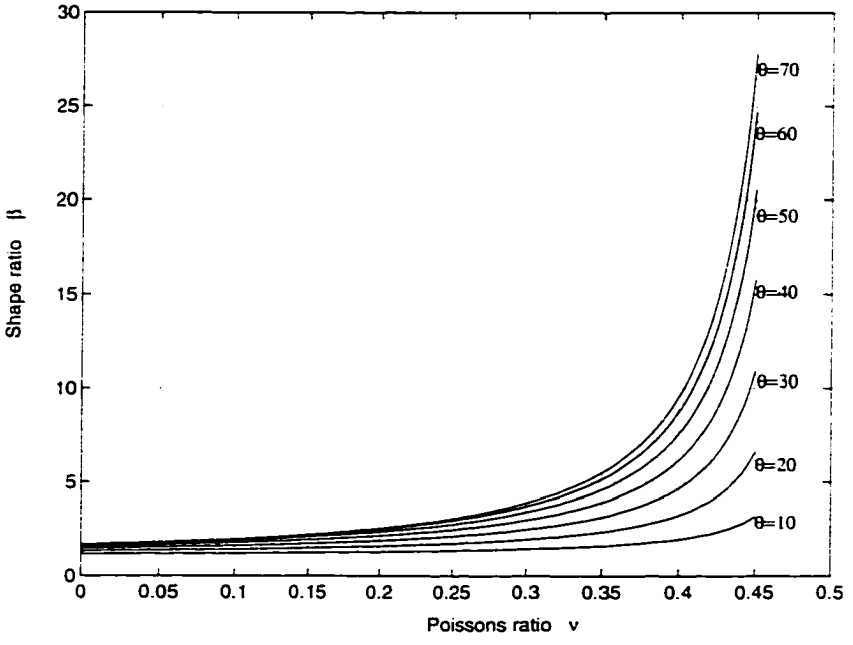

Figure 2.13: The effect of angular coordinate θ, on shape ratio β, for Tresca yield criteria.

2.8 Implications of Crack-tip Plasticity on FCGR Predictions

The retardation effect on the FCGR involves an estimation of the plastic zone formed at the crack-tip. Hence, for modelling the effect of crack-tip plasticity, the shape of the plasticity zone has been incorporated in a FCGR prediction model as is explained in Chapter 5. The number of cycles during which a fatigue crack traverses through an overload plastic zone (known as the delay cycles) is influenced in a significant manner by the type of model used for modelling plasticity. For symmetric fatigue test component geometries, the plasticity zones are symmetric for Mode-I type of loading. Hence the crucial parameter which models the effect of plasticity ahead of the crack-tip is R_P. However, H_P is important as far as the effect of plasticity in

the wake of an advancing crack is concerned. The need to study the shape of the crack-tip plasticity for fatigue crack growth rate problems has been pointed out in this Chapter. The present method is useful in that it obtains the characteristics of the plasticity zones in a simple but novel analytic procedure. The strain hardening effect has not been incorporated in the current analysis but this may also have a corresponding effect on the overall zone shape.

Finally, the effect of taking into consideration two parameter crack-tip characterizations for consideration of the shape may provide valuable information on the extent of crack closure. This is a research topic that is being studied at the current time since very little information exists on the characteristics of plasticity zones that are based upon a two parameter characterization as they relate to the influence of crack closure under CAL or SOL. The effect of crack-tip geometry in terms of blunting is not accounted for in this study. The radius of the crack-tip would have a corresponding effect on the shape of the plasticity zone. The phenomenon of crack closure can also affect the zone size because of reduction in the crack driving force, which can be incorporated through opening load, P_{open} [57]. Hence, in general, the shape of the plasticity zone is a function given as $R_f = f(\theta, \varepsilon, \nu, \rho, T_{rr}, n, Y, P_{open})$. This study focused on the first three factors of the function and clearly indicated their influence. Further consideration of Mode-II and Mode-III will provide similar results for such type of loadings.

Attention will now be turned to an investigation of fatigue crack closure.

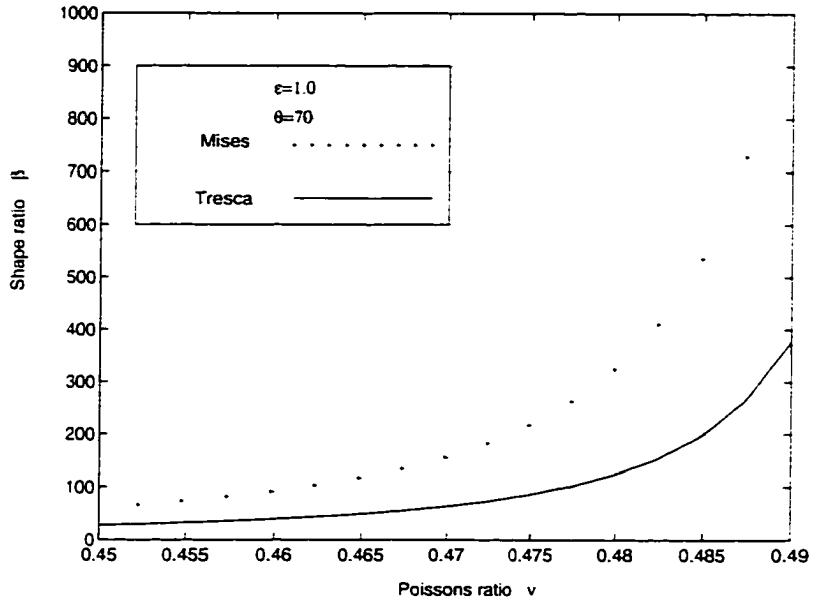

Figure 2.14: The effect of Poisson's Ratio $\nu < 0.49$ on shape ratio β.

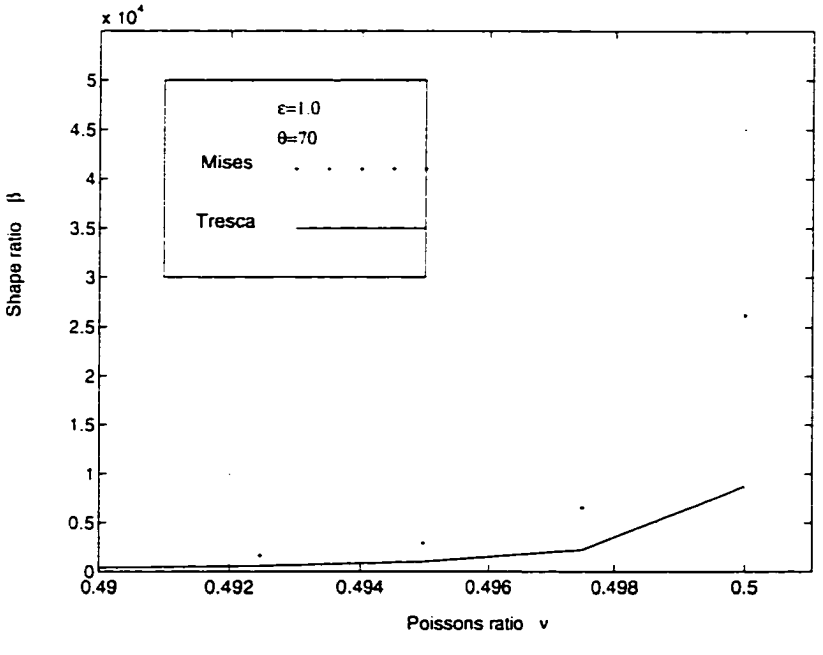

Figure 2.15: The effect of Poisson's Ratio $\nu > 0.49$ on shape ratio β minute detail.

Chapter 3

FATIGUE CRACK CLOSURE

This Chapter gives theoretical basis for fatigue crack closure phenomena. It surveys various aspects of crack closure with a review of different crack closure mechanisms. It identifies various mechanisms which may be operative in fatigue crack closure and presents the importance of plasticity induced crack closure.

3.1 Closure Concept and Experimental Evidence

In the experimental investigation of Elber [13, 58], it was found that there occurred a premature contact of crack faces during the unloading portion of a loading cycle. This premature contact has been attributed to the residual plastic stretch left in the wake of an advancing fatigue crack. During a portion of the loading cycle, the elastic constraints, acting on the residual material in the wake, will keep the crack-tip closed until those are overcome by the externally applied load. Early studies by Hertzberg and co-workers [4] report highly abraded post-overload regions on fatigue fracture surfaces, which are clear indications of crack closure.

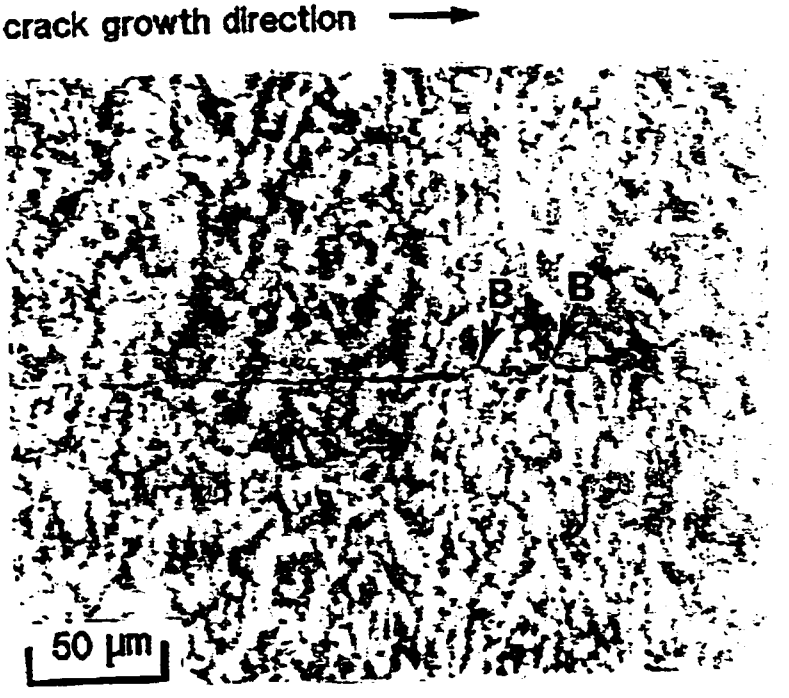

Figure 3.1: Experimental evidence of post overload crack closure. This is a micrograph of crack-path profile taken at the center thickness of the specimen after application of 100 % overload. Note the closure in region B [79].

Experimental investigations of Elber [13] on thin sheets of cracked 2024-T3 aluminum alloy indicated that fatigue cracks can close even at a far-field-tensile load. The reduction in the stress intensity factor associated with premature contact gives rise to the reduction in the fatigue crack growth rate. The details pertaining to the mechanisms of crack closure and their corresponding effect on FCGR are controversial [59], this aspect of fatigue has received considerable attention from analytical, numerical and experimental fields in the last 28 years. However, there is experimental evidence pertaining to plasticity induced crack closure, as is shown in Figure 3.1

3.2 An Explanation of Closure and its Effect

Consider the elastic load-displacement response of an ideal crack (undeformed crack wake) and a real fatigue crack (plastically deformed crack wake) Figure 3.2. While the former is associated with a linear elastic response passing through the origin, the latter shows a nonlinear elastic behavior due to the closure effect. The opening load level represents the deflection point on the load versus crack opening displacement curve, that is the point where the slope of the curve changes. The stress intensity factor associated with the crack being fully open, K_{open}, is the most important aspect of crack closure since it can be directly incorporated into life prediction models. The evaluation is dependent on the location of measurement, and the state of stress *i.e.*, whether plane stress or plane strain plasticity conditions prevail.

It was observed in the analytical crack closure model of Budiansky and Hutchinson [54], that K_{open} can be different from K_{cl} (the closure stress intensity factor) which is measured during the unloading part of a loading cycle (some further details on this aspect of closure are provided in Chapter 4 of this thesis). However, this difference is small and either of the two values can be used without any significant change in the FCGR and life prediction. In all subsequent discussions, the symbol K_{open} will be used to represent the closure behavior unless otherwise stated.

Crack closure effects are significant irrespective of the level of ΔK. In some investigations instead of stress intensity factor based results, load based results have been reported, such as, P_{open} and P_{cl} for opening and closure values of load, respectively. The maximum and minimum loads for the cycle are represented by P_{max} and P_{min} respectively. A significant difference exists in the da/dN-ΔK behavior of various alloys of aluminum and titanium over a wide range of ΔKs. This difference was reported as being due to the variation in the slip character, manifested through a crack closure

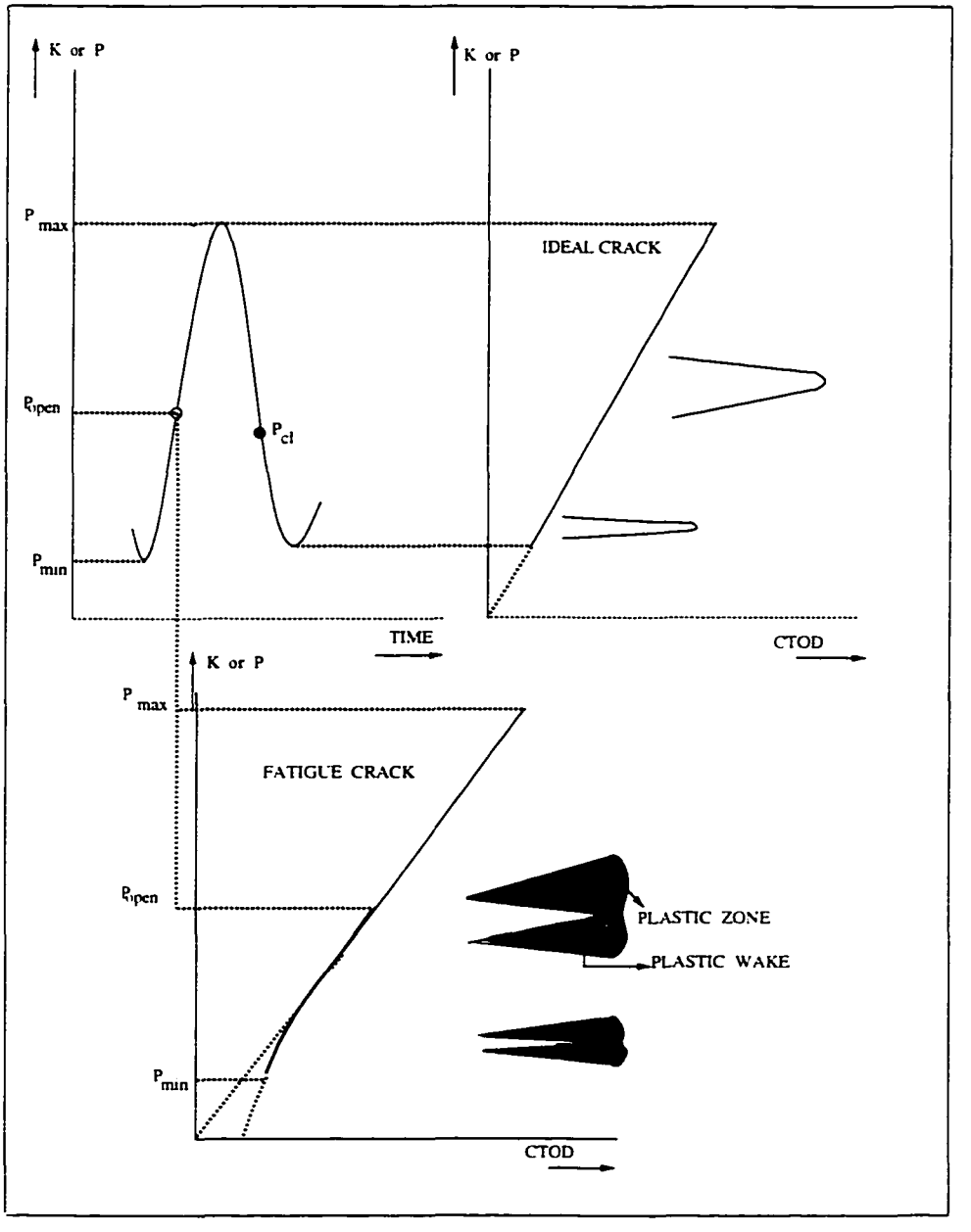

Figure 3.2: A possible representation of fatigue crack closure [60].

process, in these alloys. Majid [60] has reproduced Allison and Williams's results on the effect of closure on growth rate in titanium alloys. It is observed that different curves overlap into a single band when the crack driving force is based on effective stress intensity factor range *i.e.*, ΔK_{eff}. Some other metals such as ferrous alloys exhibit similar behavior. Numerous investigators have justified a number of fatigue crack growth characteristics such as: anomalous fast growth of small cracks, stress ratio and overload effects, as well as microstructural and environmental influences on the basis of fatigue crack closure. Over several years, other mechanisms of crack closure were identified besides Elber's mechanism, which may equally impede the FCGR, and hence the crack advance. On the basis of several research works the various forms of fatigue crack closure are given in the following Section, under constant amplitude loading condition [1, 59, 60].

3.3 Closure Mechanisms

Some exploratory experiments have revealed that several processes could be operative in the phenomenon of crack closure. The participating processes in crack closure have been grouped into following categories by McEvily [61].

- Plasticity-induced closure, this is mainly caused by residual stretch in the wake of an advancing fatigue crack-tip. It is essentially a plane stress effect, and was the first type of closure reported in the literature.

- Crack filling closure, this type of closure occurs as a result of corrosion products, oxides, fretting debris, liquids and so on. These are essentially external agents that reduce the stress intensity factor range and is discussed in detail in Appendix B.1.

- Roughness-induced closure, results from the waviness of fracture surface asperities on unloading. It occurs as a result of combined effect of Mode-I and Mode-II propagation. This type of closure occurs in plane stress as well as plane strain. Further details are provided in Appendix B.2.

- Transformation-induced closure, in some metastable alloys the stresses at the crack-tip can cause a phase transformation. In stainless steels, *e.g.*, if the transformation from austenite to martensite phase, which occurs locally in the region around the crack-tip, involves a positive volume change, the constraint of untransformed material in the immediate neighbourhood will place such regions in compression. If there is an increase in volume on transformation, closure can develop as the crack advances the transformed zone. This may result in retardation in the rate of crack growth. This type of closure is limited to specific alloys and is not a general phenomenon of closure.

- Grain boundary closure, the above mentioned forms of crack closure are crack-wake related. However, a situation may arise where the crack advance may be impeded as the crack encounters a stiffer grain. As the crack nears the grain boundary the opening level of stress intensity range is reduced and the growth rate is retarded as a consequence.

Some other forms of closure may also occur, which include, crack deflection, crack bridging or trapping, and crack-shielding via microcracking and through dislocations. Some of the mechanisms discussed above are provided in a schematic form in Figure 3.3.

Further, the crack closure occurrence through crack bridging, as reported in some investigations such as, by Ritchie, Weikang and Bucci [62] on Arall laminates, has revealed that the fatigue growth resistence of the laminate is associated with extensive

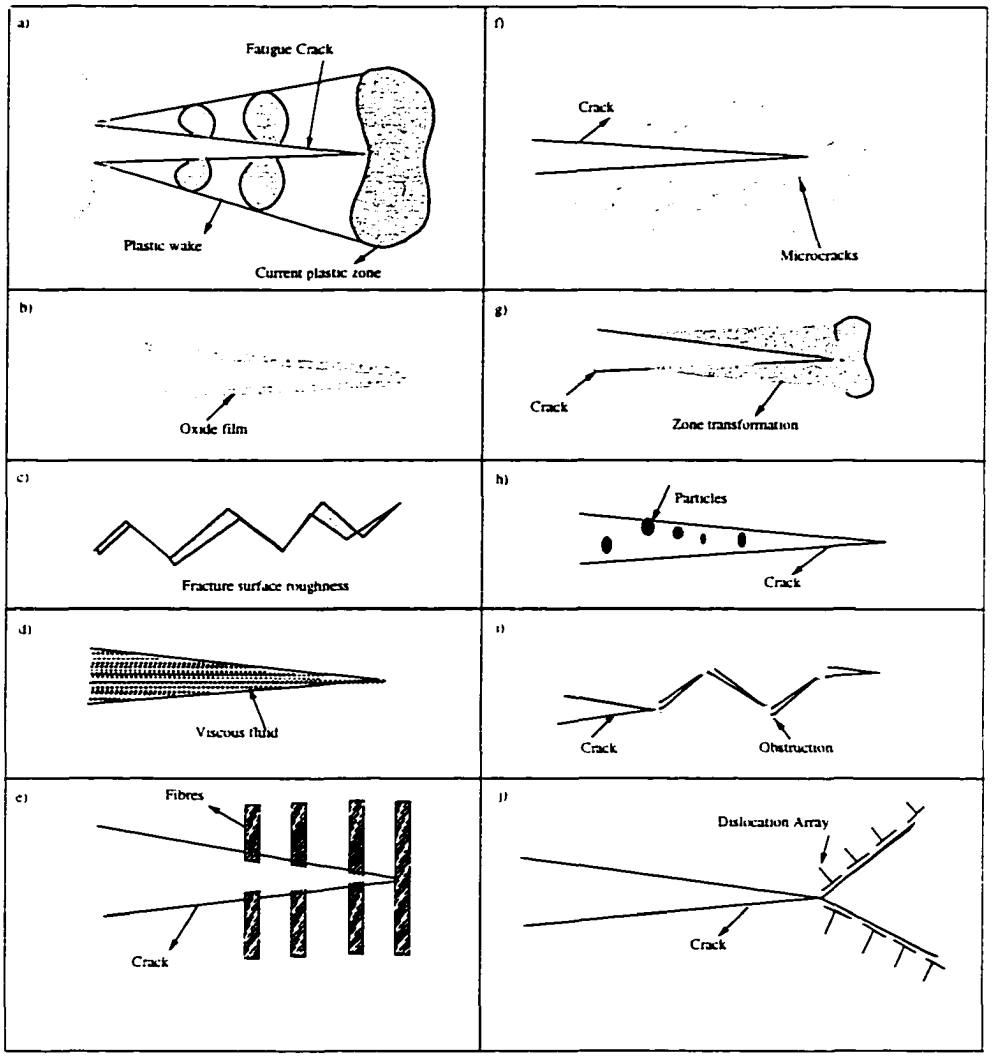

Figure 3.3: Fatigue crack closure mechanisms [1.60.61.62.63].

crack bridging from the unbroken aramid fibres in the wake of the crack with small contributions from crack closure due to waviness of the surface asperities.

3.4 Crack-tip Shielding

The crack-tip shielding phenomenon as reported by Ritchie [63], reduces the effective crack driving force at the crack-tip locally. This phenomenon has been observed in metals, composites, and ceramics. The crack-tip shielding provides a means of enhancing the resistance to crack growth. The resistance to crack growth may be achieved by the following processes:

- Intrinsic toughening, is achieved by increasing the inherent microstructural resistance by *e.g.*, coarsening particle spacings, changing the bond strengths.
- Extrinsic toughening, extension of crack is impeded by mechanical, microstructural and environmental factors, which locally reduce crack driving force.

There are several mechanisms of the crack-tip shielding. These mechanisms are broadly divided into the following categories.

- Crack deflection and meandering, in this mechanism of crack-tip shielding the Mode-I crack driving force is locally reduced by deviations of the crack path from the surface of maximum tensile stress.
- Contact shielding, this involves a direct physical contact between mating crack surfaces. This may occur by surface asperities or fibres in a composite or by means of an external medium such as corrosion debris or a fluid.

ASPECTS OF MECHANISM	MICROCRACKS	MACROCRACKS
a/o_g	Small	Large
Restraint on Slip	Low	Large
Active Slip Systems	1	2 or more
Slip Band Cracking	Possible	Difficult
Cause of Crack Growth	Decohesion	Different Mechanisms Apply
Striations	No	Yes
Plasticity in Wake	Limited	Pronounced
Fracture Surface Topography	—	Not Flat on Micro-Level

Table 3.1: Some basic differences between microcracks and macrocracks [64].

3.5 Mechanisitic Aspects of Crack Closure

For fatigue crack growth predictions usually the following two parts of the fatigue life are considered, 1) crack initiation life, 2) crack growth life. Any detailed discussion concerning different closure mechanisms necessitates a differentiation between two different types of fatigue cracks, namely *microcracks* and *macrocracks*. The crack initiation life covers the initiation and growth period of relatively small cracks, usually termed *microcracks* [64]. The basic differences between growth characteristics of microcracks and macrocracks are summarized in Table 3.1 as proposed by Schijve [64]. Some further differences have been pointed out for short crack problems in Table 3.2 (o_g in these Tables represents grain diameter).

It is difficult to consider a single numerical value for the transition crack length between microcracks and macrocracks, mainly because of the diversity and nature of the differences [60]. However, very recently, Newman [65] has provided the range for small cracks as 10 μm to 1 mm. These values may provide only an idea regarding the length of small cracks.

3.5.1 Microcrack Closure

The macrocracks are dependent on the bulk properties of the material while microcracks are highly affected by local conditions. For instance, the elastic anisotropy becomes more pronounced on the local scale and causes a non-homogeneous microstress concentration pattern, especially in materials with high elastic anisotropy [60]. Moreover, the material itself can no longer be considered as a homogeneous continuum. The salient features of the effect of grain boundaries on microcrack growth have been revealed by several microscopic studies [60]. Grain boundaries can act as crack arresters and hence impede the initial fast growth of a microcrack. Nisitani and Takao (as cited in [60]) studied the behavior of microcracks in C-steel with an optical microscope. They observed that at a maximum load an arrested crack was still closed at the tip while a growing one was fully open. Using a scanning electron microscope (SEM), Lankford *et al.* (as cited in [60]), observed closure of microcracks in 7075-T6 aluminum alloy. Morris [66] made the same observation in 2219-T851.

On the basis of above discussion, it is evident that the occurrence of *microcrack closure* might well be expected due to the microplastic deformations and mismatch between crack flank surfaces. However, it has been shown by Newman [65] that the same K_{open} will not hold for both microcracks and macrocracks because of the basic

TYPE OF CRACK	TYPICAL OBSERVATION	CAUSE
Chemically short	Environment dependent	
Mechanically short	a comparable with r_f	Initially high ΔK_{eff}
Microstructurally short	a comparable with grain ϕ_g	Microstructural Inhomogeneities

Table 3.2: Some basic differences between short cracks.

differences listed in Table 3.1. Newman [65] used a plasticity model in conjunction with some microstructural features, such as inclusion particle sizes to predict total fatigue life of the component.

The charcterization of fatigue crack growth rate on the basis of single parameter ΔK as an appropriate field parameter becomes doubtful when the crack length is very small. Modification of K_{open} to account for short crack effect will result in ΔK_{eff} as the field parameter. The small cracks at the root of a notch, are known to have initially high growth rates. This is attributed to the development of the plastic zone with respect to the advancing crack length (or the number of cycles) as is shown in Figure 3.4 and hence the closure occurs at relatively low values which implies higher ΔK_{eff}. These small cracks were labelled as *mechanically short* cracks by Schijve [64], whereas the microcracks discussed before were termed as *microstructural short* cracks by Ritchie and Suresh [1].

Some further details pertaining to the closure mechanisms, are presented in the following Sections of this Chapter. This discussion will be limited to *propagating macrocracks*.

3.5.2 Plasticity Induced Closure

According to Elber's model, a strip of yielded material is left in the wake of an advancing fatigue crack as a result of local plastic stretch at the crack-tip (see Figure 3.5). It should be noted that the plastic stretch becomes more extended in the y direction as the crack grows, since K_{max} generally increases with crack growth under constant amplitude loading condition. During the unloading portion of the cycle, the stretched material cannot be accommodated by the surrounding elastic material and a state of residual compressive stress builds up over the plastic wake which keeps the

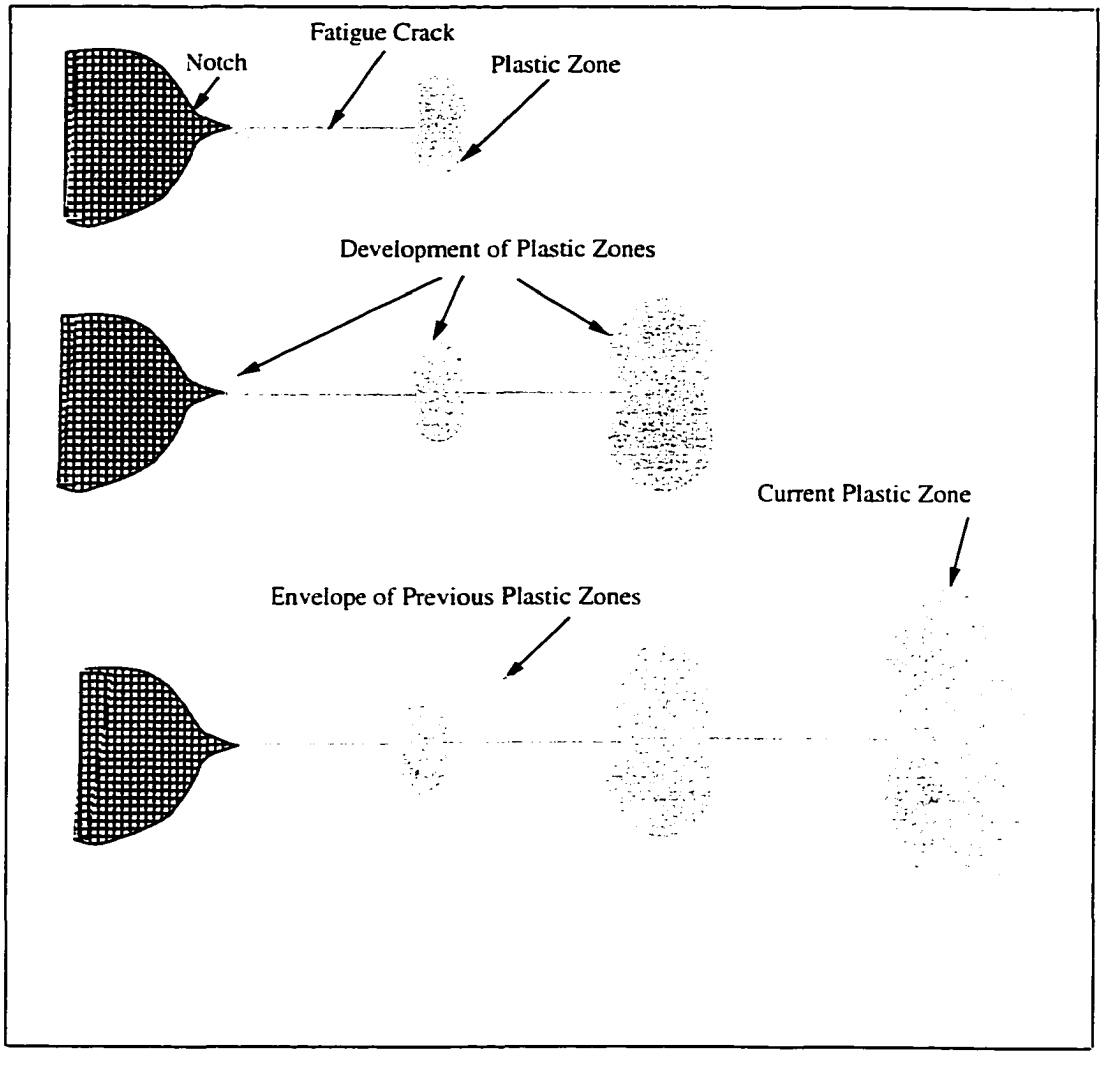

Figure 3.4: Development of plastic zone.

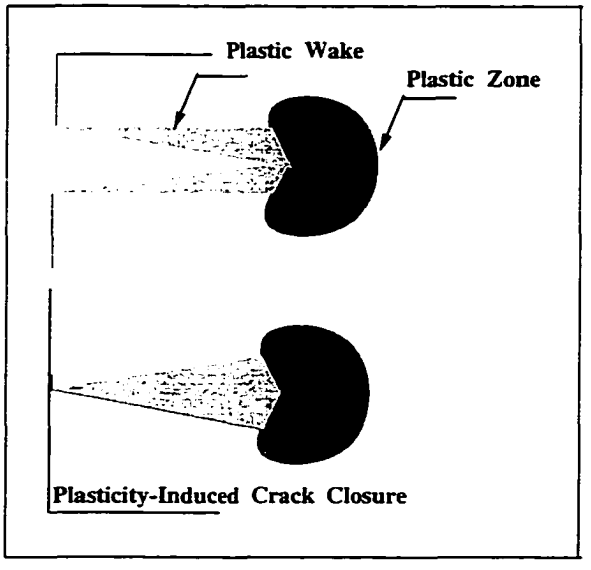

Figure 3.5: Plasticity induced crack closure.

crack faces closed together.

The plasticity induced fatigue crack closure, as shown in Figure 3.5, involves a two-dimensional mechanism for a through crack. However, the situation due to thickness of the specimen becomes more complicated. The two main component thickness related (or three-dimensional) aspects that need to be considered are:

- Plane Strain/Plane Stress transition along the crack front, and
- Shear Lips at the surface of the material.

Plane Strain/Plane Stress

If a through crack in a thick plate is considered, providing that the fatigue load is not too high, it is usually assumed that the crack front is predominantly in a state of plane strain ($\epsilon_z = 0$). On the other hand, plane stress conditions dominate near the

surface of the plate ($\sigma_z = 0$). The plastic zone size approximation, r_p, in each case is given by:

$$r_p = \frac{1}{2\alpha\pi}\left(\frac{K}{\sigma_{ys}}\right)^2. \tag{3.1}$$

where $\alpha = 3$ for plane strain and $\alpha = 1$ for plane stress, α is known as plastic constraint factor. Figure 2.4 is a schematic representation of the three-dimensional plastic zone at the crack front [5]. In Chapter 2 it was shown that α is dependent on Poisson's ratio ν. Based on plasticity model presented in Chapter 2, $\alpha = (1-2\nu)^{-2}$.

Since the plasticity-induced crack closure is inherently dependent on the plastically deformed appendages on the crack flanks, it can be anticipated that the larger plastic zone size near the outer surfaces of the plate should lead to large crack closure in those regions. Experimental results by Telesman and Fisher [67] show the effect of successive surface removal on the crack closure stress intensity factor for a 7075-T6 Aluminum alloy. While there was a significant decrease in K_{cl} with surface removal at higher stress intensity ranges (ΔK = 8.8 and 17.6$MPa\sqrt{m}$), no thickness effect was observed at a ΔK of 2.5$MPa\sqrt{m}$. It was thereby concluded that at higher ΔKs the dominant closure mechanism was plasticity-induced closure created by localized plane stress effects near the specimen surface, even though the specimen passed the ASTM E399 thickness criteria for a specimen in a predominantly plane strain condition. Instead, roughness-induced closure, which is more a function of the microstructure, was indicated as a dominant closure mechanism at the near-threshold ΔK of 2.5$MPa\sqrt{m}$.

The occurrence of more crack closure near the surface is anticipated to produce a reduction in the actual crack growth rate in this region. As a result, the ends of the crack front at the surface will trail behind the major part of the advancing crack front. Slightly curved crack fronts are quite often observed in practice.

Shear Lips

Fatigue tests on metallic materials have revealed the formation of shear lips on fracture surfaces. These shear lips are formed when crack growth occurs as a result of mixed Mode-I/Mode-III. This is essentially a PSS phenomenon and occurs in the vicinity of specimen surfaces (see Figure 3.6).

However, the situation becomes complicated by the environmental effects [1]. As regards crack closure, it can be expected that shear lips should be the first part where the crack surfaces will come into contact during unloading. Lindley and Richards [68] have observed that for mild steel the closure contacts start at shear lips. Apparently, the permanent plastic deformation is larger for the shear lips than for the tensile mode area of the fatigue fracture. A proof was provided by McEvily and Yang [69]. They found a significant crack growth delay after an overload during the testing of an aluminum alloy. A much smaller delay was found if the thickness was reduced immediately after the overload.

3.6 Crack Closure Analysis

This Section presents a brief survey of the analytical and numerical approaches to the different closure mechanisms. In general, the analytical procedures provide a better physical insight to the closure phenomenon but they are restricted to simple geometries and loading conditions. Numerical approaches are essentially applicable to complex loadings and geometries but often require large computational facilities.

[1] Vogelesang and Schijve (as cited in [64]) pointed out that in an aggressive environment, for aluminum alloys the shear lip width is smaller, which macroscopically delays the transition from the tensile mode to the shear mode to a larger crack length (or a higher ΔK value).

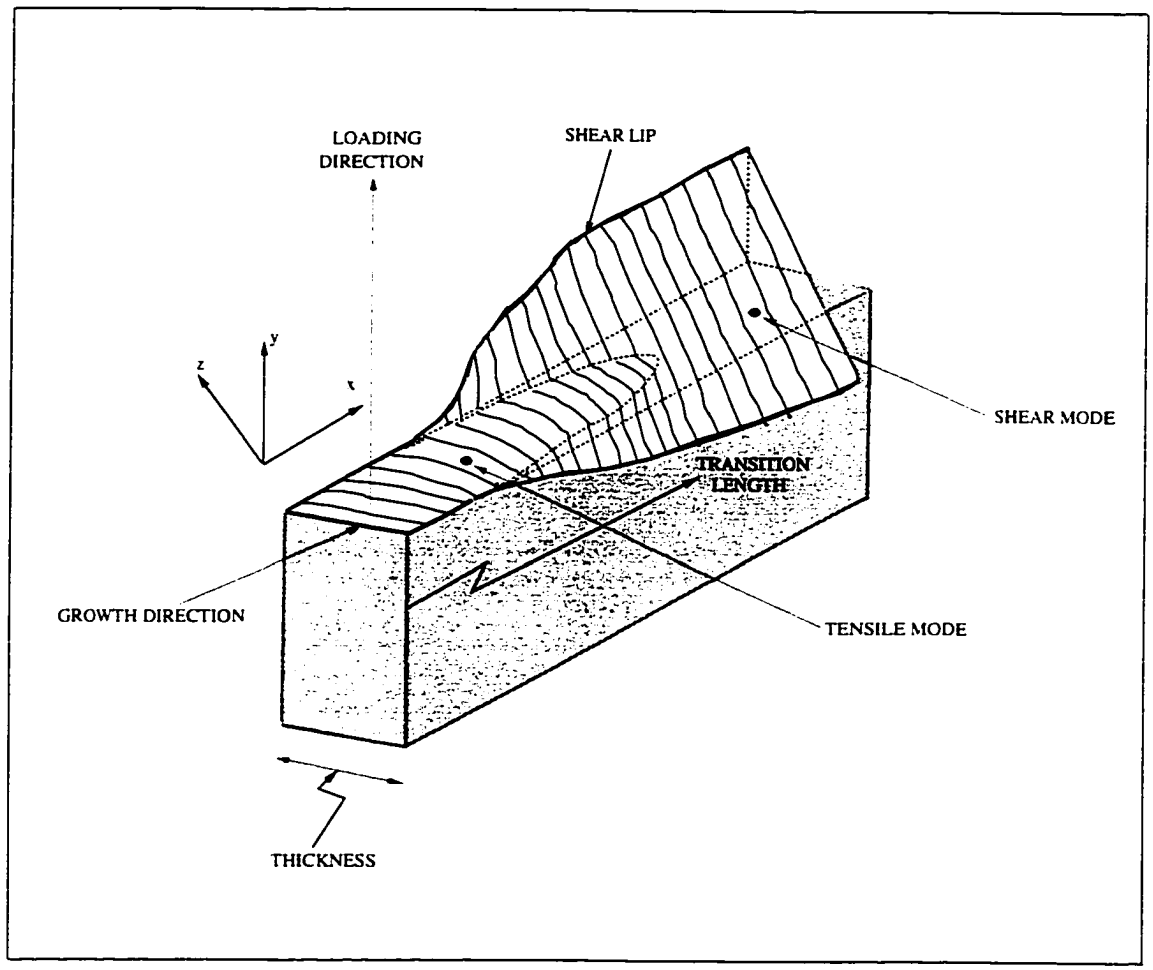

Figure 3.6: Shear lip formation in fatigue [64].

3.6.1 Plasticity-Induced Closure Models

Both analytical and numerical approaches have been implemented to investigate the occurrence of crack closure due to the formation of plastically stretched material in the crack wake. The analytical procedures are discussed first.

3.6.2 Analytical Approaches

Several analytical models pertaining to fatigue crack closure have appeared in the literature. Dill and Saff [70] presented a simple contact stress closure model. They modelled the crack surface interference as a wedge acting behind the crack-tip and calculated the contact stresses by idealizing the wedge by 25 contact stress elements. The results of the model were in good agreement with Elber's experimental expression, *i.e.*, $U = \frac{\Delta K_{eff}}{\Delta K} = 0.5 + 0.4R$. It is to be noted that Elber's expression does not agree with some experimental results reported by other investigators.

Budiansky and Hutchinson [54] proposed an analytical model for plasticity-induced closure for a central crack. Using the ideally-plastic Dugdale's model and Muskhelishvilli complex potentials, they derived plastic wake residual stretches and crack opening loads as functions of the applied load range. Their model predicts that the residual stretch would be 0.86 of the maximum CTOD. A constant value of $K_{open}/K_{max} = 0.557$ is predicted by the model. In general, it can be concluded that the model, at best, corresponds well with the available experimental data for plane stress situations alone.

Führing and Seeger [71] introduced contribution of fatigue closure in their model of fatigue growth. They calculated the contact stresses based on Dugdale's method. The results indicated that for a constant amplitude loading condition $\frac{K_{open}}{K_{max}}$ is almost independent of K_{max} and the ratio $U = \frac{\Delta K_{eff}}{\Delta K}$ increases with stress ratio R. Their

investigation was based on the behavior of an infinite sheet with collinear cracks made of an elastic-perfectly plastic material under PSS condition. These results could not be compared with an experimental work [60].

Newman [72] proposed a discrete-element model for plasticity-induced crack closure using experimentally derived information. The model was developed for a central crack in a finite-width plate subjected to a uniform applied stress. The plastic region ahead of the crack-tip and the residual plastic stretch along the crack wake were modelled as constant stress bar elements. At any applied stress level, the bar elements were considered to be either intact or broken. A constraint factor (α) was used to simulate PSS or PSN condition. The model was used to calculate crack opening stresses as a function of crack length and load history. The results were used to calculate the effective stress intensity range ΔK_{eff} and consequently the crack growth rates. In practice, a constraint factor of $\alpha = 2.3$ was found to give a good correlation under constant amplitude loading. The model was examined by Davidson [64]. He adjusted the model to simulate his own experimental results from single edge notched specimens. The results predicted by the model did not coincide with his observations [60].

A rigid insert crack closure (RICC) model was proposed by Provan and Majid [60] to account for the closure phenomenon. The overall nonlinear elastic behavior of a fatigue crack during the closing portion of the load cycle is modelled by a transitional elastic deformation caused by the superposition of a hypothetical rigid insert in an ideal crack wake. In the application of this model to the C(T) specimen, the load-crack mouth opening displacement (CMOD) is analysed which includes the derivation of simple expression for calculation of compliance or stiffness of the specimen based on CMOD data. The expression for opening load is also presented based on two experimental parameters.

3.6.3 Numerical Approaches

Numerous investigators [60, 73, 74] have studied the two-dimensional elasto-plastic finite-element analyses of crack closure and crack growth under plane-stress conditions. Further, several reports [73, 74] concerning similar analyses under plane-strain condition have appeared in the literature.

The analyses presented in [75] were carried out using constant-strain triangle-type elements, with the finest element often being 10^{-3} times the crack length. Nagagaki and Alturi (as cited in [60]) implemented a cost-effective procedure to perform a similar analysis using a rather coarse mesh. In this work, the Hutchinson-Rice-Rosengren type strain and stress singularities for strain hardening materials are embedded in special elements near the crack-tip. The analysis was carried out for a central crack tension (CCT) specimen and the opening and closure stress levels were found to be in good agreement.

Fleck [76] performed an elastic-perfectly plastic finite element analysis (FEM) of plasticity induced closure under plane strain conditions. The results lend support to the plasticity-induced crack closure in plane strain.

A three-dimensional finite-element analysis of crack growth and closure was reported by Chermahini *et al.* [77]. They simulated the crack growth by one-element-length extension per cycle as the applied stress reached the maximum level. The results showed that during unloading the crack front closes first on the free surfaces of the specimen, which implies a predominantly PSS condition. They also found that under constant amplitude loading with a maximum stress level, σ_{max}, of 0.25 times the yield strength of the material, the crack opening stress level reached a peak value of 0.34 σ_{max} at the interior and 0.6 σ_{max} at the free surfaces of the specimen which indicates that the opening level of stress is less under PSN situation when compared

with a conjugate PSS condition. The application of a single-spike overload caused the opening stress level to drop momentarily, but it rose to values higher than those calculated under constant amplitude loading after the crack advanced further. The calculated crack opening stresses for the exterior and the interior of the specimen were found to be in quantitative agreement with the already reported finite element calculations under plane stress and plane strain conditions, respectively.

In a series of papers, McClung and Sehitoglu [73, 74], presented a critical review of the previously reported finite-element based analyses and presented a different approach to tackle such problems. They also presented an elastic-plastic finite element model for crack opening and closing behavior with special emphasis to see the effects of yield stress, strain hardening, and maximum stress on crack closure. Recently, a finite-difference based analysis of plasticity-induced crack closure was reported by Llorca and Sánchez Gálvez [78]. The finite-difference method was found as being easily applicable to the modelling of fatigue crack growth as well as crack face contacts without requiring sophisticated algorithms. They considered the influence of mechanical properties of the material and testing conditions. The results were found to be in excellent agreement with those obtained from other numerical techniques.

On the basis of this study, four types of closure are observed in general: a) near-tip closure, b) far-tip closure, as reported by [79], c) crack-closure on surfaces or under PSS, and d) crack-closure in the inside of the specimen or under PSN. These general types of closure on the basis of location of occurrence are shown in Figure 3.7.

3.7 Experimental Difficulties

It is interesting to note the difficulties in the measurement of opening loads even after 30 years of research on fatigue crack closure. The determination of the opening

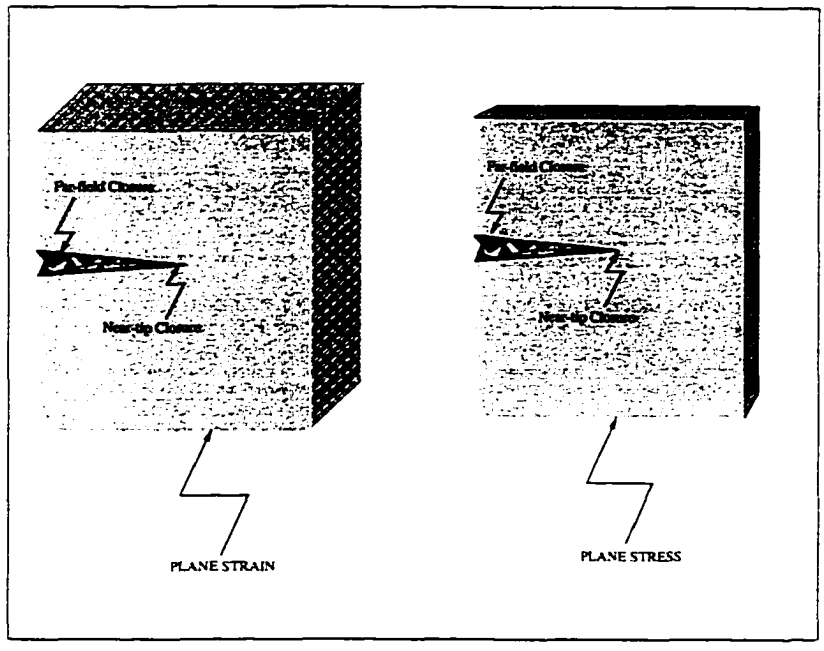

Figure 3.7: Types of closure.

load, from experimental measurements even under CAL present difficulties in terms of resolution and reproducibility [14]. These two factors not only influence the opening load measurements from compliance changes measured at various locations in a specimen but also contribute to the uncertainity, being an ongoing standardization effort within the ASTM Committee E08 [14]. In the first round robin of the ASTM [80] it was observed that there were significant differences among participating laboratories using the same analysis method and also systematic differences produced by different analysis methods. Thus, the test results showed a large dispersion. In the second round robin of ASTM [81], a standardized procedure for determining opening loads was proposed. Fourteen different laboratories participated in the testing of Aluminium alloy 2024-T351, 9 mm thick, C(T) specimens. Due to these difficulties in measurement of crack closure an interesting review paper on crack closure appeared in 1994, where the occurrence of crack closure based on plasticity is questioned [59].

It has been concluded in that investigation that based on the dislocation theory, the closure cannot occur. However, no mention is made of several plasticity models accounting for closure other than dislocation theory. For instance, the crack closure model of Budiansky and Hutchinson [54] which is based on Muskhlishavali complex potentials and gives results for opening loads under CAL, provides analytical support to crack closure. However, while the shape of the plasticity zone is ignored in [54], the importance of plasticity zone shape was emphasized in Chapter 2. Attention will now be directed to the incorporation of plasticity and closure in estimation of FCGR under CAL.

Chapter 4

CONSTANT AMPLITUDE LOADING

4.1 Introduction

The fracture mechanics based methodology to control fatigue crack propagation is mostly studied with an aim of coupling the experimental results with damage tolerant life prediction methods via the FCGR similitude principle of Paris and co-workers [9]. This principle states that equal FCGRs are produced for equal applied stress intensity ranges ΔK independent of load, crack size and specimen geometry. The crack length a versus the load cycles N is required by the designers for life predictions based on the damage tolerance philosophy.

Fatigue crack growth under CAL is an interesting research topic. Several review articles pertaining to CAL appeared in the literature recently, *e.g.*, [14, 82]. Wu *et al.*, [83] used Budiansky-Hutchinson model [54] for crack closure in conjunction with a damage law and presented a new equation for FCGR under CAL which predicted

growth rates in reasonable agreement with experimental data, but underestimated the effect of stress ratio R. Hertzberg [84] has demonstrated that incorporation of Burger's vector in fatigue crack growth calculations gives good correlation with experimental data for some metal alloys.

A component subjected to cyclic loading passes through the crack initiation and crack propagation stages during its total life. The philosophy of defect-tolerant design assumes that the engineering structures are inherently flawed: then the number of cycles required to extend a dominant flaw of an assumed initial size to a certain final length (a critical dimension, which may depend upon the fracture toughness), gives the useful life for the component. Catastrophic failure in metallic materials is generally preceded by a significantly large stage of stable crack propagation under cyclic loading conditions.

As was discussed in Chapter 3, for metallic materials fatigue cracks remain closed during a portion of the load cycle under both CAL and VAL. This effect is accounted for by modifying the Paris law [9] for FCGR in terms of closure load under CAL. The objective of this Chapter is to describe a computational method for the determination of errors which occur if the fatigue crack growth is computed on the basis of an assumed crack extension. The assumed crack extension calculations have been compared with a cycle-by-cycle approach. It is shown that for assumed crack extension to give meaningful results there is an optimal value of extension below and above which FCGR calculations are questionable. Comparisons are also presented of numerical predictions with experimental studies of other researchers. The purpose of the study was also to compare models of crack closure under PSS and PSN.

4.2 Fatigue Crack Growth under CAL

The concept of similitude permits an integration of laboratory $da/dN - \Delta K$ data into a prediction of the life of fatigue components in terms of a versus N. In addition these calculations require the loading condition, initial flaw size, and the component or specimen stress intensity factor. This Chapter compares numerically computed FCGR calculations with experimental work from different sources. Two different approaches to FCGR calculations are presented. The first approach is based on assuming crack extension Δa while the second is based on a cycle-by-cycle approach. It is shown that for the assumed Δa type of approach to give meaningful results there is an optimal value of Δa, above and below which errors could be significant.

4.3 The Assumptions for CAL

Several assumptions are inherently built into most of the models based on macroscopic considerations. The following are the assumptions for the current work.

a) Paris law adequately describes the crack growth under CAL. This assumption is justified since the focus of this work was in evaluating FCGR in the engineering regime, i.e., region-II of the $\frac{da}{dN}$ versus ΔK plot Figure 4.1.

b) The effect of environment, *e.g.*, formation of oxide layer or the roughness induced crack closure is not accounted for in this analysis.

c) The hardening of the material is not accounted for.

d) The effect of crack-tip bluntening is assumed negligible.

e) The microscopic phenomena occurring in the immediate vicinity of the crack-tip, and other related metallurgical effects such as the effect of grain size on FCGR is not explicitly accounted for in this investigation.

f) The initial size of the flaw is large enough, so that it is a *macroscopic crack* problem. Several considerations pertaining to this issue were presented in Section 3.5.

4.4 The Fatigue Crack Growth Characterization

The rate at which fatigue cracks grow under CAL is expressed in terms of the crack length increments per cycle, $\frac{da}{dN}$, the values of which for various loading conditions are determined on the basis of experimentally determined changes in crack length over a certain number of loading cycles. When the applied stress range is held constant, the rate of growth of fatigue cracks generally increases with the increasing number of loading cycles [1].

The main aim of fatigue based design approaches is to develop reliable methods for modelling crack growth rates in terms of loading parameters which can subsequently be used to determine the intrinsic resistance of the material to FCGR under various conditions of applied stress, specimen geometry and crack configuration. In the early 60's attempts were made to quantify the growth in terms of the applied stress range $\Delta\sigma$ and crack length a. One of such approaches was adopted by Liu [48], *i.e.*:

$$\frac{da}{dN} \propto \Delta\sigma^{c_1} a^{c_2}, \tag{4.1}$$

where c_1 and c_2 are the empirical constants.

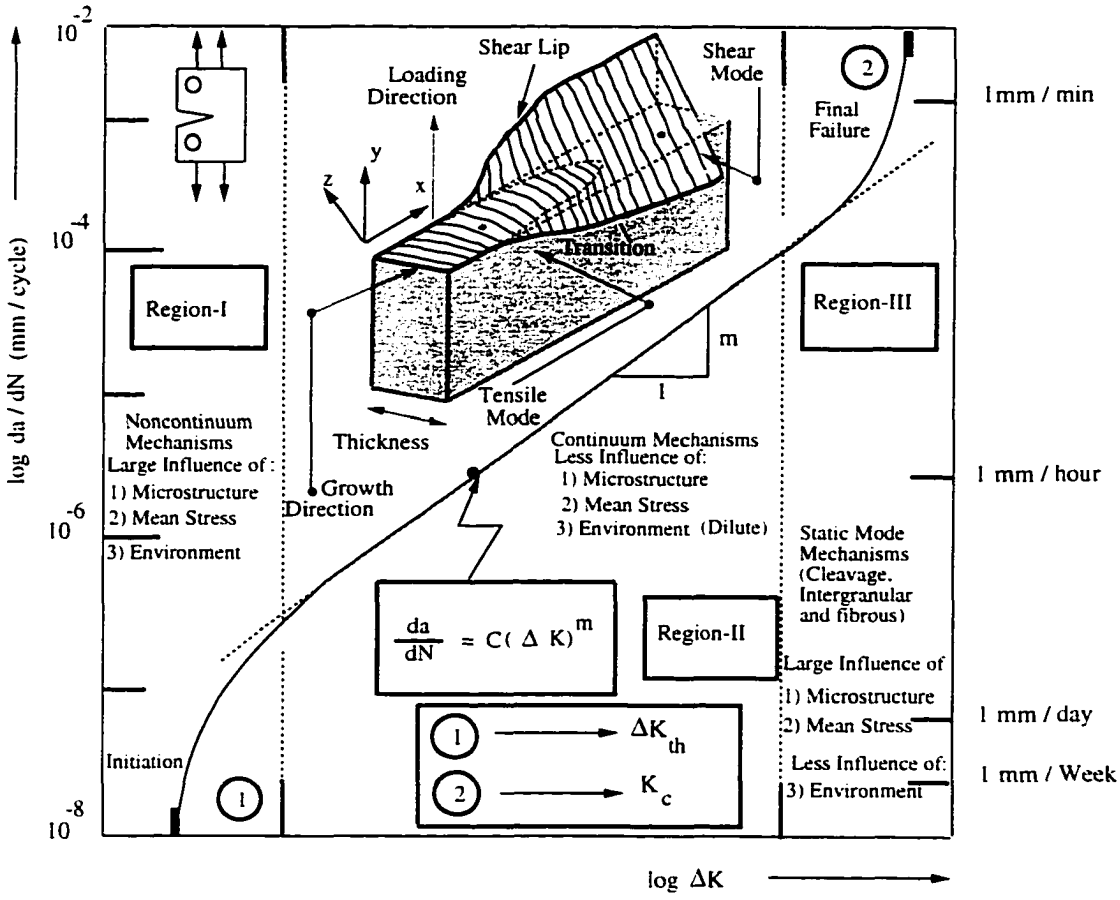

Figure 4.1: Regimes of fatigue crack growth.

Paris, Gomez and Anderson [9] proposed that for the LEFM based fracture mechanics approach of FCGR it should be based on the stress intensity factor range ΔK :

$$\Delta K = K_{max}^{CAL} - K_{min}^{CAL}. \tag{4.2}$$

where K_{max}^{CAL} and K_{min}^{CAL} are the maximum and minimum values of stress the intensity factor for a given fatigue cycle. For a cracked fatigue test specimen:

$$K_{max}^{CAL} = Y \sigma_{max}^{CAL} \sqrt{\pi a}. \tag{4.3}$$

$$K_{min}^{CAL} = Y \sigma_{min}^{CAL} \sqrt{\pi a}. \tag{4.4}$$

$$\Delta K = Y \Delta \sigma \sqrt{\pi a}. \tag{4.5}$$

$$\Delta \sigma = \sigma_{max}^{CAL} - \sigma_{min}^{CAL}. \tag{4.6}$$

where Y is the geometry factor which depends upon the ratio of crack length a to the width W of the specimen and σ_{max}^{CAL} and σ_{min}^{CAL} are the maximum and minimum values of the stress in a fatigue cycle. Paris, Gomez and Anderson [9] studied the FCGR, $\frac{da}{dN}$ and found that it is related to the stress intensity range as:

$$\frac{da}{dN} = C(\Delta K)^m. \tag{4.7}$$

The constants C and m are influenced by such variables as material microstructure, environment, test temperature, and stress ratio, R, defined as $R = \sigma_{min}^{CAL} / \sigma_{max}^{CAL}$. The value of exponent m is between two and four for ductile alloys. Although the equation is empirical, it has emerged as one of the most important fundamental relationships in characterization of fatigue crack growth for a vast spectrum of materials and fatigue test conditions. The experimental data pertaining to a wide range of metallic

materials has confirmed relationship despite some controversy in early 1960s [1]. In particular the crack growth experiments on aluminum alloys for different stress ranges and with various crack lengths and crack configurations [49] unambiguously established the validity of such a characterization.

4.5 Fatigue Crack Growth Calculations

It was discussed in Chapter 3 that experimental and theoretical research in fatigue has revealed that fatigue cracks remain closed for a substantial portion of their loading cycles. As a consequence, the Paris law cannot be used directly for FCGR calculations. The crack driving force reduction that occurs as a consequence of closure is incorporated through the use of effective stress intensity range *e.g.*, ΔK_{eff} under CAL. The fatigue crack growth in Paris regime under CAL is given by:

$$\left(\frac{da}{dN}\right)^{CAL} = C\,(\Delta K_{eff})^m \tag{4.8}$$

where $\Delta K_{eff} = K_{max}^{CAL} - K_{open}^{CAL}$, and ΔK_{eff} is the effective stress intensity factor range under CAL conditions, K_{max}^{CAL} is the maximum value of stress intensity factor under CAL and K_{open}^{CAL} is the opening value of the stress intensity factor under CAL. C and m are the material constants.

4.6 Plasticity in Wake and Opening Loads under CAL

This section incorporates the effect of plasticity in the wake of an advancing fatigue crack from several existing models. A detailed discussion regarding some of these

models was provided in Section 3.6.2. These models are based on theoretical grounds and there are difficulties to confirm the experimentally determined values of crack opening loads. Therefore no new attempt is made to obtain information regarding the opening loads under CAL.

The effect of plasticity in the wake of an advancing fatigue crack results in a decrease in the crack driving force in terms of the stress intensity factor. This decrease in crack driving force is incorporated through Elber's crack closure concept [58]. The use of crack closure results in effective stress intensity factor range ΔK_{eff} which is used in this research. For evaluation of ΔK_{eff}, closure loads (or closure stress intensity factors) are required. The FCGR can be evaluated on the basis of an estimate of the opening value of the stress intensity factor, K_{open}^{CAL}, since the value of K_{max}^{CAL} is fixed by the given loading history.

There are several models from which the opening loads may be deduced under PSS or PSN. In this research the opening loads were obtained from Newman [57] for CAL. This allows the opening load evaluation under both PSS and PSN with a choice for variable plastic constraint factor. It was observed in this study that opening loads obtained from Llorca and Gálvez's [78] model (L & G Model), for PSN loading conditions, Figure 4.2, also give results very close to [57] under PSN. Further, for the PSS situation, the opening load maps were obtained from the analytical work of Budiansky and Hutchinson [54] (B & H Model). For the PSS loading condition, Figure 4.3 provides equally good results to that of [57] under PSS. In order to account for the crack closure phenomenon, the effective stress intensity range approach ΔK_{eff} is used in this investigation. In this way the value of K_{open}^{CAL} for CAL are determined from previously existing models.

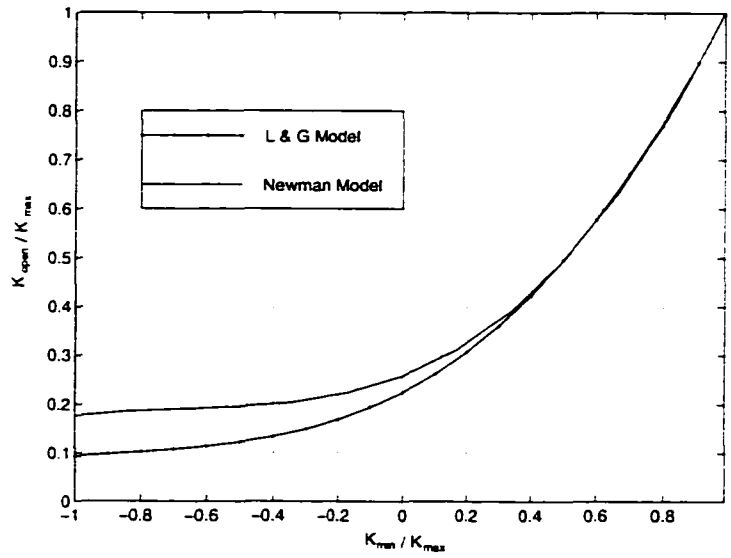

Figure 4.2: Crack opening load map for PSN.

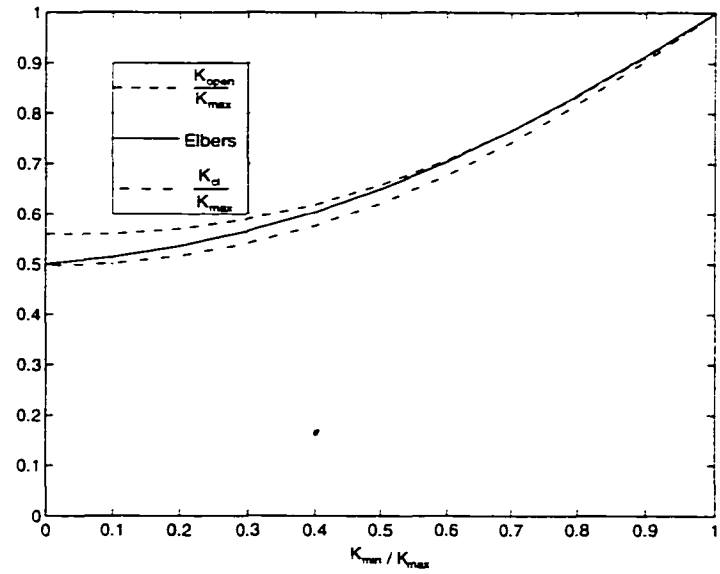

Figure 4.3: Crack opening load map for PSS.

4.7 Opening Loads under PSS and PSN

The value of the plasticity constraint factor α plays a very important role for evaluation of opening loads under PSS or PSN situations. It was shown in Chapter 2 that α is a strong function of poisson's ratio. The opening loads under PSS and PSN situation are obtained from Newman [57] with $\alpha = 1$ for a fully PSS situation and $\alpha = 3$ for a fully PSN situation. The opening load equations as given by [57] are as follows:

$$\frac{\sigma_{open}^{CAL}}{\sigma_{max}^{CAL}} = A_{00} + A_{01}R + A_{02}R^2 + A_{03}R^3 \qquad R \geq 0. \tag{4.9}$$

$$\frac{\sigma_{open}^{CAL}}{\sigma_{max}^{CAL}} = A_{00} + A_{01}R \qquad -1 \leq R < 0. \tag{4.10}$$

The coefficients in eqns(4.9 and 4.10) are:

$$A_{00} = \left(0.825 - 0.34\alpha + 0.05\alpha^2\right)\left(cos\left(\frac{\pi\sigma_{max}^{CAL}Y_{cc}}{2\sigma_o}\right)\right)^{\frac{1}{\alpha}}. \tag{4.11}$$

$$A_{01} = (0.415 - 0.071\alpha)\frac{\sigma_{max}^{CAL}}{\sigma_o}. \tag{4.12}$$

$$A_{02} = 1.0 - A_{00} - A_{01} - A_{03}. \tag{4.13}$$

$$A_{03} = 2.0A_{00} + A_{01} - 1. \tag{4.14}$$

In the above equations σ_{open}^{CAL} is the opening stress value, and σ_{max}^{CAL} is the maximum value of the stress in a given loading cycle. The flow stress σ_o is taken to be the average between the uniaxial yield stress and uniaxial ultimate strength of the material. The coefficient α is varied to simulate PSS or PSN conditions.

A comparison of FCGR results for a fully PSS situation was made using opening loads obtained from the B & H model [54] with Newman's [57] results using $\alpha = 1$ in opening load equation. For an edge crack or a C(T) specimen, the stress σ_{max}^{CAL} is replaced by $\frac{P_{max}^{CAL}}{Wt}\frac{Y_{et}}{Y_{cc}}$, where Y_{et} is the geometry correction for an edge crack type of specimen or a C(T) specimen, Y_{cc} is geometry correction factor for a central crack type of specimen and P_{max}^{CAL} represents the maximum load for a CAL cycle. W is the width and t is the thickness of the specimen. The opening and closure loads are shown in Figure 4.3 based on PSS. It is interesting to note that Budiansky and Hutchinson's model for crack closure cannot be used directly for fatigue crack growth problems. Equations were fitted to their results in terms of K_{max}^{CAL} and K_{min}^{CAL}. The equation obtained under CAL for the opening load is:

$$\frac{K_{open}^{CAL}}{K_{max}^{CAL}} = 0.4856\left(\frac{K_{min}^{CAL}}{K_{max}^{CAL}}\right)^2 - 0.046\left(\frac{K_{min}^{CAL}}{K_{max}^{CAL}}\right) + 0.5599. \tag{4.15}$$

Under CAL the closure load is:

$$\frac{K_{cl}^{CAL}}{K_{max}^{CAL}} = 0.505\left(\frac{K_{min}^{CAL}}{K_{max}^{CAL}}\right)^2 - 0.0017\left(\frac{K_{min}^{CAL}}{K_{max}^{CAL}}\right) + 0.4965. \tag{4.16}$$

Similar equations were obtained from Llorca and Gálvez model (L & G model) [78] for a fully PSN condition. The opening loads for PSN are shown in Figure 4.2. Budiansky and Hutchinson's model is probably the only analytical model of plasticity induced crack closure that distinguishes between crack opening and closure loads. Since the difference in the values of opening and closure loads is small, it was found in this investigation that the number of cycles to failure did not change significantly using either K_{open} or K_{cl} and hence, the closure values and opening values of K, have been assumed equal. Moreover, there is good agreement between Elber's experimental results [58] and the work in [54] so that assumption of no distinction between K_{open} and K_{cl} is justified as is shown in Figure 4.3.

4.8 FCG Calculations - Examples

There are two possible ways to compute FCGR under CAL. The approach-I of this investigation is based on assuming a value for the extension of the crack and then computing the stress intensity factor K and the final length of the crack as the fracture toughness is reached. The approach-II is based on a cycle-by-cycle approach.

4.8.1 Example - I

A design example from [5] is taken for comparison. The pertinent data of the problem are:

Material : A514 Steel

$\sigma_{ys} = 689\ MPa$

$K_c = 165\ MPa(m)^{0.5}$

$a_0 = 7.6\ mm$

Geometry : Edge Crack

$\sigma_{max}^{CAL} = 310\ MPa$

$\sigma_{min}^{CAL} = 172\ MPa$

$\Delta\sigma = 138\ MPa$

$a_f = 71.1\ mm$

In this example an initial flaw of $7.6\ mm$ is propagated to a final dimension of $71.1\ mm$ for the given stress range of $\Delta\sigma = 138.0\ MPa$. The two independent approaches have been used to obtain the number of cycles to failure/or the life of the component numerically. The component is deemed to have failed after the flaw size reaches a permissible dimension, which is itself obtained from fracture toughness or from some other considerations. Results on Rolfe and Barsom's data for steel are shown in Figure 4.4. The comparison of values for the number of cycles to failure

from two different approaches is provided with Rolfe and Barsom's [5] value in Table 4.1. Rolfe and Barsom assumed value of crack extension $\Delta a = 2.54$ mm. The effect

Type	N_f
Approach-I	84845
Approach-II	85077
Rolfe and Barsom	86700

Table 4.1: A comparison of N_f with Rolfe and Barsom [5].

of an increase in stress range $\Delta\sigma$ is well known [5]. As the value of $\Delta\sigma$ increases the fatigue cracks grow faster. A comparison between the two different approaches by increasing $\Delta\sigma$ twice and thrice the initial value is made. The effect of stress range $\Delta\sigma$ on the number of cycles to failure is provided for $\Delta\sigma = 276.0\ MPa$, and $\Delta\sigma = 414\ MPa$ in Table 4.2. The results have been presented in Figure 4.5 using a cycle-by-cycle approach. In these cases the initial length of the crack and final length of the crack are same as is for $\Delta\sigma = 138.0\ MPa$. Referring to Table 4.2, it is observed that the predicted life from the approach-I is within 4.5 % of the values obtained from approach-II if the errors are minimised. Doubling $\Delta\sigma$ reduces the life by 4.81 times and increasing the $\Delta\sigma$ thrice reduces life by 11.68 times the case in which the initial stress range of $\Delta\sigma = 138\ MPa$.

Type	N_f	$\Delta\sigma$
Approach-I	17775	276.0 MPa
Approach-II	17000	276.0 MPa
Approach-I	7159	414.0 MPa
Approach-II	7000	414.0 MPa

Table 4.2: A tabular comparison with Rolfe and Barsom [5].

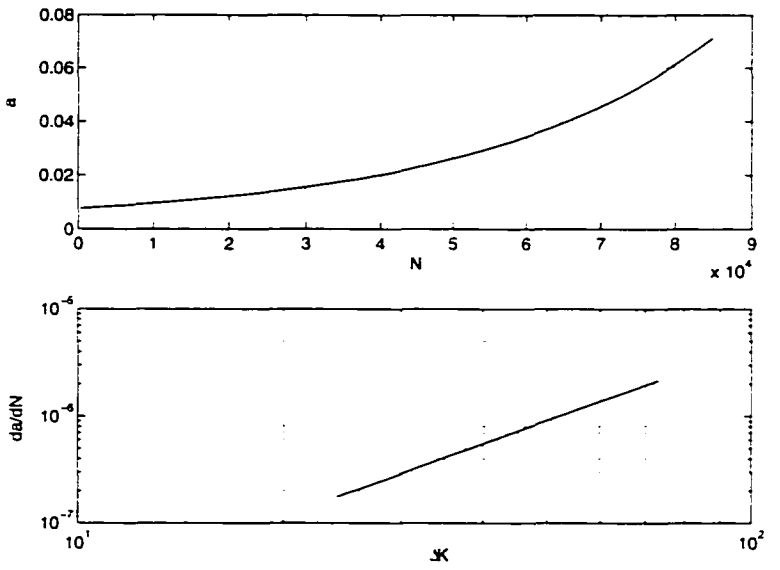

Figure 4.4: The CAL result on Rolfe and Barsom's data [5].

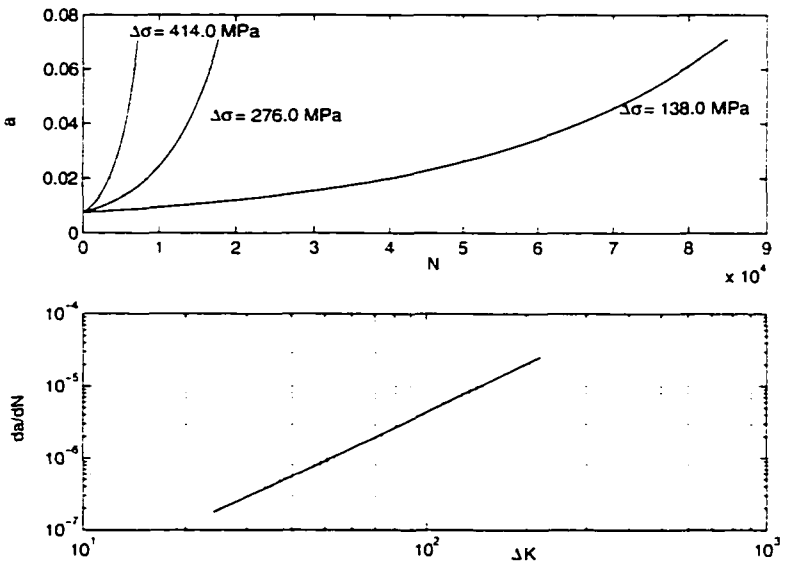

Figure 4.5: Crack length versus N and ΔK versus FCGR for various stress range.

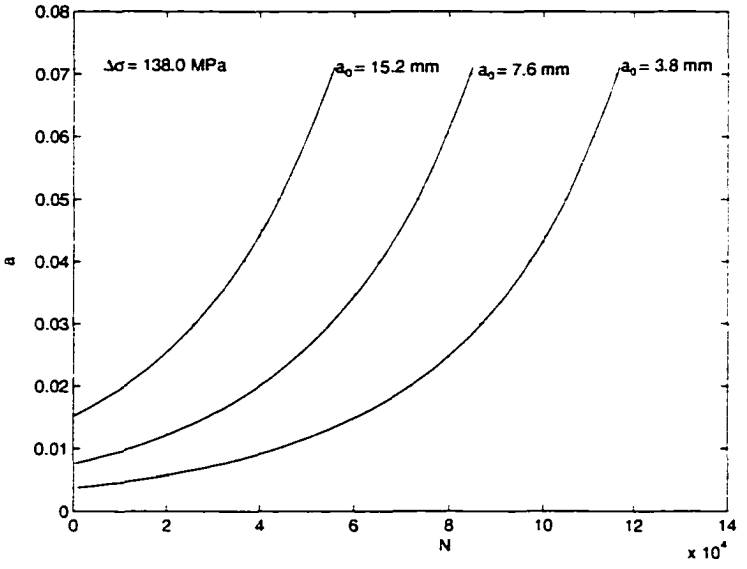

Figure 4.6: Crack length for various initial lengths of crack.

The effect of initial length of the crack on FCG is shown in Figure 4.6, for the same final length of the crack and the same stress range. It is observed that for a 50% reduction in initial flaw size *i.e.*, $a_0 = 3.8\ mm$, the life of the component is 38.43% more than the case when the initial flaw size is 7.6 mm. When the initial flaw size is doubled, *i.e.*, $a_0 = 15.2\ mm$ the life of the component is 66.9% of the case when the initial flaw size is 7.6 mm.

4.9 Further Examples

Some examples pertaining to CAL have been chosen for different specimen geometries and materials. Life prediction was performed using approach-II for all the subsequent problems, which is a cycle-by-cycle analysis. Effective stress intensity approach was incorporated in the calculations as discussed in previous sections.

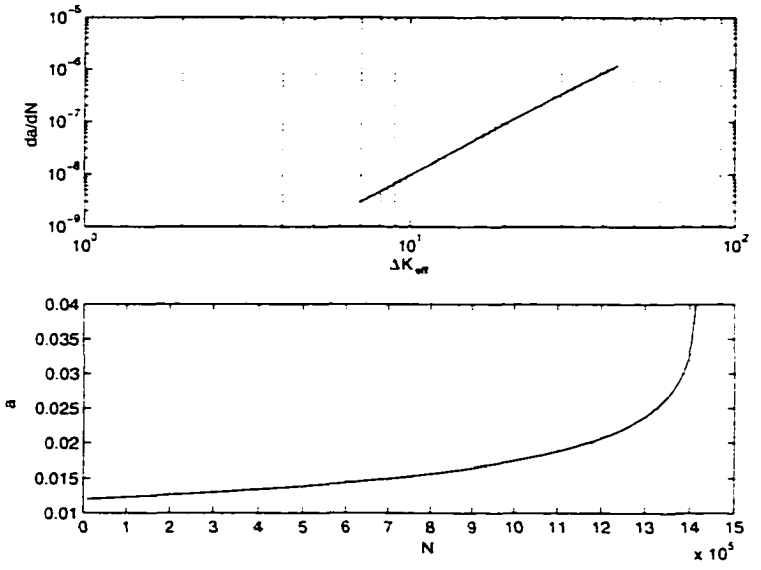

Figure 4.7: The CAL result on Farhangdoost's data [85].

4.9.1 Example - II

For CAL problems the comparison was also made with the experimental work of Farhangdoost [85]. The results for C(T) specimen of Ti-6Al-4V alloy are obtained on a cycle-by-cycle basis, as shown in Figure 4.7. The predicted life of the C(T) specimen from theoretical study is 75% of the average experimental value obtained from 18 different tests of [85]. The important observation in that investigation was the change in growth rate which occurred in all such tests. Thus two transition points, namely, at $\Delta K_{eff} \approx 8 - 9 MPa\sqrt{m}$, and $\Delta K_{eff} \approx 12 - 13 MPa\sqrt{m}$ were pointed out in that work. Due to this situation the Paris constants C and m can be defined in any of the three regions.

4.9.2 Example - III

The comparison was also made with Zhang *et al.*, [86] for various values of R as shown in Figures 4.8, 4.9 and 4.10. The FCGR on the basis of effective stress intensity factor

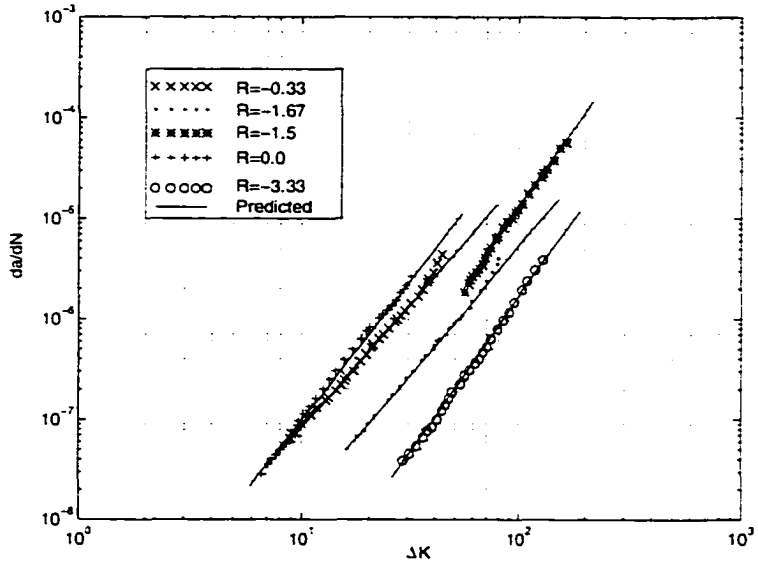

Figure 4.8: The CAL result on Zhang's data [86].

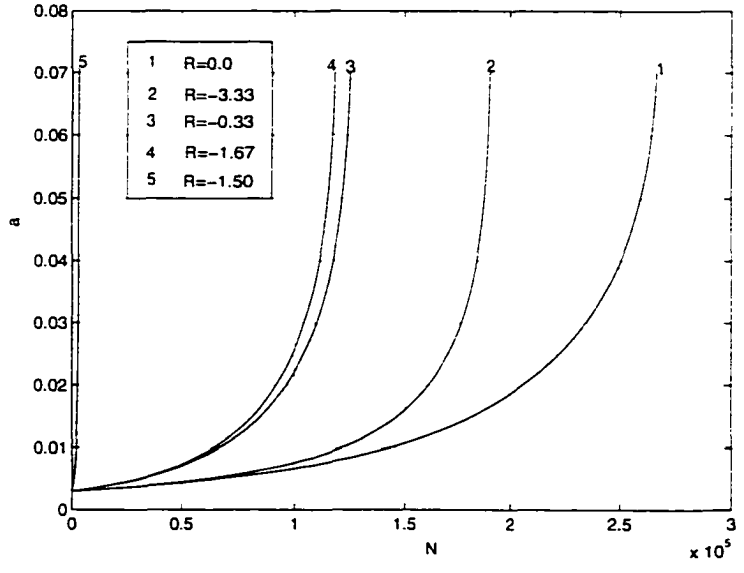

Figure 4.9: The CAL result on Zhang's data for crack length [86].

is given in Figure 4.11. The material is a high strength aluminum alloy Al 7475-T351. The specimen geometry was CCT, with 8 mm thickness and 160 mm width, with an initial notch of 3 mm. In the Figure 4.8 the crack propagation behavior both for positive and negative R-values is presented. The individual sets of data for different R-ratios follow parallel lines. The value of R and maximum applied stress are important for FCGR. For $R = -1.5$ and $\sigma_{max} = 200\ MPa$ the FCGR is highest for a given ΔK. This is shown in Figure 4.9, where the number of cycles to failure are least compared to the other cases. For the situation with $\sigma_{max} = 60\ MPa$ and $R = 0.0$, the number of cycles to failure are maximum. To obtain further details regarding negative R ratios for a fixed $\sigma_{max} = 60 MPa$, a plot of $\frac{da}{dN}$ versus a is shown in Figure 4.10. For the same crack length the curves with the negative R values show higher $\frac{da}{dN}$ values than those with $R = 0$.

The FCGR based on effective stress intensity range ΔK_{eff} is shown in Figure 4.11. On the basis of effective stress approach all the constant amplitude data falls on a single line. The governing equation for FCGR is as follows:

$$\frac{da}{dN} = 4.64 \times 10^{-7} (\Delta K_{eff})^{2.972}. \tag{4.17}$$

where, $\frac{da}{dN}$ is in $mm/cycle$ and (ΔK_{eff}) is in $MNm^{-1.5}$.

The effect of plastic constraint factor α on the fatigue life of the components is shown in Figure 4.12. It is observed that α has strong influence on life prediction. Doubling the value of α implies that the life of the component is $\approx$ 36% of the value for $\alpha = 1.0$, while the life prediction for the case with $\alpha = 3.0$ is 24% of the value for $\alpha = 1.0$. This clearly indicates that the component will fail in PSN relatively earlier than under PSS condition. Moreover, for the same component the PSS affected region (the free surfaces) will fail considerably after the PSN region (the inside portion). Therefore, the method of measurement for the number of cycles to failure (or for the determination of a versus N plot) is also important. It has

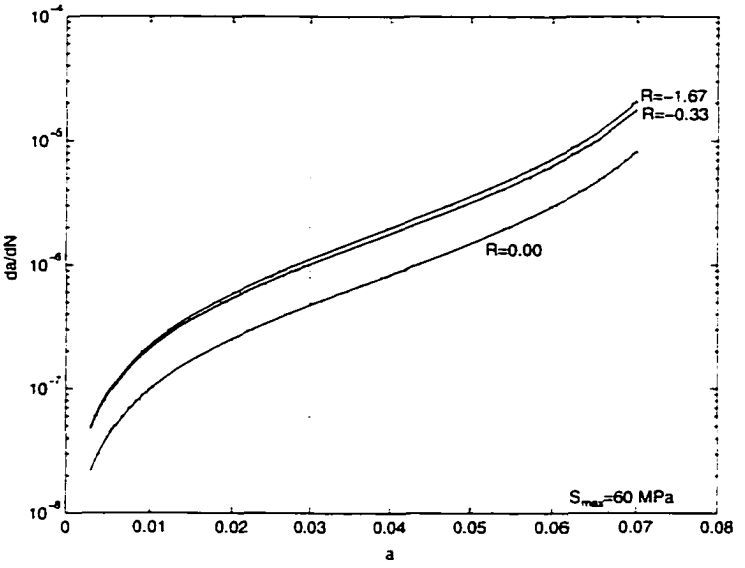

Figure 4.10: The CAL result on Zhang's data for R ratios [86].

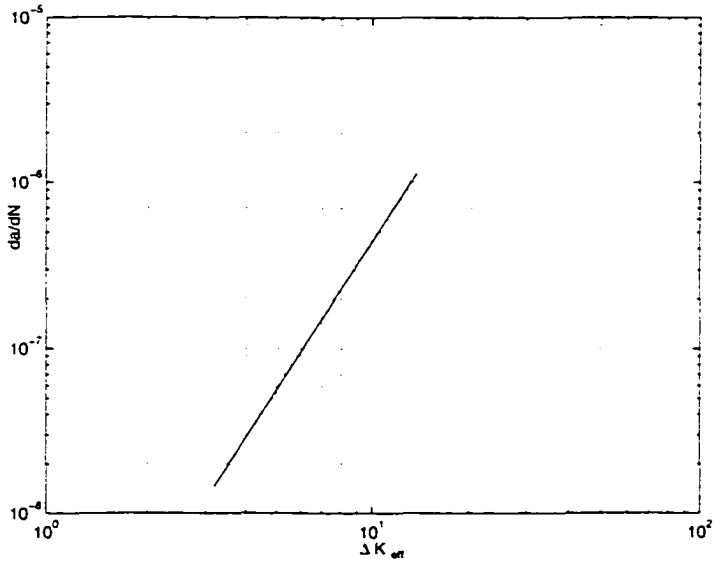

Figure 4.11: The CAL result on Zhang's data on effective stress [86].

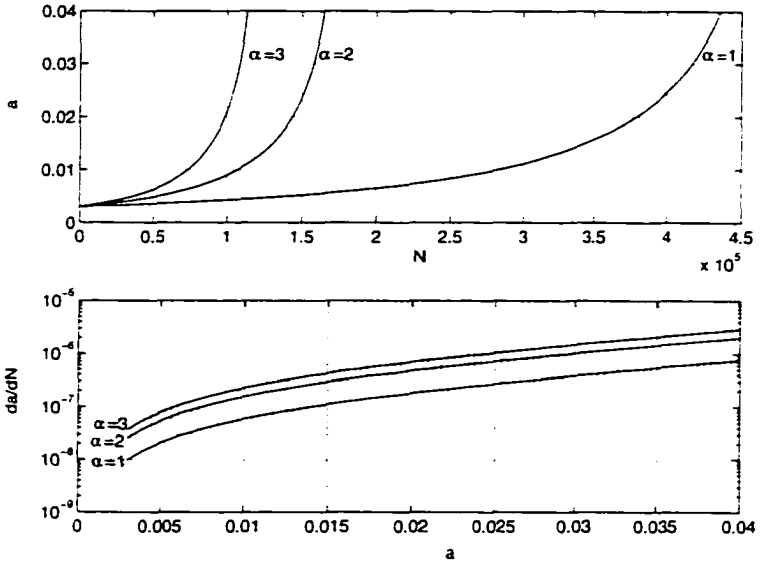

Figure 4.12: The effect of α on life of component [86].

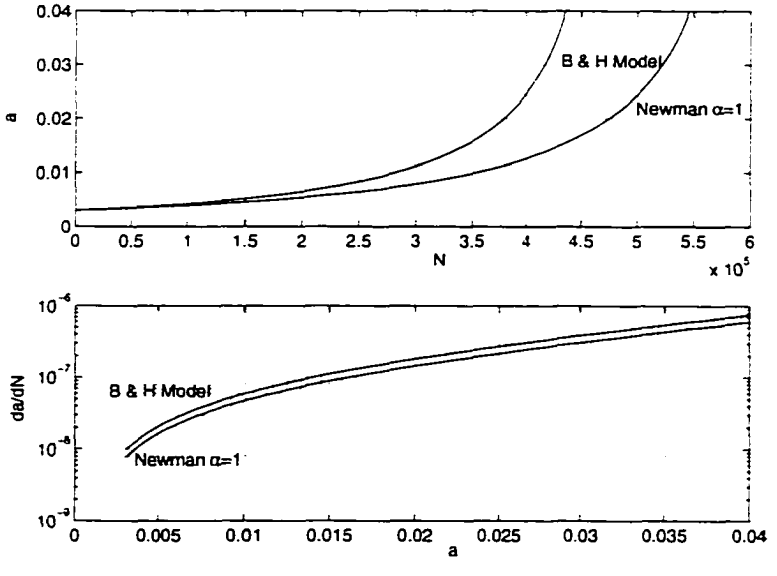

Figure 4.13: Some comparisons on Zhang's data [86].

been observed in a recent exploratory investigation by Lang and Döker [87] that for PSN measurement technique (SEM) the pattern of a versus N is different than the one for the measurement under PSS obtained from an optical microscopy technique measurement of the same component. A comparison of fatigue life estimate from the closure model of Budiansky and Hutchinson [54] and with Newman's closure model [57] is provided in Figure 4.13 . It is evident that number of cycles to failure N_f is effected by using either of these closure models under PSS condition. The number of cycles to failure from B & H model is approximately 80 % of Newman's model prediction. This indicates that for PSS situation B & H model is more conservative.

4.9.3 Example - IV

The comparison for CAL was also performed on mild steel using experimental results of Kumar *et al.* [88]. The results for three different R ratios are presented in Figure 4.14 for a constant maximum load of 11.77 kN in a cycle. It is observed that as R increases, the life of the component also increases.

4.9.4 Example - V

An additional example for CAL is taken from Kumar [89] for 6061-T6 Al-alloy. The work in [89] is essentially dealing with Single Overloads, however, one of the cases, under overload ratio (OLR) = 1.0 represents CAL condition. The results are provided in Figure 4.15.

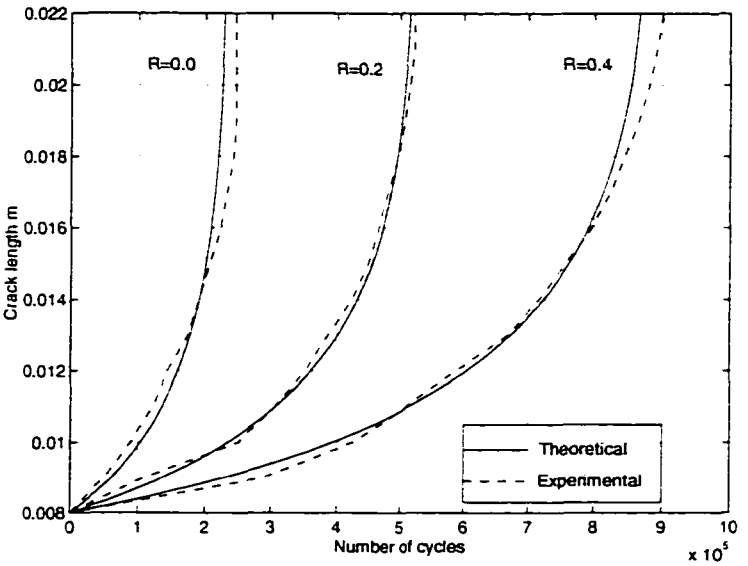

Figure 4.14: A comparison with experimental work of Kumar [88].

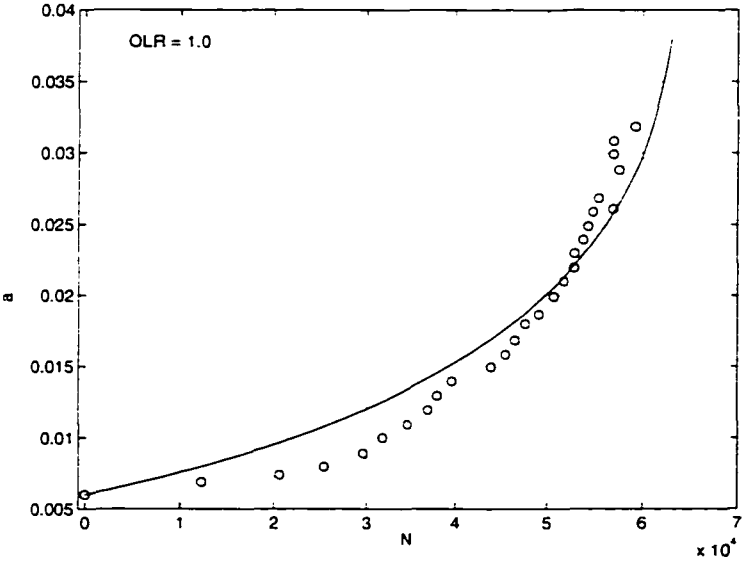

Figure 4.15: Number of cycles to failure versus crack length for CAL on Kumar's data [89]. The hollow rounds represent experimental data and firm line is the predicted values.

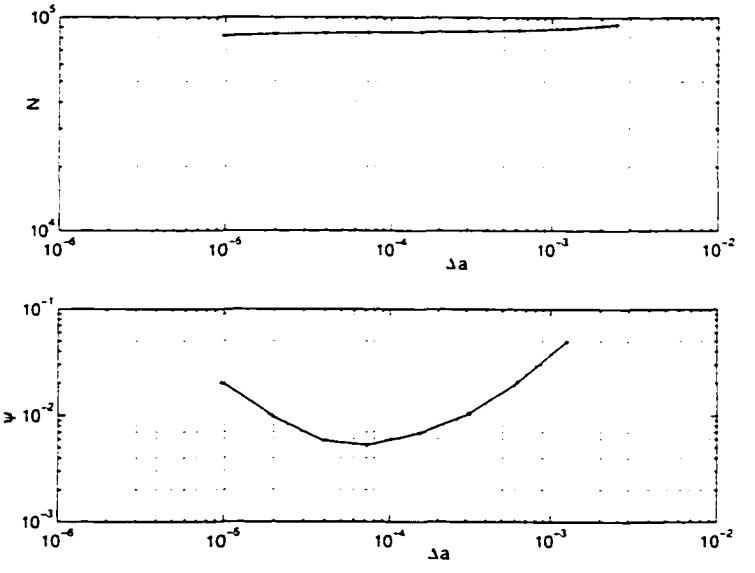

Figure 4.16: Error for various crack extensions for an a_0.

4.10 Discussion about CAL

A systematic study of the errors (which occur in approach-I) was performed for various cases, including increases in stress range, $\Delta\sigma$, and a variation in initial flaw size. Error has been defined in terms of the ratio $v = \frac{N_p - N_c}{N_R}$, where N_p is the previously obtained number of cycles to failure, N_c is the current number of cycles to failure and N_R is the reference number of cycles to failure which is obtained from approach-II. The error study was conducted on the design example of Rolfe and Barsom [5]. It was found that the errors drop for a decrease in the assumed extension and then start to grow again. This is shown in Figure 4.16. In this investigation it was observed that for approach-I to give meaningful and accurate results there is an optimal value for assumed crack extension. The errors normalised w.r.t. reference value of number of cycles to failure N_R are provided in Table 4.3 for an initial crack length of 7.6 mm. The value of N_R is taken from approach-II and represents the number of cycles to failure, and is obtained

Δa	N	Difference $N_p - N_c$	Error $v = \frac{N_p - N_c}{N_R}$
2.500000e-3	92737	—	—
1.250000e-3	88524	4213	0.0495
6.250000e-4	86774	1750	0.0205
3.125000e-4	85885	889	0.0104
1.562500e-4	85296	589	0.0696
7.182500e-5	84845	451	0.0530
3.906250e-5	84370	475	0.0580
1.953125e-5	83532	838	0.0980
9.765625e-6	81808	1724	0.0202

Table 4.3: Cases used in investigation.

from a cycle-by-cycle method of evaluation of crack extension. The variation of error is shown for the selected values of crack extensions in Figure 4.16. The number of cycles to failure is influenced by the assumed value of crack extension, the error v is minimum at a particular value of crack extension and the corresponding number of cycles to failure represent accurate number of cycles to failure. The pattern of errors using approach-I are provided in Tables 4.4 and 4.5 for $\Delta\sigma = 276.0\ MPa$ and $\Delta\sigma = 414\ MPa$ respectively. These errors are also presented in Figure 4.17. It is observed that optimal point shifts toward higher side of Δa, for higher values of $\Delta\sigma$ and errors become more pronounced for higher values of $\Delta\sigma$.

The pattern of errors with regard to the effect of initial length of the crack on FCG is shown in Figure 4.18, for the same final length of the crack. It is observed that the optimal point shifts toward higher values of Δa for a decrease in the initial length of the crack a_0. In Tables 4.6 and 4.7 the errors have been tabulated for an initial crack length $a_0 = 3.8\ mm$ and $a_0 = 15.2$ respectively.

It has been shown in the present investiagation, that there are two distinct ways

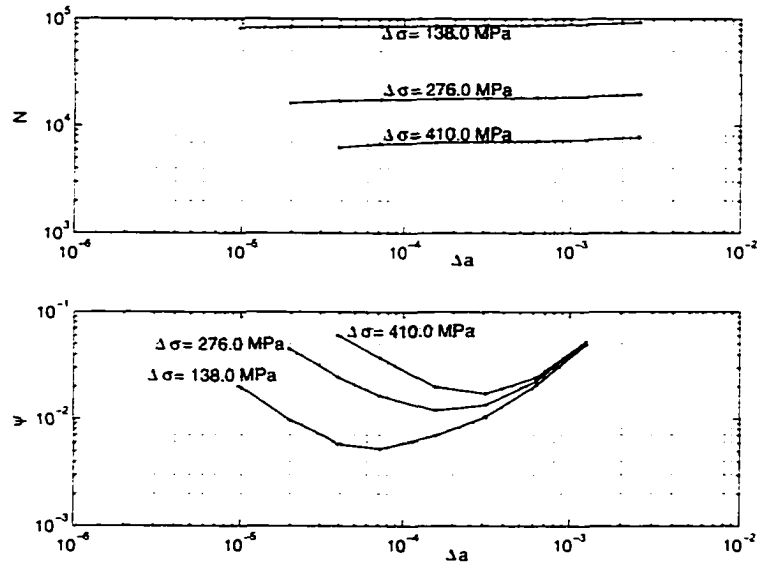

Figure 4.17: Error for various values of crack extension for various values of $\Delta\sigma$.

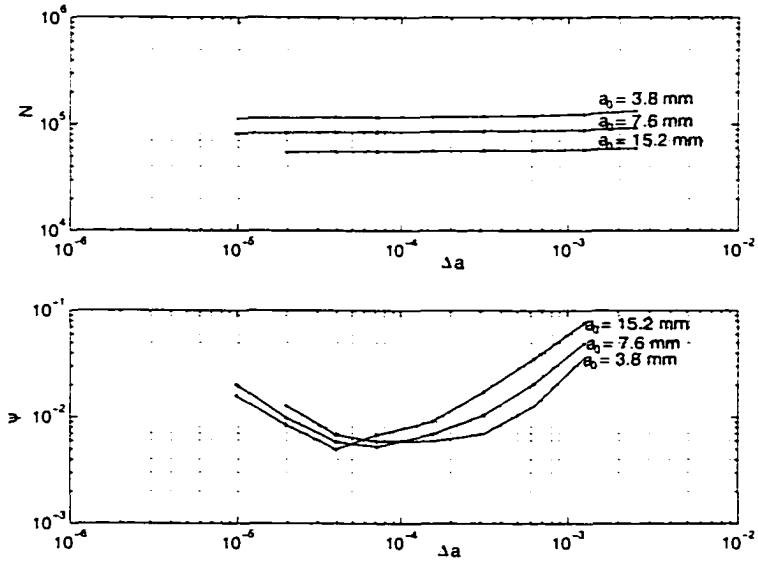

Figure 4.18: Error for various initial values of crack length a_0.

Δa	N	Difference $N_p - N_c$	Error $\epsilon = \frac{N_p - N_c}{N_R}$
2.500000e-3	19486	—	—
1.250000e-3	18591	895	0.0526
6.250000e-4	18207	384	0.0225
3.125000e-4	17978	229	0.0134
1.562500e-4	17775	203	0.0119
7.182500e-5	17496	279	0.0164
3.906250e-5	17097	417	0.0245
1.953125e-5	16328	769	0.0452

Table 4.4: Errors for $\Delta\sigma = 276.0\ MPa$.

of FCGR calculations. The errors that result by using one of the approaches, which is based on assumed crack extension, have been pointed out in a detailed study of a design problem. It was observed that cycle-by-cycle analysis gave results in agreement with the experimental values, while for the assumed crack extension method gives accurate results only for an optimal value of crack extension.

Incorporation of an effective stress intensity approach was also emphasized by several design examples and comparisons with experimental results of some investigations were also presented. The crack-tip opening loads were obtained from already existing models. In this way the crack closure models can be tested for their limitations and accuracy.

Having placed on a solid foundation the important aspects of plasticity, fatigue crack closure and the method by which fatigue crack growths are simulated, these factors will now be incorporated into an analysis of the influence of single peak overloads on fatigue crack growth retardation and its corresponding rate.

Δa	N	Difference $N_p - N_c$	Error $\psi = \frac{N_p - N_c}{N_R}$
2.500000e-3	7819	—	—
1.250000e-3	7450	369	0.0527
6.250000e-4	7279	171	0.0244
3.125000e-4	7159	120	0.0171
1.562500e-4	7020	139	0.0198
7.182500e-5	6759	269	0.0372
3.906250e-5	6335	424	0.0605

Table 4.5: Errors for $\Delta\sigma = 414.0\ MPa$.

Δa	N	Difference $N_p - N_c$	Error $\psi = \frac{N_p - N_c}{N_R}$
2.500000e-3	133579	—	—
1.250000e-3	124683	8896	0.0762
6.250000e-4	120540	4143	0.0355
3.125000e-4	118520	2020	0.0173
1.562500e-4	117451	1069	0.0916
7.182500e-5	116656	795	0.0681
3.906250e-5	116075	581	0.0497
1.953125e-5	115097	978	0.0838
9.765625e-6	113248	1849	0.0158

Table 4.6: Errors for $a_0 = 3.8\ mm$.

Δa	N	Difference $N_p - N_c$	Error $v = \frac{N_p - N_c}{N_p}$
2.500000e-3	59610	—	—
1.250000e-3	57592	2018	0.0359
6.250000e-4	56878	714	0.0127
3.125000e-4	56489	389	0.0693
1.562500e-4	56155	334	0.0595
7.182500e-5	55824	331	0.0589
3.906250e-5	55442	382	0.0680
1.953125e-5	54724	718	0.0127

Table 4.7: Errors for $a_0 = 15.2\ mm$.

Chapter 5

SINGLE PEAK OVERLOADS

5.1 Introduction

As has been discussed the fatigue crack growth behavior of metals is known to depend upon a number of variables which include the mechanical properties and material microstructure, specimen size, environmental conditions, the state of stress and strain at the crack-tip, the plasticity in the wake of the advancing crack-tip, the plasticity ahead of the crack-tip and the type of applied loading. As detailed in previous Chapter, there is now a reasonable understanding of CAL type FCGR problems. However, variable amplitude problems are still under active investigation.

Since many engineering applications, such as: the proof testing of pressure vessels, the overspeed testing of rotating machinery and the peak loading of offshore and aircraft structures, involve occasional or periodic single overloads (SOL), variable amplitude loads (VAL) or random loads (RL), it is of utmost importance to first predict the FCGRs following single overloads. This loading history or loading environment can have a significant effect on the prediction of fatigue lifetimes in any

such application.

For a safe operation of any component it is essential to have improved predictive models of crack propagation under VAL. Prediction under SOL is, then, a basic building block for a model to be useful under VAL condition. This requires an estimation of the influence of real life loading spectra with SOL on FCGRs. Therefore, this Chapter presents a model for prediction of FCGR and crack propagation in general under SOL.

5.2 Wheeler's Approach and its Impact

An analytical approach to the solution of crack growth prediction in metals subjected to variable amplitude loading that takes into consideration the plasticity affected region was first presented by Wheeler [90]. The model takes into account the yield zone ahead of the crack-tip. There has been extensive work done on the Wheeler model *e.g.*, [91, 92, 93, 94, 95]. Wheeler has shown that this model gives reasonable predictions for the crack growth rates in D6ac steel and titanium. The Wheeler model shows, by fitting curves to previously observed data, that the size of the yield zone is the main factor governing the retardation. Growth rates during the retardation event due to the application of an overload were reported very recently by Goel and Satish [93] Figure 5.1. Growth rates following overloads were not reported by Wheeler [90]. It was shown by Broek and Smith [95] that Wheeler's model provides reasonably accurate results for crack propagation under flight-by-flight loading, provided the model was adjusted on the basis of experimental results with similar types of loading. After adjustment, good predictions can be made for many spectrum variations.

An experimental method for determination of Wheeler exponent, m_w, has been performed by Shue, Song, and Hwang [92] for 5083-O and 6061-T651 aluminum alloys

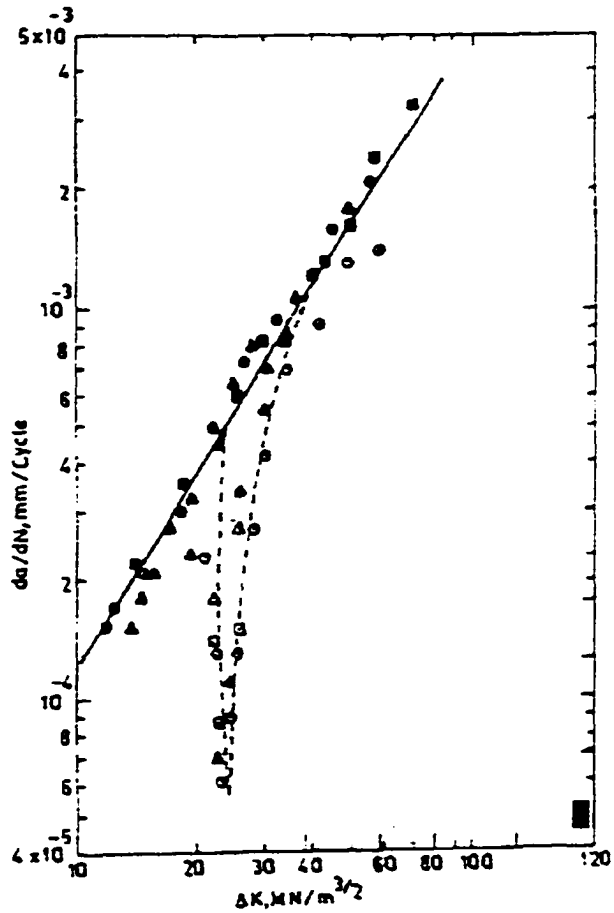

Figure 5.1: da/dN versus ΔK by Goel and Satish from an experimental perspective. Notice the sharp triangular dip in da/dN [93].

respectively. The value of m_w was found to depend on the material, OLR and initial crack length.

Crack growth rates can be predicted with a fair degree of accuracy for some simple crack configurations for specimen subjected to constant-amplitude loading. However, for complex loading sequences the results are conservative by a factor of 3 or 10 or more [96] . This was as a result of ignoring the plasticity affected zone in front of the crack-tip and in the wake of the crack-tip. As is discussed in Chapter 3, analytical models, finite element models and experimental techniques, have revealed that the crack is effectively open for only a portion of the load cycle and the reduction was attributed to the deformations in the neighborhood of the crack and plasticity affected area in the wake of the crack.

Another possible way to look at load interaction effects is the presence of compressive residual stresses in the plane of the crack which subsequently retards the crack growth. Willenborg, Engle and Wood [97] have developed a quantitative retardation model based on the residual stresses in the overload plastic zone with an effective stress intensity factor that varies in a specified manner. The model uses a modified crack growth equation that gives the crack growth in the overload effected region. The models used by Willenborg and Wheeler have been used extensively but these lack a rigorous theoretical foundation, according to Russel [98]. Recently Bolotin and Lebedev [99] used the residual stress approach for a single overload problem. Their model did not give triangular spike-dip (which is observed in experimental investigations) in the da/dN versus ΔK plot as shown in Figure 5.2. None of these retardation models account for the interaction between overload-induced crack closure. A model that accounts for this kind of interaction was reported by Russel [98]. In that analytical crack closure model, work of Budiansky and Hutchinson [54] is incorporated. That work uses a complex variable technique in conjunction with the Dugdale strip-yielding

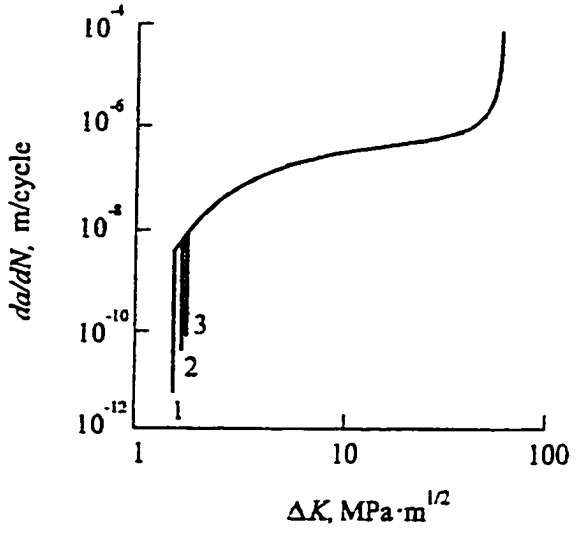

Figure 5.2: da/dN versus ΔK by Bolotin and Lebedev from a different theoretical approach than the current work. (1) Regular loading (2) Single overloading and (3) Two overloadings. Notice the absence of sharp triangular dip in da/dN for overload situations (2) and (3) [99].

model. Lo [100] extended the work to study the crack closure from the perspective of a step increase in constant amplitude loading. and it is of interest to note that model of Lo [100] predicts an acceleration in the FCGR. which is a momentary phenomenon following overloads. while the overall effect is impeding in nature. The models of Russel [98] and Lo [100] give purely theoretical grounds for closure with SOL. However. both of these models lack FCGR predictive capabilities. This is the reason that both of these models have not found application in the area of fatigue crack growth rate prediction or for obtaining information of fatigue crack growth. *i.e.*, a versus N. In view of these details. Wheeler's model if used with proper modifications . such as. a proper characterization of crack-tip plasticity and exponent m_w is the right option for an SOL situation.

5.3 Other Approaches and Some Experimental Works

Recently a review paper on FCGR under VAL and SOL by Geary [101] appeared in the literature. Several aspects pertaining to SOL and VAL were discussed and new areas of research were pointed out. It was shown that the work on VAL fatigue loading reported in the open literature has been conducted on aluminum and titanium alloys, while a relatively small amount of work has been conducted on low alloy steels. The variable magnitude SOL problem has been overlooked and predictions of FCGR in such a situation deserve to be addressed. Moreover, data pertaining to a versus N, da/dN versus ΔK and information regarding opening loads under SOL for the same test conditions, specimen geometry and material is very rarely reported together. Several references on VAL and SOL are provided in [101], and some other issues will be discussed below.

Chakrabarti [102] developed a new retardation model based on the theory of dislocation pile-ups. The results based on this model are in good agreement with some of the experimental observations. A crack growth model based on an approximate description of the crack closure behavior, with provision for the acceleration and retardation effects observed under variable amplitude loading, is reported by de Koning [96]. This paper also provides a comparison of results with experimental data for 7075-T6 aluminum alloy thin sheet material.

The effect of multiple overloads on subsequent fatigue propagation in 2024-T3 aluminum alloy specimens was studied by Trebules, Roberts and Hertzberg [103]. In this purely experimentational work, the retardation effect following overloads has been explained on the basis of crack closure. The tests were run for 1, 2, 10, 100, 1000, 5000 overload cycles. They obtained typical triangular dips in da/dN versus

ΔK plots, which were reported later by other researchers in this field of study.

An analytical model of fatigue crack growth rates based on the plastic-blunting mechanism was developed by Sahasakamontri and Horii [104]. They presented some results pertaining to variable amplitude loading. The formulation employs Muskhelishvilli complex stress functions in terms of which the stress and displacement components were written. The dislocation based plasticity approach is adopted in that paper, and it is predicted that the residual plastic deformation in the wake of an advancing crack has a large influence on the crack growth behavior. The reported results also lend theoretical support to plasticity induced crack closure under plane strain conditions. This contradicts some of the observations made in reference [59], that, based on dislocation theory, closure could not occur. However, this paper does not provide any information on a versus N and da/dN versus ΔK, which is a very important check on the validity of the model.

The phenomenon of retardation following overloads has also been explained on the basis of the closure concept [98, 105]. Several attempts have been made to develop simple analytical models (see *e.g.*, Provan and Majid [60, 106]) to determine closure loads, which are required for a meaningful assessment of the fatigue life of components under VAL situations. Although it is well known that FCGR, following overloads, is significantly influenced by load interaction-effects, yet the cause of these interaction-effects is still under active investigation. Several exploratory experimental works on various Aluminum alloys with single overloads (SOL) have appeared in recent years which show retardation following single overloads [89, 92, 93, 99, 107]. As was mentioned in earlier Sections of this Chapter, some investigations have pointed out that, for the description of load-interaction effects the important factor is plasticity induced crack closure. Several prominant models of predicting crack growth rates under variable amplitude loading are based on the crack closure concept. Direct

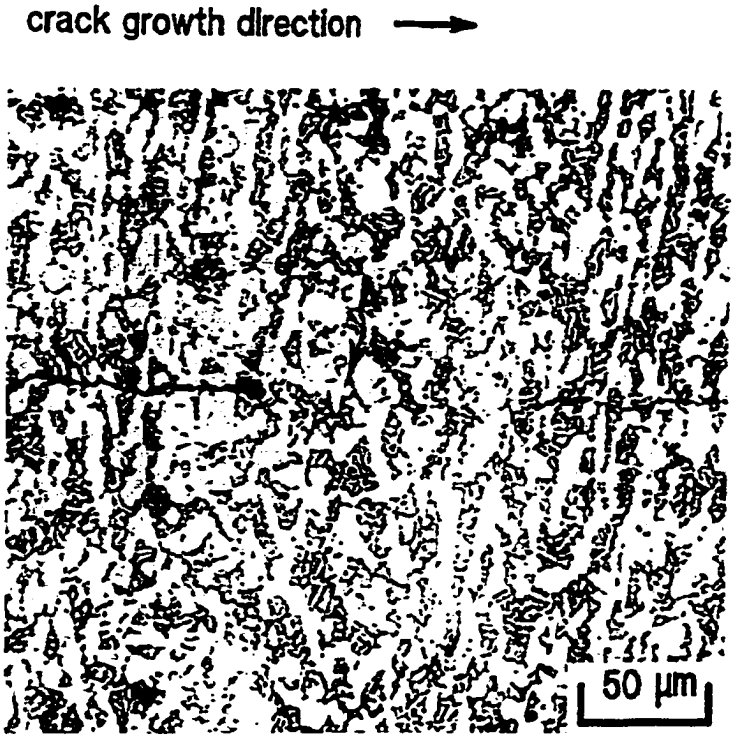

Figure 5.3: Experimental evidence of plasticity induced crack closure. Notice closure over a considerable crack length following overload, this is indicated by marker "A". A pronounced crack-tip opening displacement at the eve of application of overload is conspicuous [79].

experimental evidence for this salient feature of FCG under SOL is available through some recent works, *e.g.*, [79] as is shown in Figure 5.3. In that investigation the evidence of crack closure under SOL, on the basis of SEM pictures, is revealed and a reasonable agreement between experimental results and theoretical prediction based on Newman's model [72] of crack closure is also presented. A crack closure model for VAL type of loading was presented by Newman [72]. The development and application of this analytical model of cyclic crack growth with crack closure effects was based on a concept like Dugdale model but modified to leave plastically deformed material

in the wake of advancing crack. Subsequently this model has been used for FCGR under VAL and SOL respectively [79, 108]. The opening loads obtained on the basis of that model have large oscillations and a special averaging technique was used by Newman [72] to overcome this behavior. That averaging also resulted in a reduction in the computation time.

5.4 Generations of Retardation Models

The models for FCGR retardation for load interaction effects may be broadly classified into the following generations.

The first generation models were mainly based on Wheeler [90] and Willenborg [97] type of approach.

The second generation models such as CORPUS, ONERA, PREFFAS (for details see ASTM STP 982 [109], and reference [110] by Ling and Schijve for some critical notes on these models) were essentially based on closure as a domineering mechanism governing the load-cycle interaction. The opening loads were obtained from empirical relations in these models. It is interesting to note that the CORPUS and ONERA models account for PSS/PSN effects, while in PREFFAS, it is introduced empirically. All the above mentioned models do not predict a delayed retardation effect as is found in some of the experimental investigations. The CORPUS, ONERA predict a constant opening load following an overload. However, the actual opening load measurements indicate a special trend [107] following an overload. The present model provides this trend, while, the initial delayed effect does not appear in the results.

The third generation models are based on Dugdale strip yield models. The model COSMIC by Newman [111] and another model by de Koning *et. al* [109] fall in this category. These models make provision for plastic deformations in the wake of an

advancing crack and take closure into account. The models also predict a cycle-by-cycle variation of opening loads. However, it is interesting to note that the opening loads have been obtained in COSMIC by a special averaging technique because of very large oscillations in the predicted opening loads. This averaging has also reduced the computation time.

The modelling of crack-tip plasticity in strip-yield models is crude according to Ling and Schijve [110]. Therefore, in the current investigation a different approach to crack-tip plasticity was adopted which allows for the PSS/PSN effect and also accounts for the shape of the plasticity zone.

The fourth generation models are now attempting to incorporate closure effects into the earlier generation models, based on issues of the proper characterization of crack-tip plasticity. Also, a distinction between closure effects under CAL and an additional closure part resulting from an overload is incorporated into earlier generation models, so that role of plasticity zone is clearly understood. Furthermore, the information pertaining to closure loads under SOL is obtained through the modified retardation factor based models. The issue of PSS/PSN transition is also not fully understood. It was pointed out by McClung and Sehitoglu [73], that limitation of experimental techniques in identifying critical behavior, such as displacement histories at the mid section in a thick specimen, may be because they are essentially inaccessible by any conventional measuring technique. However, more recently, Lang and Döker [87] have presented SEM results, with marker load position identification, (PSS) compared with potential drop methods (PSN). The results for crack length versus the number cycles to failure reveal that specimen fails relatively early in the interior (PSN region) when compared to the fully PSS regions.

There is also ongoing research activity using FEM methodology. However, it is yet in its embryonic state. The limitation of the finite element model for FCG was

discussed in detail in [73], indicating crack advance must occur in relatively large jumps, corresponding to the element size, rather than in a relatively continuous and smooth series of infintesimally small Δa values which correspond to the physical situation.

The second limitation is that there is no consensus on the quantitative basis of the mechanism that actually causes crack advance. The most important shortcoming of finite element models is therefore related to the crack advance schemes, which are arbitrary and unrealistic. The FCGR calculations require a realistic estimate for crack advance and is generally obtained from the Paris law in analytical and quasi-numerical models. It is interesting to note from reference [73] for element width $\frac{\Delta a}{W} = 0.002$ where Δa is the crack advance and W is the width of specimen, that the time for execution was 100 h on an HP-9000 and 20 min on a CRAY. The FCGR is typically of the order of $10^{-11}m$ near the threshold region and of the order of $10^{-9}m$ in the Paris region. Therefore, the assumed extension of the crack extension cannot simulate the FCGR calculations.

5.5 Need for Model under SOL

On the basis of information provided in previous Sections of this Chapter, and Chapters 2, 3 and 4, it is evident that despite the existence of so many crack growth retardation models, there is scope for a model for FCGR under SOL. The model should account for crack closure, predict growth rates reasonably well under CAL and SOL with an effective stress intensity approach, and take into account load interaction effects. The present model has all these features and also accounts for the plasticity zone size and shape. The model is user friendly and computationally efficient. Furthermore, the closure that occurs as a result of overloads, primarily because

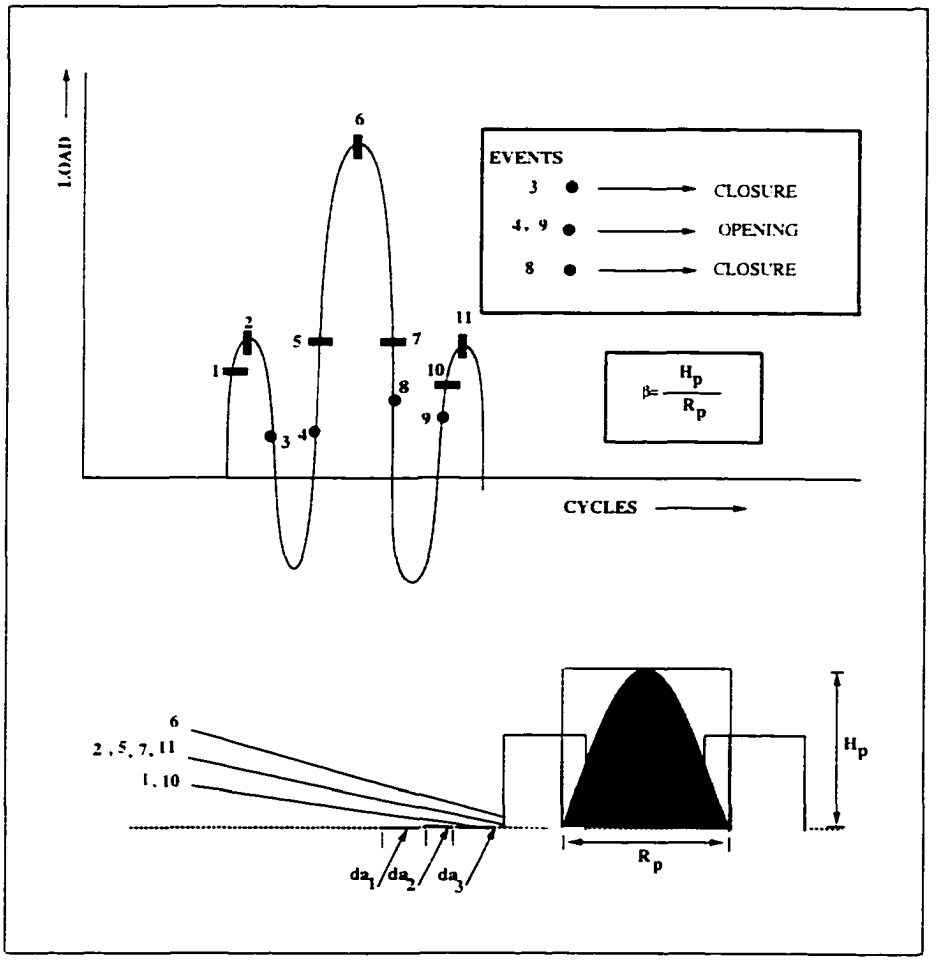

Figure 5.4: Schematic showing events after an overload application.

of the plasticity effect, is incorporated. The schematic of plasticity effect following SOL is presented in Figure 5.4. This kind of effect has been established from experimental evidence as shown in Figure 5.3. The objective of this Chapter is to calculate the FCGR in specimens under variable magnitude SOL. More specifically, the purpose is to explore interaction effects on the crack growth characteristics using this novel approach. The new approach to evaluate the effects of load interaction has been developed after examining the various models which already exist. In view of

striation spacings appearing as *a posteriori* evidence for fatigue, a cycle-by-cycle prediction model is more realistic. The importance of the cycle-by-cycle approach was emphasized in Chapter 4 of this thesis.

The current work compares numerical predictions with experimental studies [89] of the fatigue crack growth rate behavior associated with variable magnitude, single overloads under plane stress (PSS) or plane strain (PSN) conditions in 6061-T6 Al-alloy for various overload ratios (1.75, 2.0, 2.15, 2.25, 2.5). From the many reported experimental works on SOL, Kumar's [89]work was chosen since it provided a versus N information, and da/dN versus ΔK data very candidly. The a versus N data, in particular, is provided for various overload ratios which was not reported previously in the open literature for a variable magnitude SOL problem.

On the basis of this investigation a power law for the retardation exponent is obtained. The model is then used to provide opening loads for 2024-T3 Al-alloy and compared with [107] . This work also proposes a cycle-by-cycle analysis following modifications to the Wheeler's model. Since the concept of crack closure was in its embryonic state when Wheeler's model first appeared [90], it was not based on the effective stress intensity factor approach. Moreover, the effect of plasticity was incorporated very crudely in [90]. In this study the opening loads under CAL from Newman's investigation [57] are used; this is discussed in detail in Chapters 3 and 4. The retardation factor has been obtained on the basis of the concept of plasticity affected ranges, as was discussed in Chapter 2. The model also relates the exponent of the retardation factor to the overload ratio and thus allows the model to be used without reliance on data fitting. It incorporates a model for crack-tip plasticity which can be used under both plane stress PSS and plane strain PSN situations, Figure 2.7. The model can be used to provide closure loads following an overload.

The objective of the current work was to compare numerical predictions with

experimental studies of the fatigue crack growth rate behavior associated with variable magnitude, single overloads. The purpose of the study was also to determine the role of crack closure (in terms of magnitude and location). The retardation effect following overload was obtained on the basis of the retardation factor. The closure load was decomposed into two components, one that would result under CAL and the second component, which is an additional part, which exists as long as the crack remains within the overload plastic zone.

5.6 Modelling

The model is composed of three regions. 1) A linear elastic region with a fictitious crack length of $a + r_f$, where a is the crack length, and r_f is the forward plasticity affected range, 2) A plasticity affected region of length of r_f, and 3) a plasticity affected region left in the wake of the crack with residual deformations. The magnitude of r_f depends on plastic constraint coefficient and has been evaluated from the model presented in Chapter 2.

5.6.1 Opening Loads

Both CAL and SOL require evaluation of opening loads. Since it has been pointed out in the above discussions that experimental verification of opening loads is a subject of controversy due to problems of reproducibility and resolution even under CAL, it is appropriate, therefore, for single overload (SOL) problems that a novel way of theoretically evaluating the opening loads following an overload be presented. The opening load is divided into two components, one that would result from a constant amplitude block, and the other from an additional component due to the application

of an overload. The second component exists for the portion of the crack propagation within the overload plastic zone. As soon as the crack-tip comes out of the overload plastic zone the additional component vanishes.

5.6.2 Plasticity in the Wake

The effect of plasticity in the wake results in the decrease in the crack driving force in terms of the stress intensity factor. The opening loads have been evaluated for CAL from Newman's [57] analysis. The additional component has been obtained by equating the FCGR resulting from opening load approaches with a modified Wheeler type retardation concept. Fatigue crack closure under SOL has been evaluated on the basis of plasticity range load interaction in conjunction with the closure effects under CAL. It is essential to consider fatigue crack growth rates under constant amplitude loads, to compute the opening loads under SOL.

Several assumptions have been made while arriving at the formula for opening loads under SOL while the crack is propagating through the overload plasticity range, r_f^{SOL}. The assumption for the model, in addition to those presented in Chapter 4, is as follows. The plasticity affected range has been considered to be the crucial part of the plastic zone and responsible for the retardation effect as the crack passes through the plastic zone. In Chapter 2 it was shown that the plasticity zone formed at the tip of the crack has a height and a range associated with it. The crack propagates through the plasticity affected range, r_f, for C(T) or CCT specimens due to the symmetry about the axis of the crack. Moreover, the plasticity affected range denotes the shortest plasticity affected radius from the crack-tip towards a perpendicular line drawn to the propagation direction.

5.7 Crack Growth Calculations

The information regarding the opening loads for the constant amplitude loading CAL is provided in Chapter 4. However, the situation under SOL condition is different. The crack length under SOL after any q cycles is given by the following formula which applies for a model that takes retardation into consideration:

$$a_q = a_0 + \sum_{i=1}^{q} f\left(\Delta K_{eff} - K^{*}_{open}\right)_i. \tag{5.1}$$

Here a_q is the crack length after q cycles. a_0 is the initial physical length of the crack. $(\Delta K_{eff})_i$ is the effective stress intensity factor range, and $(K^{*}_{open})_i$ is the second component of opening stress intensity factor for a given cycle i. There are several choices available for $f\left(\Delta K_{eff} - K^{*}_{open}\right)_i$; however, this study will be restricted to the Paris law for FCGR. A thorough discussion regarding the evaluation of K^{*}_{open} will be presented in the following Sections of this research.

At the application of a SOL, the value of the maximum stress intensity factor, K^{SOL}_{max}, is known from the loading history. However, the value of opening stress intensity factor following SOL, K^{SOL}_{open} is not known. Unlike the constant amplitude loads where several models exist, there is not an accepted model for the determination of opening loads under SOL. The method of computing the opening loads under SOL is based on the Plasticity Range Interaction (PRI) concept. The formulae are developed in three steps. The first step is to place the crack growth rate under SOL in terms of the retardation factor. The second step is to put the retardation factor in terms of a stress intensity format. The third step is to obtain the opening load expression by incorporating the opening loads under CAL.

5.8 Plasticity Range Interaction (PRI) Model

From the information presented in Chapter 2, an estimate for the plasticity affected range r_f may be obtained. This is utilised to evaluate the retardation factor under SOL.

The value of r_f immediately ahead of the crack-tip is given by:

$$r_f = \alpha_j \left(\frac{K_{max}}{\sigma ys} \right)^2 . \tag{5.2}$$

$$\alpha_j = \left(\frac{(1-2\eta)^2}{2\pi} \right) \tag{5.3}$$

where, $\eta = 0.0$ is for PSS and $\eta = \nu$ is for PSN situation. The value of r_f as given in eqn(5.2) is valid for both Tresca and von Mises yield criteria.

5.8.1 Load Retardation Range Concept (LRR)

A proper characterization of crack-tip plasticity, which exists because of a prior load spectrum, must be taken into consideration in any crack growth retardation model. The extent of such a zone, which could account for load interaction effects is referred to as the load retardation range (LRR). The radius of this zone was taken to be the plastic zone radius created under PSN by Wheeler [90] . However, others [94] have suggested that plastic zone radius under PSS is a more appropriate approximation.

In this investigation, it has been shown in Chapter 2 that the plasticity zone formed ahead of the crack tip has a plasticity affected height, h_f, and a plasticity affected range, r_f, associated with it. In the present model, the size of this interacting zone has been chosen to be the plasticity affected range, r_f, since this is the most probable path for crack to propagate in a symmetrically loaded fatigue specimen and,

hence, represents the critical dimension in the plastic zone. The values of this range can be computed under both PSS and PSN and is highly sensitive to poisson's ratio, ν, and load ratio, ε.

Referring to Figure 5.5, P^{SOL} denotes the applied overload at the crack length a_1, that creates a plasticity affected range, r_f^{SOL} and is assumed to extend to some future crack position a_4. At some intermediate crack length a_2 a plasticity affected range r_f^{CAL} is associated with the load P^{CAL}, which extends up to some future crack position a_3. Then, using Wheeler's retardation concept [90] :

$$a_2 + r_f^{CAL} \geq a_1 + r_f^{SOL}, \qquad \text{no retardation.} \tag{5.4}$$

If the load P^{CAL} develops r_f^{CAL}, which extends beyond any previously created plasticity affected ranges, then the growth increment associated with P^{CAL} loading is calculated on the basis of a constant amplitude loading procedure. Conversely, if the load interaction range at a_2 is smaller than the previously created SOL plastic range, then the retardation is assumed. Thus, for retardation to exist the following condition must prevail:

$$a_2 + r_f^{CAL} \leq a_1 + r_f^{SOL}, \qquad \text{retardation.} \tag{5.5}$$

The crack growth rate under SOL is as follows:

$$\left(\frac{da}{dN}\right)^{SOL} = F_R \left(\frac{da}{dN}\right)^{CAL}. \tag{5.6}$$

where F_R is retardation factor. In the proposed model of plasticity affected ranges for an existing retardation condition it is given as:

$$F_R = \left(\frac{r_f^{CAL}}{r_f^{SOL}}\right)^{m_w}, \qquad r_f^{CAL} \leq r_f^{SOL}. \tag{5.7}$$

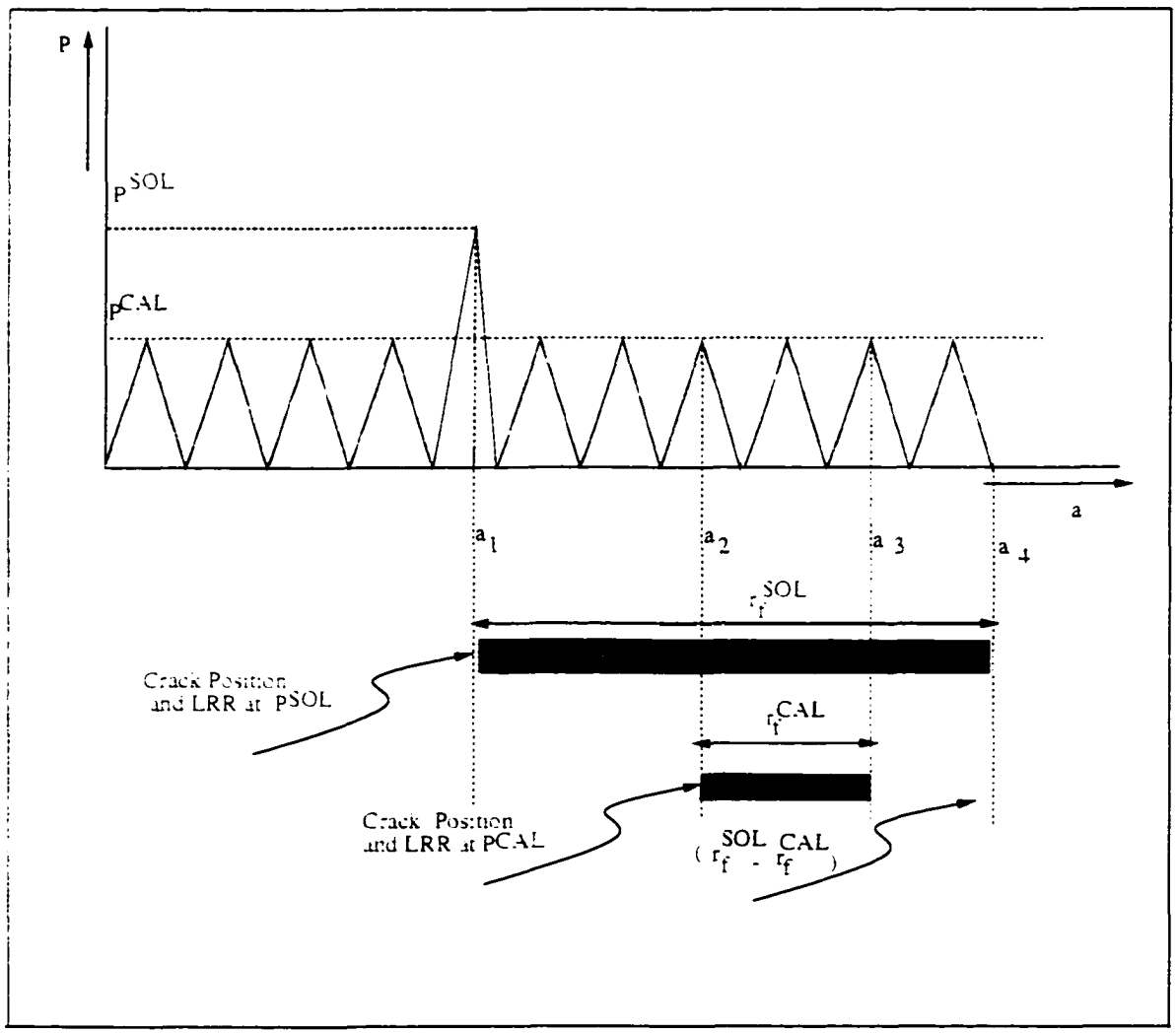

Figure 5.5: Plastic range interaction.

and for no retardation to occur the following condition prevails.

$$F_R = 1, \qquad r_f^{CAL} \geq r_f^{SOL}. \tag{5.8}$$

r_f^{CAL} denotes the plasticity affected range of the current plastic zone caused by the current maximum stress intensity factor K_{max}^{CAL}, and m_w denotes Wheeler's exponent, which may depend on material, OLR and the type of loading spectrum.

If the range r_f^s denotes the difference between the previously applied overload plasticity affected range and the crack growth increment since the overload was applied, then the conditions for retardation may be expressed as:

$$r_f^s = r_f^{SOL} - \Delta a, \tag{5.9}$$

$$r_f^s = r_f^{CAL}, \qquad \text{no retardation.} \tag{5.10}$$

It is obvious from the eqns(5.9 and 5.10) that as the crack grows away from position a_1, r_f^s decreases until some state later $r_f^s = r_f^{CAL}$. At this point he constant amplitude loading conditions exist.

For r_f^s there is an associated stress intensity factor K_{max}^s which decays such that:

$$K_{max}^s = K_{max}^{SOL} \left\{ \left(1 - \frac{\Delta a}{r_f^{SOL}} \right) \right\}^{0.5}. \tag{5.11}$$

The stress intensity format of the retardation factor, based on the plasticity affected range concept of the present work and using the retardation study of Gray and Gallagher [94], is as given below:

$$F_R = \left(\frac{K_{max}^{CAL}}{K_{max}^s} \right)^{2m_w}, \qquad K_{max}^{CAL} \leq K_{max}^s. \tag{5.12}$$

The above equation is valid for retardation effect to exist, while, for the no retardation condition, the following equation is valid:

$$F_R = 1, \qquad K_{max}^{CAL} \geq K_{max}^s. \tag{5.13}$$

5.8.2 Evaluation of Exponent m_w

The value of exponent m_w is unknown and requires to be determined either experimentally or from a theoretical reasoning. Two conditions on m_w are known, 1) the value of m_w is zero immediately outside the overload plastic zone, 2) it has a maximum value at the beginning of the overload zone and then decays to zero. Thus, if OLR denotes the overload ratio then a factor of the form $(OLR-1)$ or any powers of it, will be involved in the function for evaluation of m_w. The following function was found to give reasonably good results for m_w:

$$m_w = (OLR-1)\left(OLR + \frac{n_0}{OLR}\right). \tag{5.14}$$

In the above function, n_0 is a constant which is independent of the OLR and may depend on the type of material and the pattern of loading. The values of n_0 were obtained for each overload by calibrating against the experimental values of FCGR.

There are other possible forms of above function which can also give the same value for m_w. Some of the functions for m_w are:

$$m_w = (OLR-1)^{\gamma_{0i}}\left(OLR + \frac{n_{oi}}{OLR}\right). \tag{5.15}$$

The values of n_{oi} for corresponding values of OLR are provided in Table 5.1 for

OLR	m_w	n_0	n_{01}	n_{02}	n_{03}	n_{04}	n_{05}
2.5	3.03	-1.2	-2.883	-4.005	-4.75	-5.25	-5.38
2.25	2.92	0.20	-0.857	-1.69	-2.37	-2.909	-3.34
2.15	3.14	1.00	0.482	-0.169	-0.76	-1.266	-1.703
2.00	2.45	0.80	0.80	0.80	0.80	0.80	0.80
1.75	3.00	4.00	6.27	9.38	13.53	19.06	26.43

Table 5.1: Variation in values of n_0 and n_{0i}.

several values of m_w. The γ_{0i} are arbitrary constants, and in Table 5.1, γ_{0i} have been chosen 1 through 5. The values of n_{oi} were also obtained by calibrating against the experimental values.

5.9 Concept of Opening Load Decomposition:

Associated with K^s_{max} is an opening load, because of the plasticity in the wake of the crack, which can be computed for each crack extension. The opening load following the SOL is decomposed into two components, P_{OP1} and P_{OP2}. The value of P_{OP1} is obtained from the CAL history. The second component, P_{OP2}, is an additional part to P_{OP1} after a SOL is applied. The total opening load P_{OP} is given by the following expression:

$$(P_{OP})_i = (P_{OP1})_i + (P_{OP2})_i . \tag{5.16}$$

The value of P_{OP2} is a maximum when the overload is applied and as the crack advances. Outside the overload plasticity range r_f^{SOL}, it vanishes. The magnitude of P_{OP2} within r_f^{SOL} part of the crack extension can be computed as described as follows. Fatigue growth rate with SOL $\left(\frac{da}{dN}\right)_i$, for a given cycle i, using Paris law is:

$$\left(\frac{da}{dN}\right)_i = C\,(\Delta K_{eff} - K^*_{open})_i^m . \tag{5.17}$$

where, (ΔK_{eff}) is the effective stress intensity range and K^*_{open} denotes the second component of the stress intensity factor which is a maximum when the overload is applied and then decays to zero immediately outside the overload zone.

The FCGR may also be obtained from the retardation factor concept. Thus, within the overload plastic zone the following equation applies:

$$\left(\frac{da}{dN}\right)_i = C F_R (\Delta K_{eff})_i^m . \tag{5.18}$$

Since the FCGR is unique for a loading history the eqns(5.17 and 5.18) can be equated and after some simplifications the following equation results:

$$(K^{-}_{open})_i = (\Delta K_{eff})_i \left\{ 1 - \left(\frac{r_f^{CAL}}{r_f^{SOL}} \right)^{\frac{m_w}{m}} \right\}. \tag{5.19}$$

Therefore, in terms of the effective load ΔP_{eff}, the second component of opening load P_{OP2} is as follows:

$$(P_{OP2})_i = (\Delta P_{eff})_i \left\{ 1 - \left(\frac{r_f^{CAL}}{r_f^{SOL}} \right)^{\frac{m_w}{m}} \right\}. \tag{5.20}$$

5.10 Results

The results obtained using the concept of PRI are presented in Figure 5.6. The comparison was made with experimental work of Kumar [89]. The material investigated was 6061-T6-Al-alloy in the form of 180 x 50 x 3 mm thin sheets. The loading pattern is provided in Figure 5.7. The initial physical length of the crack was 6 mm and the geometry of the specimen is single-edge-notched (SEN). For the same geometry a CAL crack propagation study was presented in Section 4.9.3 on a cycle-by-cycle basis. A good agreement was observed between predicted and experimental results. The number of cycles to failure from predicted analysis was within 0.04 % of the experimental value. In Chapter 4 it was shown that a cycle-by-cycle method of evaluation of FCGR gives better results than an assumed crack extension method. In the single overload problems the approach-II was modified to account for single overload which occurred at a crack length of 8 mm for the present set of problems.

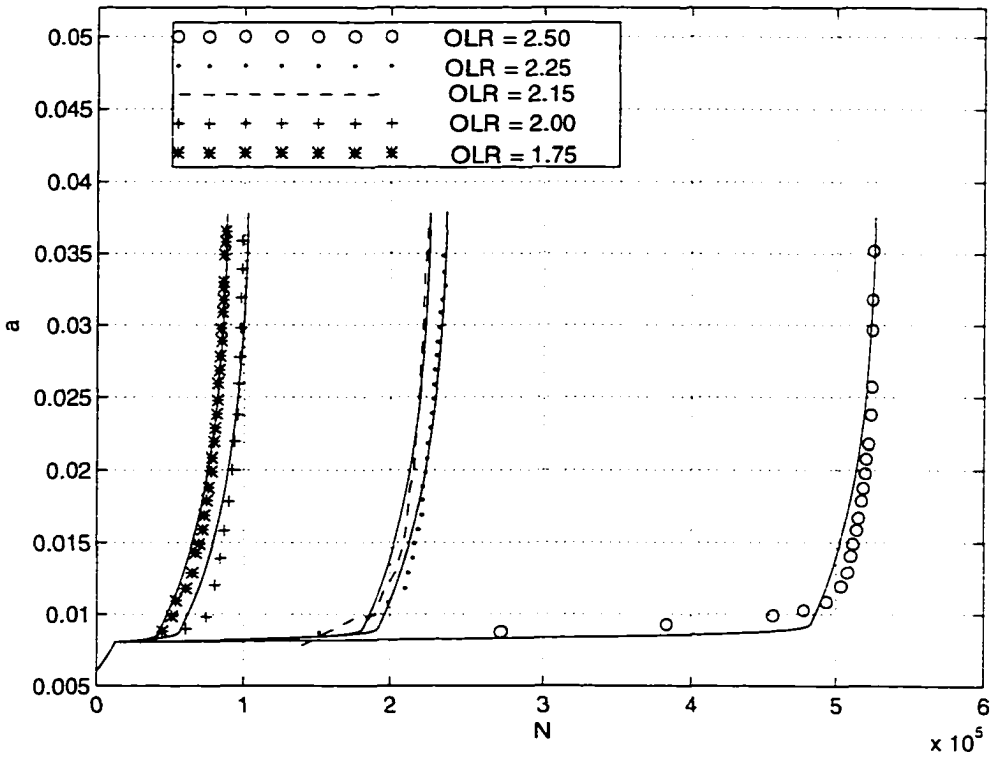

Figure 5.6: Comparison for SOL with experimental work of Kumar [89]. The solid lines represent the predicted values based on current model of plasticity affected ranges for each OLR.

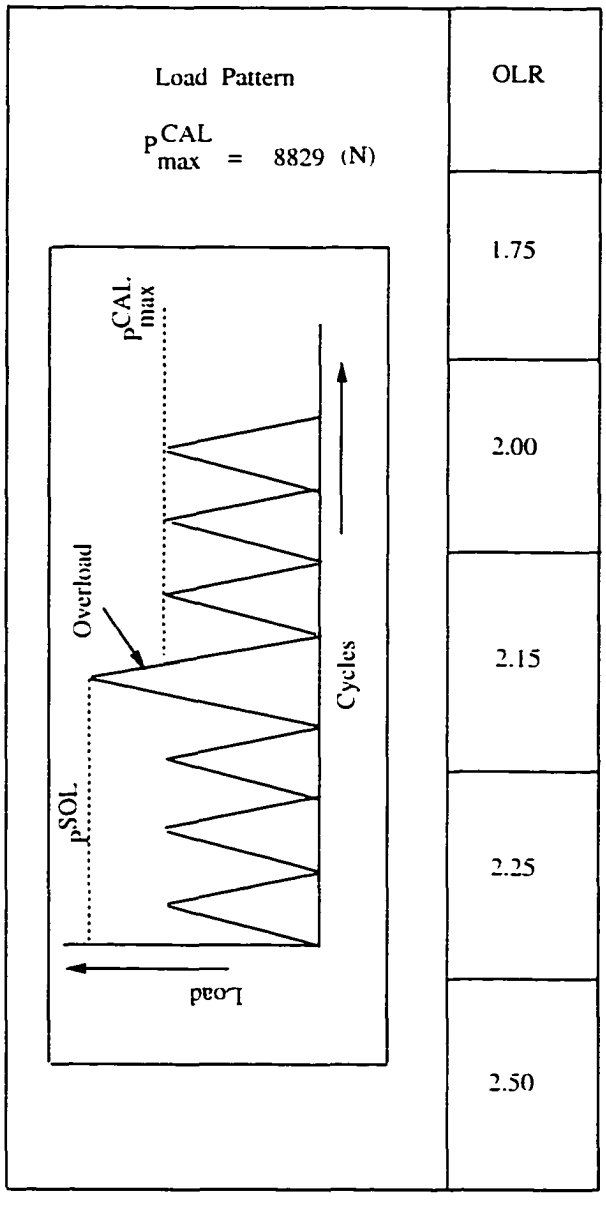

Figure 5.7: The load pattern for comparison with work of Kumar [89].

The results in Figure 5.6. are provided for five different OLR. namely 1.75. 2.00. 2.15. 2.25 and 2.50. It is observed that an increase in magnitude of OLR gives a corresponding increase in the life of the specimen which results from a retarded crack growth rate. The life of the component is increased from a value of 89233 to 526491 as is provided in Table 5.2. In Table 5.2. N_T and N_f is the number of cycles to failure from experiment and theory, respectively. and N_D represents delay cycles because of application of overload. For an $OLR = 2.50$ it would imply that the increase in life of the specimen is approximately 5.9 fold. Also the tabulated values in Table 5.2 provide information regarding the the number of delay cycles (which is the number of cycles a crack spends in the overload plasticity range r_f^{SOL}). N_D. For example. for an $OLR = 2.50$ applied at a crack length of 8 mm. the estimated number of delay cycles $N_D = 482787$. The experimentally determined value of $N_D = 462000$. which is within 4.5 % of the predicted value. The results pertaining to $\frac{da}{dN}$ versus ΔK are presented in Figures 5.8 and 5.9 for $OLR = 2.5$ and $OLR = 2.25$ respectively. Similar results were obtained for other values of OLR and the results are provided in Figures 5.10 and 5.11 respectively. The FCGR is found to significantly decrease during the number of cycles which the fatigue crack spends in the overload plasticity range. which itself is created as a consequence of single overload. There is a fair agreement between the experimental and predicted values of FCGR as is evident from Figures 5.8. 5.9. 5.10 and 5.11. Initially the FCGR decreases with increase in ΔK. while at a further increase in ΔK. there is an increase in FCGR as the CAL condition is approached. It was also observed that a minimum crack growth rate is obtained at the maximum overload ratio of 2.50. Thus, it is clear from this investigation that plasticity range interactions between the overload plasticity range resulting from the single overload and the plasticity range resulting from CAL is responsible for the retardation effect. The number of delay cycles N_D in Table 5.2, are a representative of the time the crack takes to pierce through the overload plasticity range.

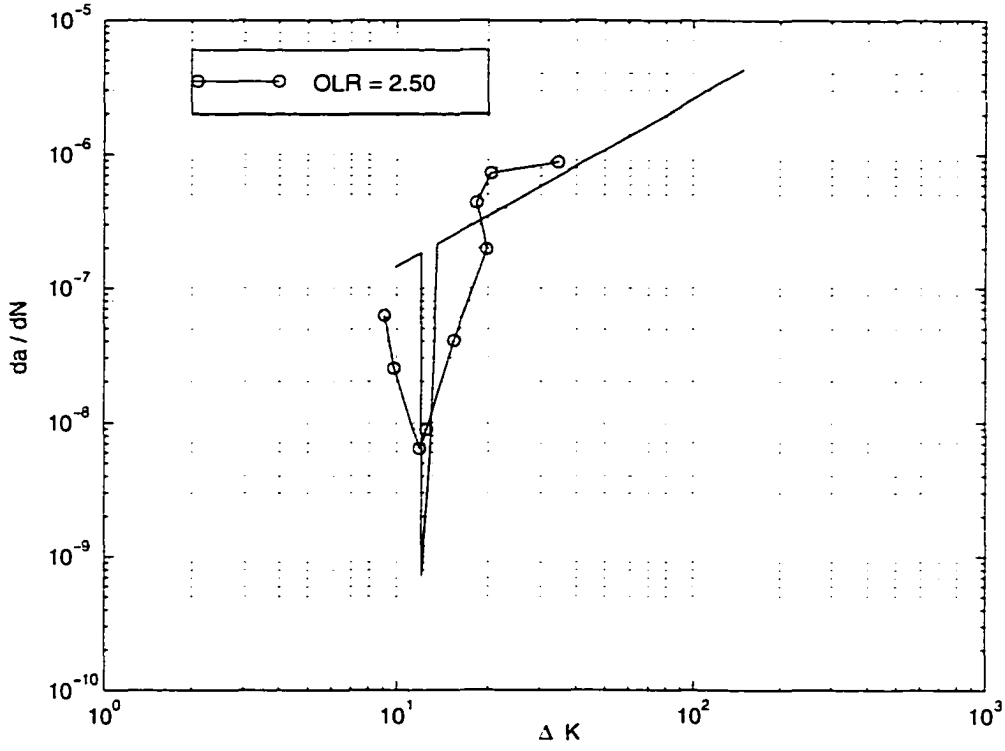

Figure 5.8: FCGR variation w.r.t. stress intensity factor range. The connected hollow rounds represent experimental work [89] and the solid line is the prediction of the model.

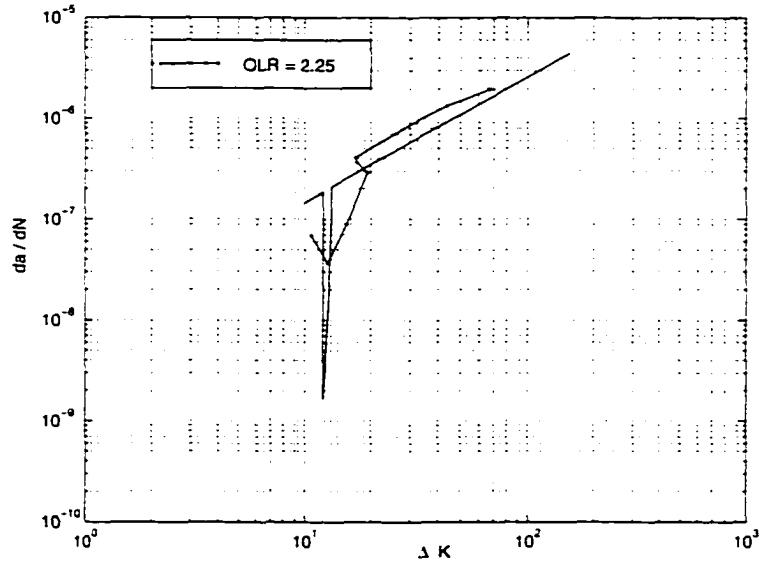

Figure 5.9: FCGR variation w.r.t. stress intensity factor range for $OLR = 2.25$. The connected dotted line represent experimental work [89] and the solid line is the prediction of the model.

5.11 An Interpretation of Results Based on Opening Load Decomposition

The results were also obtained on the basis of opening load decomposition. As shown in the Figure 5.12, the second component of opening load P_{OP2} decays to zero outside the overload plastic zone. So, if the FCGR is modelled by incorporation of the decomposition concept of opening loads instead of the retardation concept, similar results are obtained. This is an equivalent way of accounting for the retardation effect accompanying a single overload. It is indicated in Figure 5.12 that for the maximum value of $OLR = 2.5$ the value of P_{OP2} is maximum, and it takes the respective delay cycles N_D to decay to zero.

A direct comparison with experimental work regarding the second component of

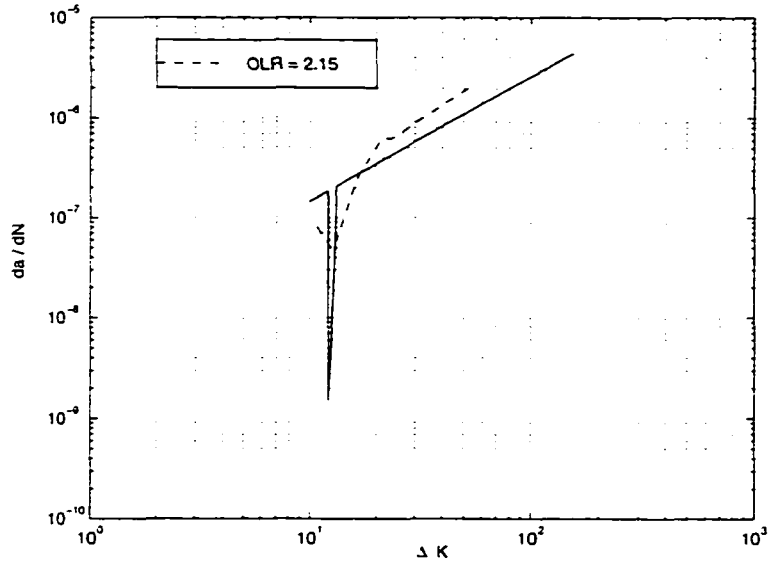

Figure 5.10: FCGR variation w.r.t. stress intensity factor range for $OLR = 2.15$. The dashed line represents experimental work [89] and the solid line is the prediction of the model.

opening load is provided by another example in which a comparison is made with a recent reference of Yisheng and Schijve [107]. In this example, which was chosen to demonstrate the use of the new concept of opening load decomposition, a sheet specimen of 2024-T3 with a central crack is considered. The width and thickness of the specimen was 105 mm and 6.35 mm respectively. In Figure 5.13, the FCG is shown, with the overload ($\sigma_{max}^{SOL} = 200.MPa$) being inserted in CAL ($\sigma_{max}^{CAL} = 100.MPa$ and $\sigma_{min}^{CAL} = 0.0.MPa$) after 76000 cycles. The delayed fatigue crack growth is obvious after the overload is applied. The corresponding crack opening stress is provided in Figure 5.14. Except for the value of crack opening stress just after the overload is applied, the agreement between experiment and prediction based on the current model is reasonable. This anomalous behavior was attributed to crack-tip blunting by Yisheng and Schijve [107]. Since the effect of blunting is not considered by the present model that focus is on the interaction of plasticity ranges, this probably is

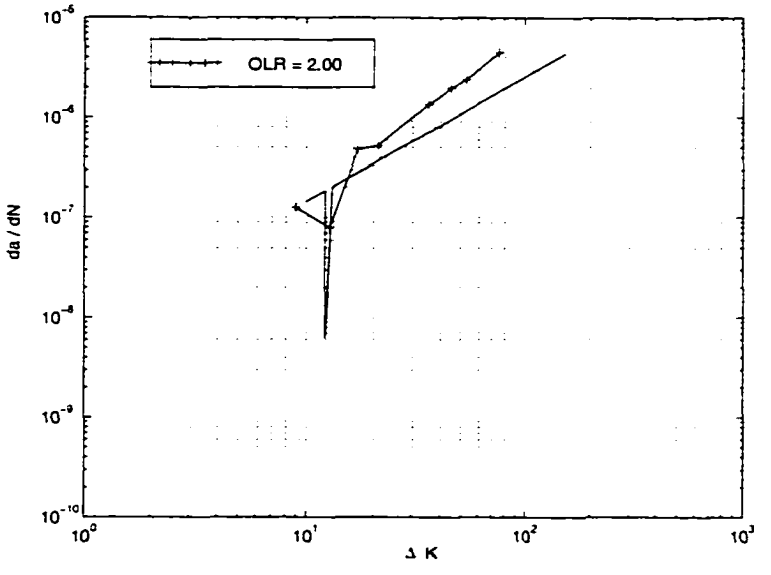

Figure 5.11: FCGR variation w.r.t. stress intensity factor range for $OLR = 2.0$. The connected '+' line represent experimental work [89] and the solid line is the prediction of the model.

the cause. The zones outside the overload effected region basically represent CAL.

In this example, for CAL regions, there is a fair amount of disagreement between theory and experiment because of crack opening displacement (COD) meter position in the investigation of Yisheng and Schijve [107], and their selection of method-III. The tabulated results as presented in [107] and are reproduced here in Table 5.3. They show a very high scatter. In Table 5.3 the method-I is based on the intersection of two tangent lines to upper and lower parts of the P-COD curve. The fatigue crack opening stress is defined as the intersection point of the tangent lines. The method-II is based on the variation of slope. The method-III is based on simulating the upper part as a linear function and the lower part as a second order polynomial. For a CAL situation, a thorough study of the effects of the COD meter on fatigue crack opening stress is provided in [107]. It is obvious that the values of fatigue crack opening

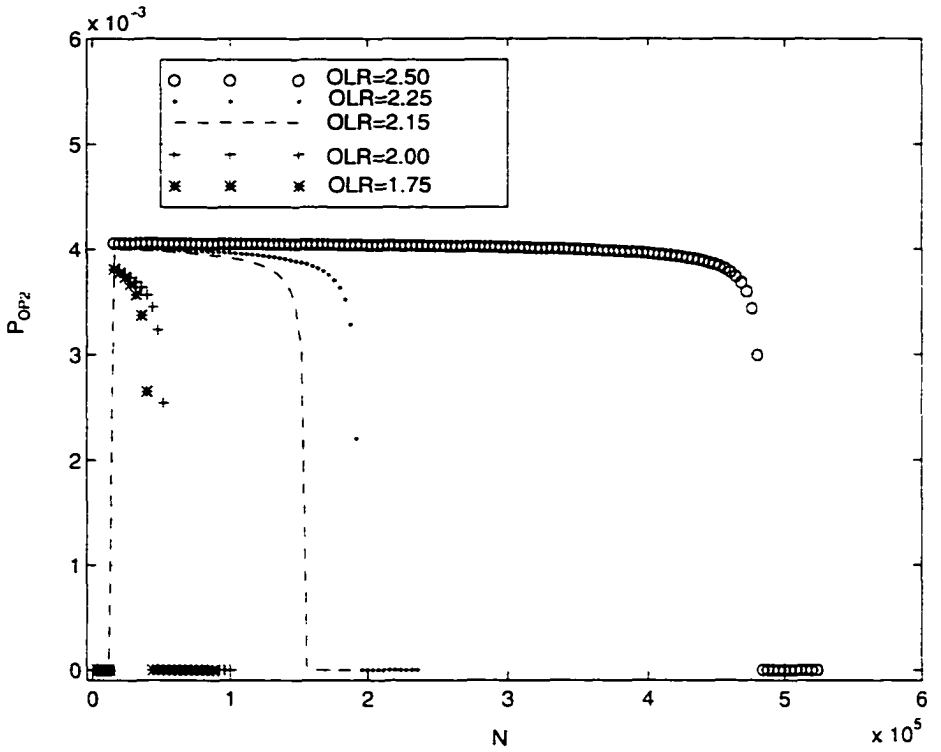

Figure 5.12: Second component of opening loads P_{OP2}.

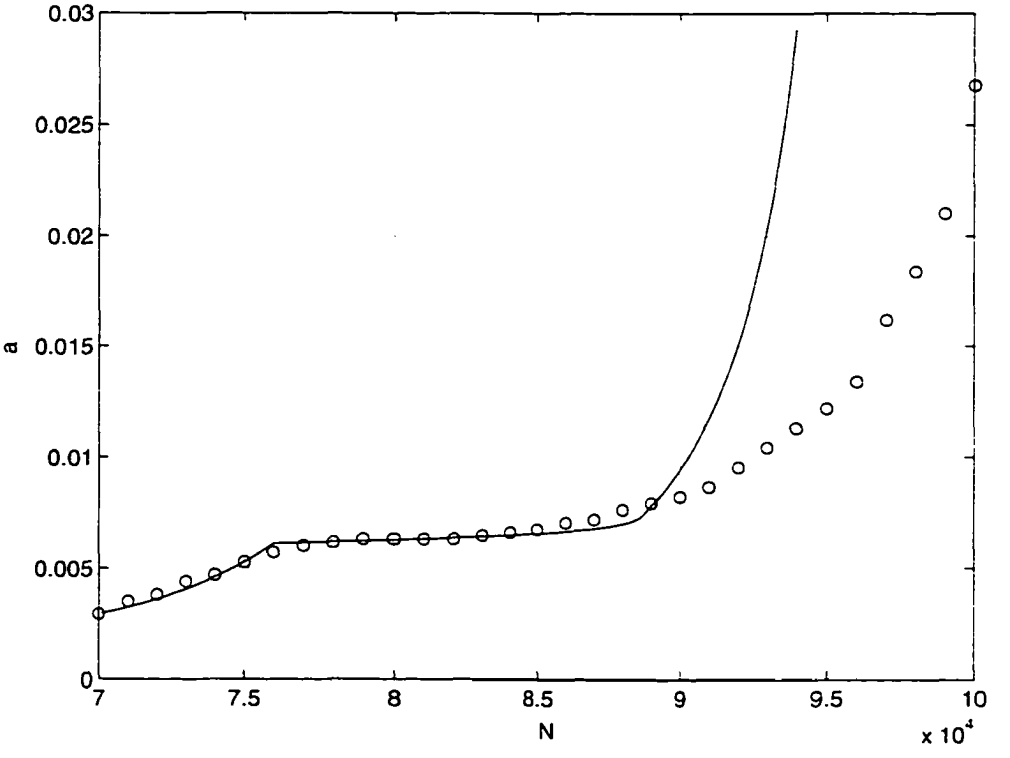

Figure 5.13: Fatigue crack length versus number of cycles. The hollow rounds represent experimental work of Yisheng and Schijve [107]. solid line is the prediction of the model.

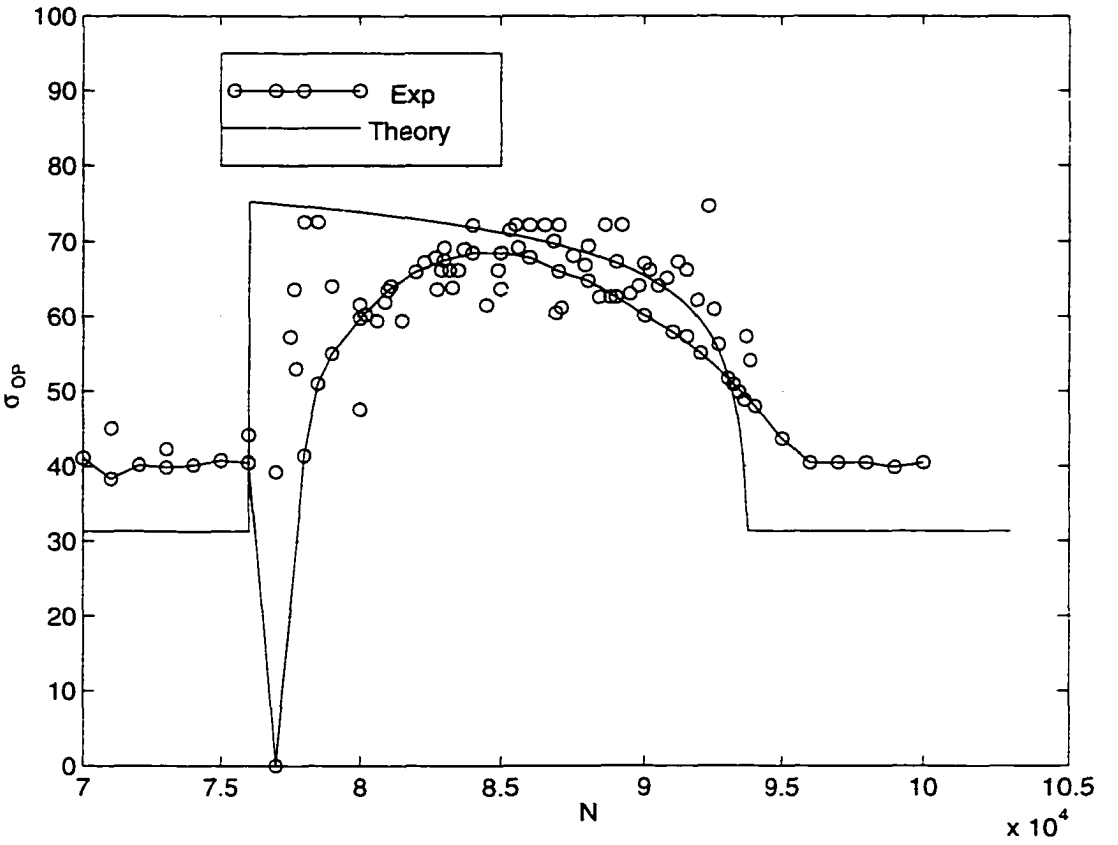

Figure 5.14: The decomposition of opening stresses, a comparison with experimental work of Yisheng and Schijve [107].

stress are not affected by the location of measurement for method-I and method-III. However, it is noticed in [107] that the values from method-II and method-III are higher than their corresponding values from method-I. Therefore, [107] discarded method-I and selected method-III for their final results. In the research reported here, it was noticed that predicted values under CAL are very close to method-I.

5.12 Discussion

Two different methods of accounting for the retardation effect on FCGR problems have been presented. The first method is based on the retardation factor obtained on the basis of the interaction of plasticity ranges, which occurs as a result of an overload application. The second method is based on opening load decomposition, in which the fatigue crack opening stress is divided into two portions, the first portion occurs under CAL, while the second portion results as a consequence of applied overload. The second portion on the basis of predicted values is a maximum immediately after the application of overload and then decays to zero. The aspect of its maximum value immediately after the overload is contrary to experimental findings, where it is momentarily zero and then rises suddenly to decay to zero outside the overload plasticity range as shown in Figure 5.14. The value of m_w for this method of decomposition was obtained from the first example which was based on comparison with Kumar [89].

The evaluation of m_w was performed by calibrating the theoretical results against the experimental values until a best match was observed, as shown for $OLR = 2.5$, in Figure 5.15. Similarly, for other values of OLR corresponding values of n_0 were obtained. The value of m_w was deduced based on the information regarding n_0. In this way the values of m_w were obtained for each OLR value. Finally, a polynomial was fitted to m_w. This is shown in Figure 5.17. Since there are other possible values

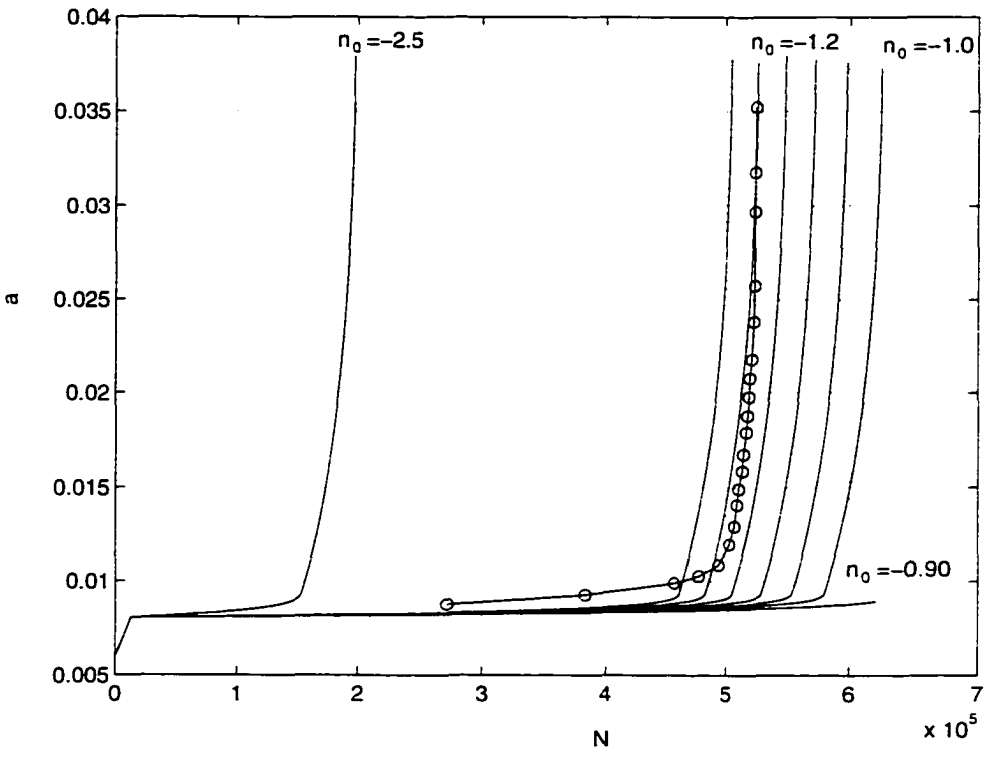

Figure 5.15: Example of calibration for various values of n_0. The hollow rounds represent experimental values for an $OLR = 2.5$. Kumar [89].

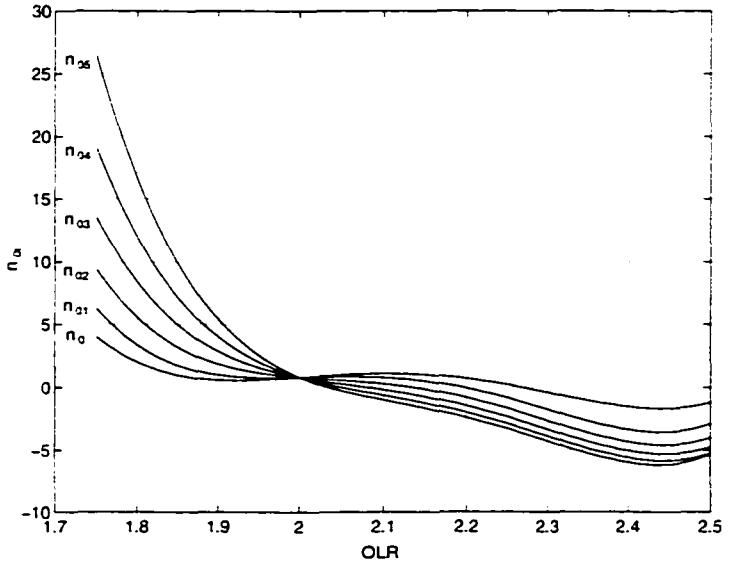

Figure 5.16: n_{0i} versus OLR.

of n_{oi} that lead to the same value of m_w, the corresponding families of n_{oi} are provided in Figure 5.16 for various values of OLR. Some of the values so obtained for n_{oi} are provided in Table 5.1 along with the corresponding values of m_w. The dependence of delay cycles N_D, and the life of the specimen N_f is provided in Table 5.4. For this research, the best matching of the experimental results with predicted values, was the criteria for selecting m_w. The Table 5.4 is for an overload ratio of $OLR = 2.5$. Similar results were obtained for other OLR for m_w.

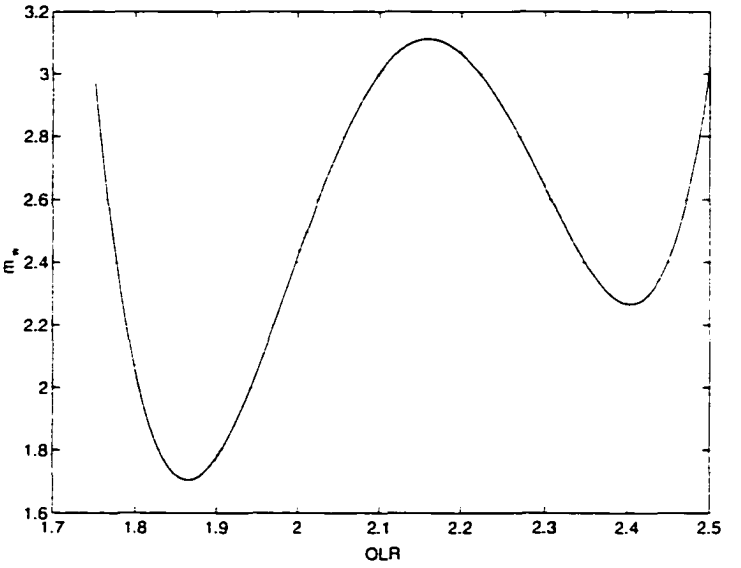

Figure 5.17: Exponent m_w versus OLR.

OLR	N_f	N_D	N_T	$\frac{N_f}{N_T}$
2.50	526491	482787	524720	1.00337
2.25	238104	192977	233770	1.01853
2.15	200562	154896	225960	0.8875
2.00	100319	53876	100210	1.00108
1.75	89233	41594	89440	0.9976

Table 5.2: N_f, N_D and N_T values for various values of OLR.

Position of COD meter	Method-I	Method-II	Method-III
Center	33.10 ± 2.59	33.90±2.12	45.00 ± 3.19
4.0 mm behind tip	34.90 ± 1.87	41.30±0.64	44.10 ± 2.02
2.5 mm behind tip	34.00 ± 2.19	44.40±1.62	45.90 ± 3.01
1.0 mm behind tip	34.00 ± 2.61	44.50±2.11	44.80 ± 7.10

Table 5.3: Crack opening stress obtained by Yisheng and Schijve from three different methods [107].

m_w	n_0	N_f	N_D	$\frac{N_f}{N_D}$	$\frac{N_f}{N_T}$
3.03	-1.0	624358	580654	1.0752	1.18
3.12	-1.05	598084	554380	1.0788	1.139
3.09	-1.10	573054	529350	1.0825	1.092
3.06	-1.15	549209	505505	1.0864	1.046
3.03	-1.20	526491	482787	1.0905	1.003
3.00	-1.25	504847	461142	1.0947	0.962
2.25	-2.50	197411	153706	1.2843	0.370

Table 5.4: N_D and N_f values for various values of m_w during calibration with experimental work of Kumar [89], for an $OLR = 2.5$.

Chapter 6

CONCLUSIONS

6.1 General Conclusions

Fatigue life prediction of a specimen or a structure is a function of many variables, including stress level, flaw size, environment, geometry, loading history and metallurgical condition of the material. Small changes in the specimen or test conditions can significantly affect fatigue behavior. One such condition is the loading history. Several phenomenon occur as *a posteriori* evidence of an overload, which include the retardation on crack growth, spike-dip in FCGR and crack closure. Life prediction models are typically complicated by these issues, and accuracy and cost of computation. Also, the PSS/PSN transition, plasticity zone formation, striation spacings and shear lip formation add to these complicacies. The objectives of this thesis were intended to address some of the issues pertaining to the loading history.

The results presented in Chapters 2, 4 and 5 demonstrate that the objectives of the present study, as summarized in Section 1.6 were accomplished. Detailed study of crack-tip plasticity was presented in Chapter 2; the issue of plasticity zone shape

was discussed in detail. It was shown that an increase in Poisson's ratio, ν, and load ratio, ε, have opposite effects on the size of the plasticity zone; ν has shrinkage effects while ε has swelling effects. Furthermore, it was shown, with the help of shape ratio, β, that the use of Dugdale's model [21] for modelling fatigue crack-tip plasticity is contradictory to various experimental findings. Consequently, it was demonstrated how assuming plasticity zone of vanishingly small heights can be resolved by adopting new approach. In this approach, plasticity affected range, R_P, the dimension of plasticity zone on which load interaction effects should be based, was identified.

The effective stress intensity factor range ΔK_{eff} based calculations were presented in Chapter 4, and some closure models were tested for fatigue crack growth under CAL situations. It was shown that for fatigue crack growth and FCGR calculations, incorporation of closure stress intensity factors from the model of Newman [57] give results in agreement with the experimental results. It also gives opening loads under both PSS and PSN situations on the basis of, α, the plasticity constraint factor. Furthermore, the B & H model for closure under PSS, and the L & G model for PSN were also investigated for FCGR under CAL. It was found that incorporation of the closure stress intensity factors from the B & H model into fatigue crack growth calculations based on Paris law give conservative results for the number of cycles to failure compared with Newman's fully PSS condition. A thorough comparison with several experimental results showed a good agreement between predictions and experimental results based on Paris law with modification for effective stress intensity factor range, ΔK_{eff}. Chapter 4 also presents an evaluation of errors in FCGR calculations that can occur on the basis of the assumed crack extension method under CAL. A detailed design example was chosen to account for this particular aspect.

In Chapter 5 a model for predicting the life of components subjected to single overloads was presented. The model provides prediction capability with good precision

for variable magnitude, single overload situations. The three different characteristics which accompany an overload situation namely, retarded fatigue growth, a special trend in closure stress, and the spike-dip in FCGR, have been explained using a simple model based on a suppression factor obtained on the basis of plasticity affected ranges (details are presented in Chapter 2). The effect of opening loads under SOL was discerned by decomposition into two components. By subtracting the opening loads that result under CAL from an SOL type of loading following overloads, the change in opening loads that results from application of overloads was obtained by equating the FCGR obtained from this approach with that of retardation factor approach. Simulations were compared with experimental results. The results indicate excellent agreement for FCG, FCGR and a fair agreement for the closure loads within the overload zone. The momentary phenomena of spike-dip in closure loads is not appearing in the results. This is attributed to crack-tip blunting.

It has been shown that the overload plasticity affected range, r_f^{SOL}, and its interaction with the current plasticity affected range, r_f^{CAL}, is responsible for the retardation effect. This effect lasts while the crack-tip is within the overload plasticity affected range and then vanishes immediately outside the overload zone. It has been demonstrated that the concept of plasticity affected range interaction and effective stress intensity approaches are equivalent ways of accounting for retardation effects.

6.2 Recommendations for Future Work

This study provides foundation work, which can be used in future studies with variable amplitude loads. The load interaction effects for a spectrum loading can be simulated on similar lines as is discussed in this thesis for an SOL problem. These loading situations are typically complicated due to selection of opening load model on one

hand and the three dimensional aspect of PSS/PSN transition, on the other.

The load interaction effects provide a severe test for plasticity models and effective stress intensity factor range approach. The prediction of the life of components subjected to variable amplitude loads, with provision for obtaining closure loads, by incorporating the present model for accounting for plasticity effects will extend this hybrid model to such loading situations as, multiple overloads, programmed block loads, and finally to random loading.

References

[1] Suresh, S., *Fatigue of Materials*, Cambridge University Press, New York, 1991.

[2] N. Shute N., *No Highway*, William Heinemann Ltd. London, 1959.

[3] Smith R. A., "Thirty Years of Fatigue Crack Growth -An Historical Review in Fatigue Crack Growth 30 Years of Progress," *Proceedings of a Conference on Fatigue Crack Growth Cambridge, UK*, 20th September, 1984.

[4] Hertzberg, R. W., *Deformation and Fracture Mechanics of Engineering Materials, Fourth Edition*, Wiley, New York, 1996.

[5] Rolfe, S. T., and Barsom, J. M., *Fracture and Fatigue Control in Structures, Applications of Fracture Mechanics*, Prentice-Hall, New Jersey, 1987.

[6] Parton, V. Z., *Fracture Mechanics from Theory to Practice*, Translated from Russian by Lucia Man, Gordon and Breach Science Publishers, Philadelphia, 1992.

[7] Timoshenko, S. P., *History of Strength of Materials*, McGraw-Hill Book Company, New York, 1953.

[8] Provan, J. W., "An Introduction to Fatigue," *Journal of Materials Education*, Vol. 11, No. 1 and 2, pp. 1-104, 1989.

[9] Paris, P. C., Gomez, M. P., and Anderson, W. P., "A Rational Analytic Theory of Fatigue," *The Trend in Engineering*, Vol. 13, pp. 9-14, 1961.

[10] Provan, J. W., "An Introduction to Fracture Mechanics," *Journal of Materials Education*, Vol. 10, No. 4, pp. 331-428, 1988.

[11] Irwin, G. R., *Handbuch der Physik*, Vol. VI, S. Flügge, *ed.*, Springer, pp. 551-590, 1958.

[12] Irwin, G. R., "Fracture Mechanics," *Structural Mechanics: Proceedings, Goodier, J. N., and Hoff, N. J., eds.*, Pregamon Press, New York, pp. 557-594, 1958.

[13] Elber, W., *Fatigue Crack Propagation: Some Effects of Crack Closure on the Mechanism of Fatigue Crack Propagation Under Cyclic Tension Loading*, PhD Dissertation, University of New South Wales, 1968.

[14] Gangloff, R. P., Piascik, R. S., Dicus, D. L., and Newman, Jr., J. C., "Fatigue Crack Propagation in Aerospace Aluminum Alloys," *Journal of Aircraft*, Vol. 31, No. 3, May-June, 1994.

[15] Broek, D., *The Practical Use of Fracture Mechanics*, Kluwer Academic Publishers, Netherlands, pp. 1-21, 1989.

[16] Westergaard, H. M., "Bearing Pressures and Cracks," *Journal of Applied Mechanics*, Vol. 61, pp. A49-53, 1939.

[17] Hellen, K., *Introduction to Fracture Mechanics*, McGraw-Hill Book Company, New York, 1984.

[18] Irwin, G. R., "Analysis of Stresses and Strains Near the End of a Crack Traversing a Plate," *Journal of Applied Mechanics*, Vol. 24, pp. 361-364, 1957.

[19] Harlin, G., and Willis, J. R., "The Influence of Crack Size on Ductile-Brittle Transition," *Proceedings of Royal Society of London*, Vol. A 415, pp. 197-226, 1988.

[20] Hauf, D. E., Parks, D. M., and Lee, H., "A Modified Effective Crack-Length Formulation in Elastic-Plastic Fracture Mechanics," *Mechanics of Materials*, Vol. 20, pp. 273-289, 1995.

[21] Dugdale, D. S., "Yielding of Steel Sheets Containing Slits," *Journal of the Mechanics and Physics of Solids*, Vol. 8, pp. 100-108, 1960.

[22] Tada, H., Paris, P. C., and Irwin, G. R., "The Stress Analysis of Cracks Handbook (2nd. ed.)," *Del Research Corporation*, Saint Louis, MO, 1985.

[23] Hutchinson, J. W., "Plastic Stress and Strain Fields at a Crack Tip," *Journal of Mechanics and Physics of Solids*, Vol. 16, pp. 337-347, 1968.

[24] Rice, J. R., and Rosengren G. F., "Plane Strain Deformation Near a Crack Tip in a Power-Law Hardening Material," *Journal of Mechanics and Physics of Solids*, Vol. 16, pp. 1-12, 1968.

[25] Edmunds, T. M., and Willis, J. R., "Matched Asymptotic Expansions in Nonlinear Fracture Mechanics-III. In-Plane Loading of an Elastic Perfectly Plastic Symmetric Specimen," *Journal of Mechanics and Physics of Solids*, Vol. 25, pp. 423-455, 1977.

[26] Sham, T. L., "A Finite-Element Study of the Asymptotic Near-Tip Fields for Mode I Plane-Strain Cracks Growing Stably in Elastic-Ideally Plastic Solids, in: Shih, C. F., and Gudas, J. P., *eds.*," *Elastic-Plastic Fracture: Second Symposium*, Volume I - *Inelastic Crack Analysis*, *ASTM STP 803*, *American Society for Testing and Materials* pp. I-52-I-79, 1984.

[27] Hilton, P. D., and Hutchinson, J. W., "Plastic Intensity Factors for Cracked Plates," *Engineering Fracture Mechanics*, Vol. 3, pp. 435-451, 1971.

[28] Larsson, S. G., and Carlsson, A. J., "Influence of Non-Singular Stress Terms and Specimen Geometry on Small Scale Yielding at Crack Tips in Elastic-Plastic Material," *Journal of Mechanics and Physics of Solids*, Vol. 21, pp. 263-277, 1973.

[29] Williams, M. L., "On the Stress Distribution at the Base of Stationary Crack," *Journal of Applied Mechanics*, Vol. 24, pp. 109-114, 1957.

[30] Leevers, P. S., and Radon, J. C., "Inherent Stress Biaxiality in Various Fracture Specimen Geometries," *International Journal of Fracture*, Vol. 19, pp. 311-325, 1982.

[31] Rice, J. R., "Limitations to the Small Scale Yielding Approximation for Crack Tip Plasticity," *Journal of Mechanics and Physics of Solids*, Vol. 22, pp. 17-26, 1974.

[32] Betegon, C., and Hancock, J. W., "Two-Parameter Characterization of Elastic-Plastic Crack-Tip Fields," *Journal of Applied Mechanics*, Vol. 58, pp. 104-110, 1991.

[33] Shih, C. F., O Dowd, N. P., and Kirk, M. T., "A Framework for Quantifying Crack Tip Constraint," in: Hackett, E. M., Schwalbe, K. H., and Dodds, R. H., *eds.*, *Constraint Effects in Fracture*, *ASTM STP 1171*, *American Society for Testing and Materials*, Philadelphia, pp. 2-20, 1993.

[34] Wang, Y. Y., and Parks, D. M., "Evaluation of the Elastic T-Stress in Surface-Cracked Plates Using the Line-Spring Method," *International Journal of Fracture*, Vol. 56, pp. 25-40, 1992.

[35] Hollister, S. C., "Experimental Study of Stresses at a Crack in a Compression Member," *Proceedings of the American Concrete Institute*, Vol. 30, pp. 361-365, 1934.

[36] Post, D., "Photoelastic Stress Analysis for an Edge Crack in a Tensile Field," *Proceedings of the Society for Experimental Stress Analysis*, Vol. 12, No. 1, pp. 99-116, 1954.

[37] Hahn, G. T., and Rosenfield, R. A., "Plastic Zones Generated by Cracks Growing Under Load," *The International Journal of Fracture Mechanics*, Vol. 4, No. 2, pp. 79-88, 1968.

[38] Hahn, G. T., Sarrate, M., and Rosenfield, R. A., "Plastic Zones in Fe-3Si Steel Double-Cantilever-Beam Specimens," *The International Journal of Fracture Mechanics*, Vol. 7, No. 4, pp. 435-446, 1971.

[39] Wilson, W. K., "Geometry and Loading Effects on Elastic Stresses at Crack Tips," Westinghouse Research Report 67-1D7-BTLPV-R1 Properietary Class 3, July 3, 1967.

[40] Loye, C., Bathias, C., Retali, D., Devaux, J. C., "The Plastic Zone Ahead of a Fatigue Crack in 316 Stainless Steel," *Fatigue Mechanisms: Advances in Quantitative Measurement of Physical Damage, ASTM STP 811, American Society for Testing and Materials*, pp. 427-444, 1983.

[41] Ranganathan, N., Jendoubi, K., and Merah, N., "Experimental Characterization of the Elastic-Plastic Strain Fields at the Crack Tip due to Cyclic Loading," *Transactions of the ASME, Journal of Engineering Materials and Technology*, Vol. 116, pp. 187-192, 1994.

[42] Csizmazia, A., and Czoboly, E., "Determination of Plastic Zones in Compact Specimens of Aluminium," *Theoretical and Applied Fracture Mechanics*, Vol. 8, pp. 11-19, 1987.

[43] Tuba, I. S., "A Method of Elastic-Plastic Plane Stress and Strain Analysis," *Journal of Strain Analysis*, Vol. 1, pp. 115-120, 1966.

[44] Swedlow, J. L., "Elasto-PLastic Cracked Plates in Plane Strain," *International Journal of Fracture Mechanics*, Vol. 5, pp. 33-44, 1969.

[45] Ayres, D. J., "A Numerical Procedure for Calculating Stress and Deformation Near a Slit in a Three-Dimensional Elastic-Plastic Solid," *Engineering Fracture Mechanics*, Vol. 2, pp. 87-106, 1970.

[46] Head, A. K., "On the Growth of Fatigue Cracks." *The Philosophical Magazine*, 44(7c), pp. 725, 1953.

[47] Liu, H. W., *Crack Propagation in Thin Metal Sheet Under Repeated Loading*. PhD Dissertation, Department of Theoretical and Applied Mechanics, University of Illinois, Urbana, IL, 1959.

[48] Liu, H. W., "Fatigue Crack Propagation and Applied Stress Range." *Transactions of the ASME, Journal of Basic Engineering*, Vol. 85 D (1), pp. 116-122, 1963.

[49] Paris, P. C., and Erdogan, F., "A Critical Analysis of Crack Propagation Laws." *Transactions of the ASME, Journal of Basic Engineering*, Vol. 85D (4), pp. 528-534, 1963.

[50] Paris, P.C., *The Growth of Cracks Due to Variations in Loads*, PhD Dissertation, Bethelhem: Lehigh University, 1960.

[51] Rice, J. R., "Mechanics of Crack Tip Deformation and Extension by Fatigue." In *Fatigue Crack Propagation, ASTM STP 415, American Society for Testing and Materials*, pp. 247-311, 1967.

[52] Hahn, G. T., Hoagland, R. G., and Rosenfield, A. R., "Local Yielding Attending Fatigue Crack Growth." *Metallurgical Transactions*, 3A, pp. 1189-1202, 1972.

[53] Jones, R. E., "Fatigue Crack Growth Retardation After Single-Cycle Peak Overload in Ti-6Al-4V Titanium Alloy." *Engineering Fracture Mechanics*, Vol. 5, pp. 585-604, 1973.

[54] Budiansky, B., and Hutchinson, J. W., "Analysis of Closure in Fatigue Crack Growth." *Journal of Applied Mechanics, Transactions of the ASME*, Vol. 45, pp. 267-276, 1978.

[55] Glinka, G., "A Cumulative Model of Fatigue Crack Growth." *International Journal of Fatigue*, pp. 59-67, 1982.

[56] Liu, H. W., "A Review of Fatigue Crack Growth Analyses." *Theoretical and Applied Fracture Mechanics*, Vol. 16, pp. 91-108, 1991.

[57] Newman, J. C., "A Crack Opening Stress Equation for Fatigue Crack Growth." *International Journal of Fracture*, Vol. 24, pp. 131-135, 1984.

[58] Elber, W., "Fatigue Crack Closure Under Cyclic Tension." *Engineering Fracture Mechanics*, Vol. 2, pp. 37-45, 1970.

[59] Vasudeven, A. K., Sadananda, K., and Lout, N., "A Review of Crack Closure, Fatigue Crack Threshold and Related Phenomena: Invited Review," *Materials Science and Engineering*, Vol. A188, pp. 1-22, 1994.

[60] Majid, M., *On Fatigue Crack Closure Analysis and Measurement*, PhD Dissertation, McGill University, Montreal, Canada, 1991.

[61] McEvily, A. W., "On Crack Closure in Fatigue Crack Growth," *Mechanics of Fatigue Crack Closure*, ASTM STP 982, Newman, J. C., Jr., and Elber, W., *eds.*, American Society for Testing Materials, Philadelphia, pp. 35-43, 1988.

[62] Ritchie, R. O., Weikang, Y., and Bucci, R. J., " Fatigue Crack Propagation in ARALL Laminates : Measurement of the Effect of Crack-Tip Shielding from Crack Bridiging," *Engineering Fracture Mechanics*, Vol. 32, No. 3, pp. 361-377, 1989.

[63] Ritchie, R. O., "Mechanisms of Fatigue Crack Propagation in Metals, Ceramics and Composites: Role of Crack Tip Shielding," *Materials Science and Engineering*, A103, pp. 15-28, 1988.

[64] Schijve, J., "Fatigue Crack Closure: Observations and Technical Significance," *Mechanics of Fatigue Crack Closure*, ASTM STP 982, Newman, J. C., Jr. and Elber, W., *eds.*, American Society for Testing Materials, Philadelphia, pp. 5-34, 1988.

[65] Newman, J. C. Jr., "Fatigue-Life Prediction Methodology using a Crack-Closure Model," *Journal of Engineering Materials and Technology*, Transactions of the ASME, Vol. 117, No. 4, pp. 433-439, 1995.

[66] Morris, W. L., "The Noncontinuum Crack Tip Deformation Behavior of Surface Microcracks," *Metallurgical Transactions*, 11 A, pp. 1117-1123, 1980.

[67] Telesman, J., and Fisher, D. M., "Influence of Fatigue Crack Wake Length and State of Stress on Crack Closure," *Mechanics of Fatigue Crack Closure*, ASTM STP 982, pp. 568-582, 1988.

[68] Lindley, T. C., and Richards, C. E., "The Relevance of Crack Closure to Fatigue Crack Propagation," *Materials Science and Engineering*, Vol. 14, pp. 281-293, 1974.

[69] McEvily, A., J., and Yang, Z., " Fatigue Crack Growth Retardation Mechanisms after Single and Multiple Overloads," *Fatigue 90*, 1990.

[70] Dill, H. D., and Saff, C. R., "Analysis of Crack Growth Following Compressive High Loads Based on Crack Surface Displacements and Contact Analysis," *MCAIR 76-006, McDonnell Aircraft Co.*, 1976.

[71] Führing, H., and Seeger, T., "Dugdale Crack Analysis of Fatigue Cracks Under Constant Amplitude Loading," *Engineering Fracture Mechanics*, Vol. 11, No. 1, pp. 99-122, 1979.

[72] Newman, J. C. Jr., "A Crack Closure Model for Predicting Fatigue Crack Growth Under Aircraft Spectrum Loading," *Methods and Models for Predicting Fatigue Crack Growth Under Random Loading, ASTM STP 748, Chang, J. B., and Hudson, C. M.*, eds., American Society for Testing and Materials, pp. 53-84, 1981.

[73] McClung, R. C., and Sehitoglu, H., "On the Finite Element Analysis of Fatigue Crack Closure-1, Basic Modeling Issues," *Engineering Fracture Mechanics*, Vol. 33, No. 2, pp. 237-252, 1989.

[74] McClung, R. C., and Sehitoglu, H., "On the Finite Element Analysis of Fatigue Crack Closure-2, Numerical Results," *Engineering Fracture Mechanics*, Vol. 33, No. 2, pp. 253-272, 1989.

[75] Newman, J. C. Jr., *Finite-Element Analysis of Fatigue Crack Propagation-Including the Effects of Crack Closure*, PhD Dissertation, Virginia Polytechnique Institute and State University, Blacksburg, VA, May, 1974.

[76] Fleck, N. A., "Finite Element Analysis of Plasticity Induced Crack Closure Under Plane Strain Conditions," *Engineering Fracture Mechanics*, Vol. 25, No. 4, pp. 441-449, 1986.

[77] Chermahini, R. G., Shivakumar, K. N., Newman, J. C., and Blom, A. F., "Three-dimensional Aspects of Plasticity -Induced Fatigue Crack Closure," *Engineering Fracture Mechanics*, Vol. 34, pp. 393-402, 1989.

[78] Llorca, J., and Gálvez, V. S., "Modelling Plasticity-Induced Fatigue Crack Closure," *Engineering Fracture Mechanics*, Vol. 37, No. 1, pp. 185-196, 1990.

[79] Ward-close, C. M., Blom, A. F., and Ritchie, R. O., "Mechanisms Associated with Transient Fatigue Crack Growth Under Variable-Amplitude Loading: An Experimental and Numerical Study," *Engineering Fracture Mechanics*, Vol. 32, No. 4, pp. 613-638, 1989.

[80] Phillips, E. P., "Results of the Round Robin on Opening Load Measurement Conducted by ASTM Task Group E24.04.04 on Crack Closure Measurement and Analysis," *NASA Langely Research Center*, NASA TM 101601, Hampton, VA, 1989.

[81] Phillips, E. P., "Results of the Second Round Robin on Opening Load Measurement Conducted by ASTM Task Group E24.04.04 on Crack Closure Measurement and Analysis," *NASA Langely Research Center*, NASA TM 109032, Hampton, VA, 1993.

[82] Kumar, R., "Review on Crack Closure for Constant Amplitude Loading in Fatigue," *Engineering Fracture Mechanics*, Vol. 42, No. 2, pp. 389-400, 1992.

[83] Wu, S., Mai, Y., and Cottrell, B., "A Model of Fatigue Crack Growth Based on Dugdale Model and Damage Accumulation," *International Journal of Fracture*, Vol. 57, pp. 253-267, 1992.

[84] Hertzberg, R. W., "On the Calculation of Closure-Free Fatigue Crack Propagation Data in Monolithic Metal Alloys," *Materials Science and Engineering*, Vol. A 190, pp. 25-32, 1995.

[85] Farhangdoost, K., *On the Fatigue Reliability Assessment of Ti-6Al-4V*, PhD Dissertation, McGill University, Montreal, Canada, 1994.

[86] Zhang, S., Marissen, R., Schulte, K., Trautmann, K. K., Nowak, H., and Schijve, J., "Crack Propagation Studies on Al 7475 on the Basis of Constant Amplitude and Selective Variable Amplitude Loading Histories," *Fatigue and Fracture of Engineering Materials and Structures*, Vol. 10, No. 4, pp. 315-332, 1987.

[87] Lang, M., and Döker, H., "Crack Opening Measurement During Variable Amplitude Loading," *Fatigue 96, Proceedings of the sixth International Fatigue Congress*, Lütjering, G., and Nowack, H., *eds.*, Vol. 1, pp. 437-442, 1996.

[88] Kumar, R., and Singh, K., "Influence of Stress Ratio on Fatigue Crack Growth in Mild Steel," *Engineering Fracture Mechanics*, Vol. 50, No. 3, pp. 377-384, 1995.

[89] Kumar, R., "Effect of Variable Single Cycle Peak Overload on Fatigue Life," *International Journal of Pressure Vessel and Piping*, Vol. 48, pp. 293-303, 1991.

[90] Wheeler, O. E., "Spectrum Loading and Crack Growth," *Journal of Basic Engineering, Transactions of the ASME*, Vol. 94, Series D, No. 1, pp. 181-186, 1972.

[91] Arone, R., "Application of Wheeler Retardation Model for Assessment of Fatigue Crack Lifetime Under Random Overloads," *International Journal of Fatigue*, Vol. 12, No. 4, pp. 275-281, 1990.

[92] Sheu, B. C., Song, P. S., and Hwang, S., "Shaping Exponent in Wheeler Model Under A Single Overload," *Engineering Fracture Mechanics*, Vol. 51, No. 1, pp. 135-143, 1995.

[93] Goel, H. S., Chand, S., "A Fatigue Crack Growth Model for Single Overload Tests," *Transactions of the ASME*, Vol. 116, pp. 168-172, 1994.

[94] Gray, T. D., and Gallagher, J. P., "Predicting Fatigue Crack Retardation Following Overload Using a Modified Wheeler Model," *Mechanics of Crack Growth, ASTM STP 590, American Society for Testing and Materials*, pp. 331-344, 1976.

[95] Broek, D., and Smith, S. H., "The Prediction of Fatigue Crack Growth Under Flight-by-Flight Loading," *Engineering Fracture Mechanics*, Vol. 11, pp. 123-141, 1979.

[96] de Koning, A. U., "A Simple Crack Closure Model for Prediction of Fatigue Crack Growth Rates Under Variable-Amplitude Loading," *Fracture Mechanics: Thirteenth Conference*, ASTM STP 743, Richard Roberts, *ed.*, American Society for Testing and Materials, pp. 63-85, 1981.

[97] Willenborg J., Engle, R. M., Jr., and Wood R. A., "A Crack Growth Retardation Model Using an Effective Stress Concept," *Air Force Flight Dynamics Laboratory Report*, AFFDL-TM-71-1FBR, 1971.

[98] Russell, S. G., "A New Model for Fatigue Crack Growth Retardation Following an Overload," *Engineering Fracture Mechanics*, Vol. 33, No. 6, pp. 839-854, 1989.

[99] Bolotin, V. V., and Lebedev, V. L., "Analytical Model of Fatigue Crack Growth Retardation due to Overloading," *International Journal of Solids Structures*, Vol. 33, No. 9, pp. 1229-1242, 1996.

[100] Lo, K. K., "Fatigue Crack Closure Following a Step-Increase Load," *Transactions of the ASME, Journal of Applied Mechanics*, Vol. 47, pp. 811-815, 1980.

[101] Geary, W., "A Review of Some Aspects of Fatigue Crack Growth Under Variable Amplitude Loading," *International Journal of Fatigue*, Vol. 14, No. 6, pp. 377-386, 1992.

[102] Chakrabarti A. K., "Fatigue Crack Growth Model Based upon Critical Damage Approach," *Engineering Fracture Mechanics*, Vol. 13, pp. 1-14, 1980.

[103] Trebules, V. W. Jr., Roberts, R., and Hertzberg, R. W., "Effect of Multiple Overloads on Fatigue Crack Propagation in 2024-T3 Aluminium Alloy," *Progress in Flaw Growth and Fracture Toughness Testing*, ASTM STP 536, American Society for Testing and Materials, pp. 115-146, 1973.

[104] Sahasakmontri, K., and Horii, H., "An Analytical Model of Fatigue Crack Growth Based on the Crack-Tip Plasticity," *Engineering Fracture Mechanics*, Vol. 38, No. 6., pp. 413-437, 1991.

[105] Newman, J. C. Jr., and Dawicke, D. S., "Prediction of Fatigue-crack Growth in a High-strength Aluminium Alloy Under Variable-amplitude Loading," *Advances in Fracture Research: Proceedings of the 7th International Conference on Fracture (ICF7)*, Houston, Texas, pp. 945-952, March, 1989.

[106] Majid, M., and Provan, J. W., "A New Method for the Analysis and Assessment of Fatigue Crack Closure. I: modeling," *Theoretical and Applied Fracture Mechanics*, Vol. 18, pp. 47-58, 1992.

[107] Yisheng, W., and Schijve, J., "Fatigue Crack Closure Measurements on 2024-T3 Sheet Specimens," *Fatigue and Fracture of Engineering Materials and Structures*, Vol. 18, No. 9, pp. 917-921, 1995.

[108] Newman, J., C., Jr., "Prediction of Fatigue Crack Growth Under Variable-Amplitude and Spectrum Loading Using a Closure Model," ASTM STP 761, pp. 255-277, 1982.

[109] Newman, J. C., Jr., and Elber, W., *eds.*, "Mechanics of Fatigue Crack Closure," *ASTM Special Technical Publication, 1916 Race Street Philadelphia, PA 19103*, ASTM STP 982, 1988.

[110] Ling, M. R., and Schijve, J., "Fractographic Analysis of Crack Growth and Shear Lip Development Under Simple Variable-Amplitude Loading," *Fatigue and Fracture of Engineering Materials and Structures*, Vol. 13, No. 5, pp. 443-456, 1990.

[111] Newman, J. C., Jr., "COSMIC, Fastran II - A Fatigue Crack Growth Structural Analysis Program," *NASA Technical Memorandum 104159*, Langley Research Center, Hampton, Virginia 23665, 1992.

[112] Suresh, S., Parks, D. M., and Ritchie, R. O., "Crack Tip Oxide Formation and its Influence on Fatigue Thresholds," In *Fatigue Thresholds*, (*eds.*, A. F. Blom, J. Backlund and C. J. Beevers), Warley: Engineering Materials Advisory Services, Vol. 1, pp. 391-408, 1982.

[113] Walker, N., and Beevers, C. J., "A Fatigue Crack Closure Mechanism in Titanium," *Fatigue of Engineering Materials and Structures*, Vol. 1, pp. 135-148, 1979.

[114] Suresh, S., and Ritchie, R. O., "A Geometric Model for Fatigue Crack Closure Induced by Fracture Surface Morphology," *Metallurgical Transactions*, Vol. 13A, 1627-1631, 1982.

Appendix A

Additional Plasticity Zones

Plasticity zones were presented in Chapter 2, some additional plasticity zones are given below for each of the yield criteria separately. For PSN condition Figure A.1 and Figure A.2 represent situation under Mises and Tresca yield criteria respectively. These Figures present each of the yield criteria in all the four quadrants, and display the shrinkage effect with an increase in Poisson's ratio, ν. Similar results with PSS included are presented in Figure A.3 and Figure A.4. In Chapter 2 for Figure 2.11, an information regarding Tresca plasticity zones was obstructed by von Mises cone and this is provided in the form of a plasticity cone in Figure A.5. The Figure shows the swelling effect caused by an increase in load ratio ε.

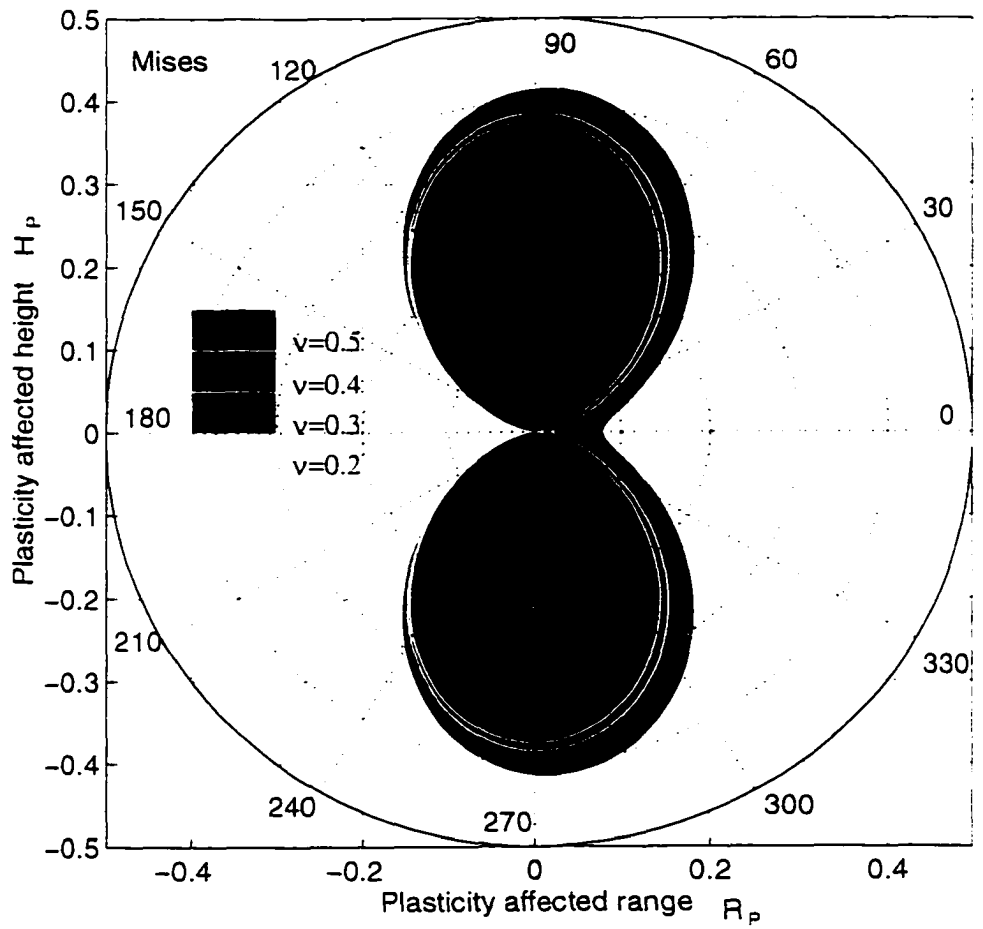

Figure A.1: The plasticity zones obtained on Mises yield criteria.

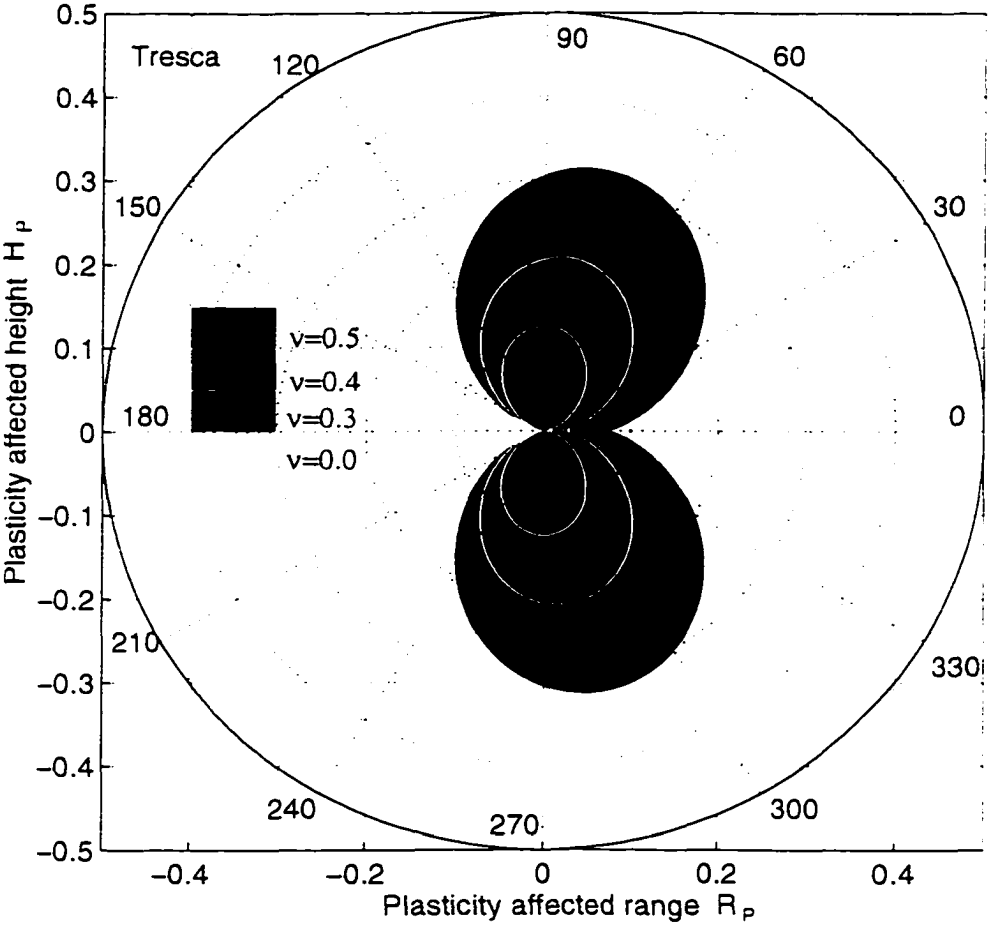

Figure A.2: The plasticity zones obtained on Tresca yield criteria.

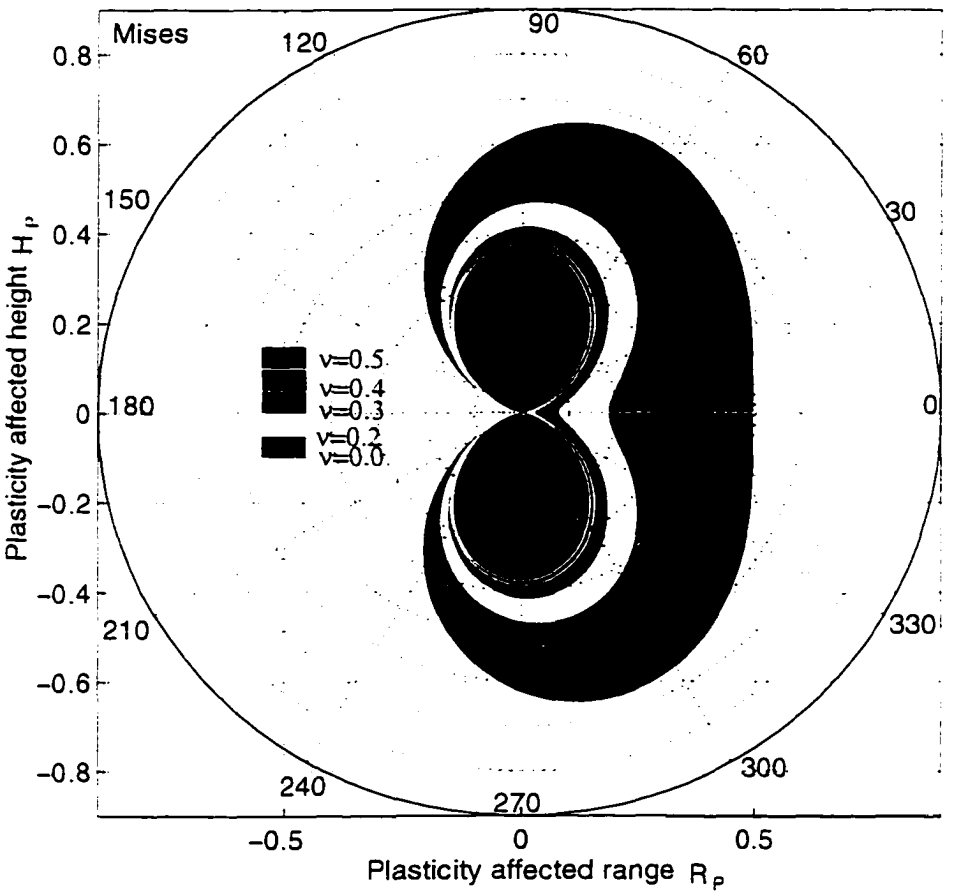

Figure A.3: The plasticity zones obtained on Mises yield criteria. PSS included.

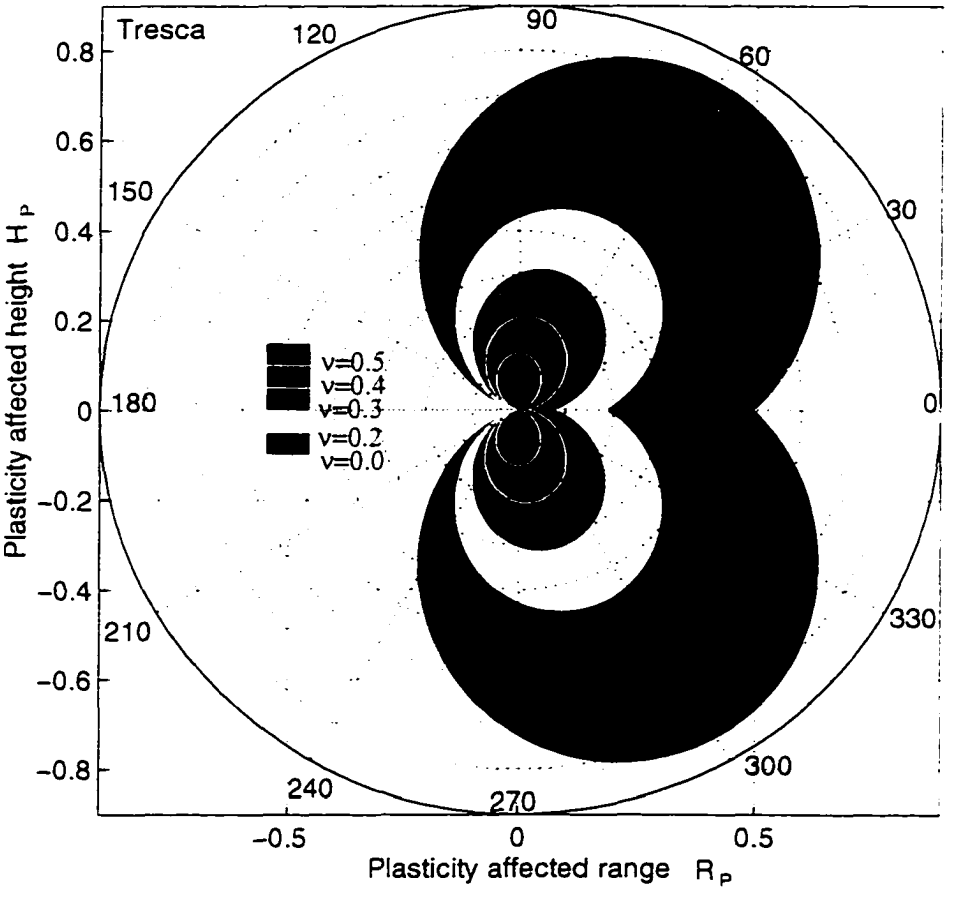

Figure A.4: The plasticity zones obtained on Tresca yield criteria. PSS included.

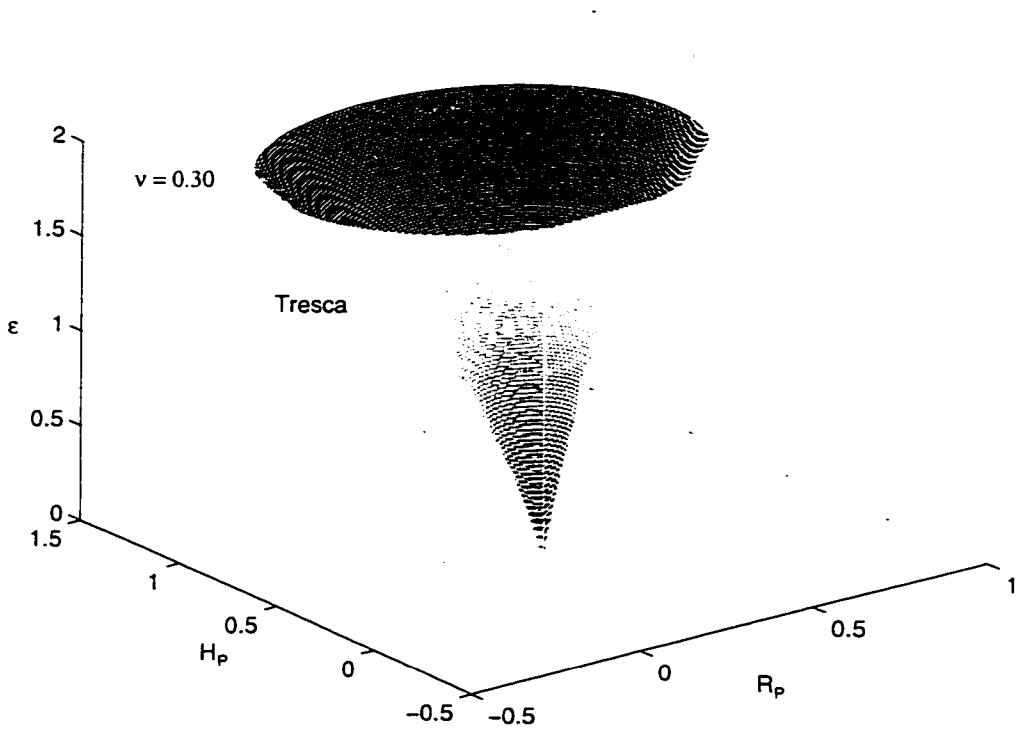

Figure A.5: The plasticity cone obtained on Tresca yield criteria.

Appendix B

Details of Some Crack Closure Mechanisms

B.1 Oxide-Induced Closure Models

Corrosion products formation in the crack wake, through the exposure of the fresh fatigue crack surfaces to a corrosive environment results in crack closure and a consequent reduction in crack driving force. Oxide debris, which is less predominant in dry oxygen-free atmospheres or at high load ratios, provides a mechanism for increased crack closure and hence a reduction in ΔK_{eff}. This mechanism of environmentally-assisted crack growth, however, is specific only to stress intensity ranges where oxide thicknesses are of the order of crack-tip opening displacements (CTOD), *e.g.*, at near-threshold levels.

The significance of oxide-induced crack closure at lower ΔK levels can be appreciated by comparing the ratio of oxide thickness to CTOD. This is shown in Table B.1 which presents oxide thickness at various ΔK values and at low R ratios of 0.05

Material	Yield Strength, MPa	R Ratio	ΔK, MPa.m$^{1/2}$	Oxide Thickness d, μm	CTOD†, μm	$d/CTOD$
Steel	500	0.05	16	0.013	0.784	0.017
Steel	500	0.05	13	0.030	0.518	0.058
Steel	500	0.05	10	0.125	0.306	0.408
Steel	500	0.05	8.2	0.200	0.206	0.971
Copper	134	0.1	7.7	0.005	0.926	0.005
Copper	134	0.1	6.4	0.156	0.640	0.244

†CTOD $= 0.49 \times \Delta K^2/2\sigma_{ys}E$, $\sigma_{ys} = yield\ strength$, $E = Young's\ modulus$.

Table B.1: Oxide thickness, d, and crack-tip-opening displacement, CTOD [60].

and 0.1. The reported results indicate that oxide thickness generally increases with decreasing ΔK because of a more significant amount of Mode-II displacements (or fretting oxidation). Accordingly, the ratio of oxide thickness to CTOD increases with decreasing ΔK. At low ΔK levels this ratio can approach 1. This behavior suggests that thick oxide deposits at low ΔK values wedge the crack-tip and promote oxide-induced crack closure.

Suresh *et al.* [112] (and reviewed later by Suresh and Ritchie, for details see references [1, 60]), modelled the effect of oxide film formation, which acts as an appendage on the virgin flanks of fractured component surface, and promotes oxide-induced crack closure, at near threshold levels, by considering the simple model of a rigid wedge inside a linear elastic crack. The model used a crack length a, and oxide layer thickness (taken to be a rigid wedge of constant thickness) d, extending along the crack length distance $2l$ behind the crack-tip, with assumptions of ignoring plasticity and roughness induced closure effects . The estimation of stress intensity factor at the crack-tip based on elastic superposition using *e.g.*, Westergaard stress function, yields the following equation:

$$K_{R_{x=0}} = \frac{E'd}{4\sqrt{\pi l}}, \tag{B.1}$$

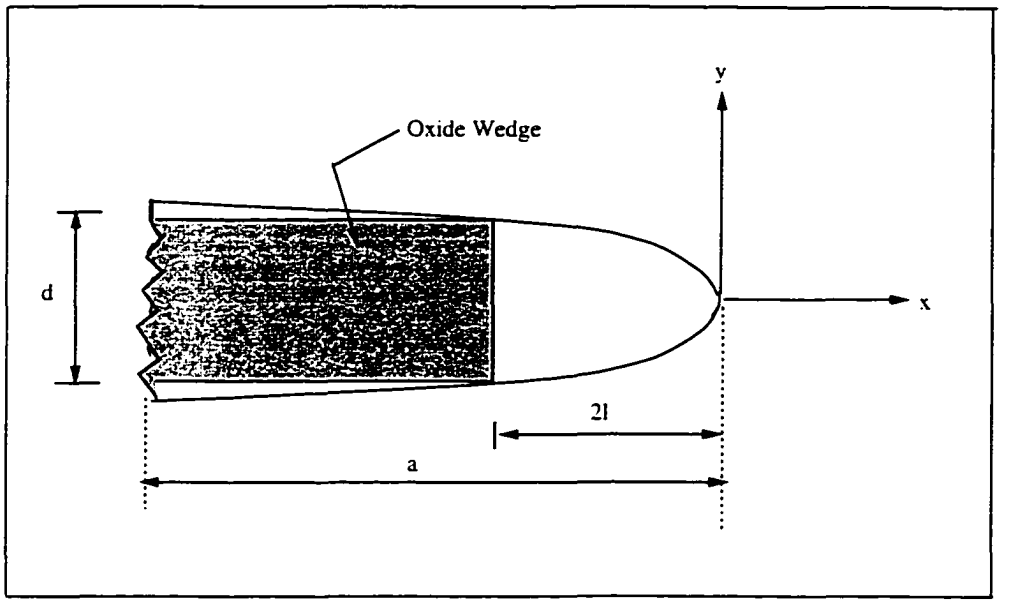

Figure B.1: Different dimensions that are used for calculation of K_R due to a rigid wedge of constant thickness d located at distance $2l$ behind the crack-tip for steel.

where d is the height of the rigid wedge, $2l$ is its location behind the tip, $E' = E$, the elastic modulus in plane stress and $E' = E/(1-\nu^2)$ in plane strain. Thus, for a fatigue cycle, the crack will close when the crack driving force equals K_R, such that K_R can be taken as closure stress intensity K_{cl}. Figure B.1 depicts how the eqn(B.1) has been evaluated for steels where $E = 2.1 \times 10^5\ MPa$ and $\nu = 0.3$, over a range of wedge thickness of 10 nm to 10 μm with $l = 10$ nm to 100 mm. It is obvious that where pronounced oxide formation occurs remote from the crack-tip, the resultant stress intensity K_R due to the wedge is insignificant for most experimentally observed oxide thicknesses (*i.e.*, $d < 1\ \mu m$). Conversely, for oxide layers which build up very close to the crack-tip K_R values become extremely large. Obviously for this linear elastic model, if oxide forms at the tip the resultant stress intensity becomes infinite.

The oxide-induced closure model given above is similar to the asperity-induced closure models in its basic assumptions. Accordingly, the comments pertaining to

those models are also applicable here. Realistic values for K_{open}, the model require the assumption that the oxide layer would form at a distance behind the crack-tip. There is some physical justification for this assumption on the grounds that at the very crack-tip the virgin area of material is not fully exposed to the surrounding conditions. The accuracy of the predicted K_R is dictated by a precise measurement of the oxide thickness and its distance from the crack-tip.

B.2 Asperity-Induced Closure Models

After a complete unloading, the fatigue crack surfaces would fit ideally. However, an ideal match between two fracture crack flank surfaces does not occur because of material structure inhomogeneties which leads to waviness (asperity) formation. It was first reported by Walker and Beevers [113] that crack closure may occur due to the asperity contact between the conjugate fracture surfaces during unloading. The asperity-induced closure mechanism manifests itself as a mixed Mode-I and Mode-II opening of the crack that results in interference of the asperities and thus provides several distinct contact points over the crack surfaces where load transfer may take place. Lankford and Davidson (as cited in [1]) have experimentally demonstrated the presence of mixed Mode-I and Mode-II opening of the fatigue crack. Vacuum infiltration method was used to obtain plastic castings of the crack itself by Bowles and Schijve (as cited in [60]). Applying this method to a 2024-T3 aluminum alloy it was observed that the crack closure occurred only at segregate locations of maximum mismatch between the fracture surfaces. Striation spacings were also observed on the larger part of the fracture surface. These observations should not be expected after numerous cyclic closure contacts if a perfect mating fit occurs [60]. The fracture surface topography has been shown to be dependent on a given microstructure. Based

on the type of material, several structural features, such as grain boundaries, preferred orientation in different grains (texture), inclusions, $\alpha - \beta$ phase boundaries in Ti-alloys, pearlitic colonies in steel, and so forth which may result in a tortuous crack path with different growing directions and a possibility of crack branching occurrence [64]. The microscopical roughness of the fracture surface may also be affected by the loading condition. Stubbington and Gunn (as cited in [64]) performed a test on a C(T) specimen of a Ti-6Al-4V alloy, at a low fatigue load, a fairly coarse surface morphology was obtained due to the so called *structural sensitive cracking* on preferred crystallographic planes. At higher values of fatigue loads a relatively flat, structure insensitive, crack plane resulted. Schijve [64] obtained the formation of macroscopically dark bands on the fatigue fracture surfaces of 2024-T3 specimens subjected to a flight-simulation loading. He concluded that it was partly due to some quasistatic crack extension during the maximum load of the severe flight but mainly due to a kind of rubbing debris, produced during delayed crack growth after the severe flights. Suresh [1] discussed the fracture surface roughness during delayed crack growth after an overload. He mentioned the tendency to observe stage I crack growth in this period.

Beever *et al.* [60] obtained the closure stress intensity factor by considering an effective precompressed spring which makes line contact across the thickness and models the effect of a single through-thickness asperity (see Fig. B.2). This model is termed the Single Asperity Model and presents two different expressions for K_{cl} and K_{open}:

$$K_{cl} = (\frac{2}{\pi C_0})^{1/2}[\frac{1}{Eb} + \frac{2}{\pi GL}(1-\nu)]^{-1}. \tag{B.2}$$

$$K_{open} = \frac{LG}{2(1-\nu)}(\frac{2\pi}{C_0})^{1/2}. \tag{B.3}$$

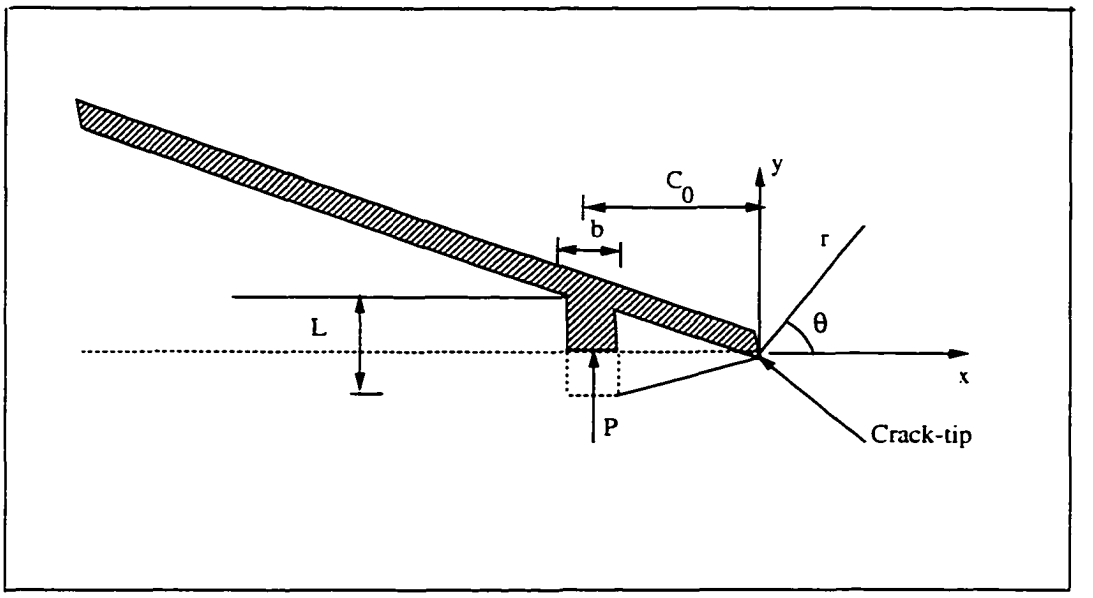

Figure B.2: Single-asperity crack closure model.

in which, L and b are the height and width of the asperity, respectively, C_0 is its distance from the crack-tip, and $E, G,$ and ν are the usual elastic constants. The model is based on assumption that the formation of the plastic zone of effective length r_p increases the dimension of C_0 to $C_0 + r_p$, which implies that K_{cl} and K_{open} decrease as σ_{ys} decreases. The resulting equation for K_{open} is:

$$K_{open} = \frac{LG}{2(1-\nu)}\left(\frac{2\pi}{C_0 + r_p}\right)^{1/2}. \tag{B.4}$$

The dimensions $L, b,$ and C_0 were measured using replicating techniques and these, when substituted in eqns(B.3 and B.4) gave a K_{open} value which agreed with the experimentally determined K_{open} value in the near threshold regime for a wrought nickel alloy. Table B.2 presents the reported results.

The model was reviewed by some other researchers [60] and for both single and multiple asperity with Mode-II crack opening displacements. Several other models on asperity induced crack closure have been summarised in recent text by Suresh [1].

a/w	C_0 μm	L μm	b μm	P^1_{open} kN	P^2_{open} kN	P^3_{open} kN
0.39	15	0.100	9	3.23	2.75	1.86
0.41	16	0.100	9.5	2.90	2.36	1.96
0.44	28	0.125	11	2.51	2.14	2.01

Table B.2: The predicted opening loads. P^1 from eqn(B.3) and P^2 from eqn(B.4) compared with the observed opening loads P^3 [60].

and some details pertaining to some other models are given in [60].

A model for computing the influence of the fracture surface roughness and the mixed Mode-I and Mode-II opening of the crack has been sketched by Suresh and Ritchie [114]. Their 2D geometrical model assumes the crack to have a simple saw-tooth shape and proposes the following expression for closure stress intensity factor:

$$K_{cl}/K_{max} = [(2\gamma x)/(1 + 2\gamma x)]^{1/2}. \tag{B.5}$$

Here, γ is the ratio of the height to the width of the sawtooth and x denotes the ratio of the Mode-II to Mode-I crack-tip displacement. The parameter γ is the direct measure of the angular direction of the crack elements and the ratio x could be related to shear in planes inclined to the main fracture plane. The value of γ estimated from surface coating and profilometric studies when substituted in eqn (B.5) together with the experimentally determined K_{cl} and K_{max} values, give a value of x or Mode-II displacement, u_{II}, which is consistent with the experimental examination of crack-tip motion using stereoimaging procedures.

IMAGE EVALUATION
TEST TARGET (QA-3)

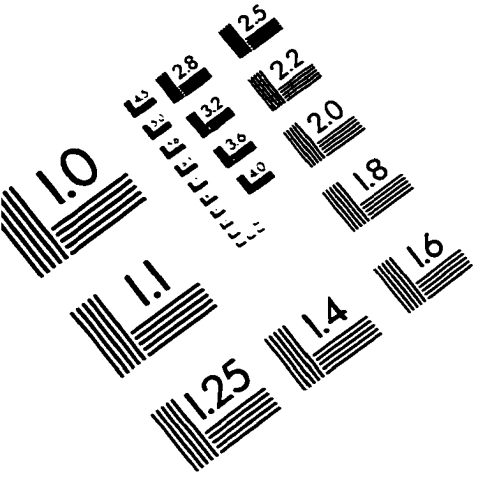

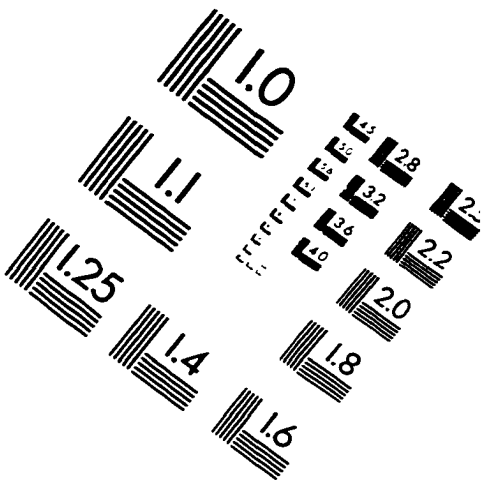

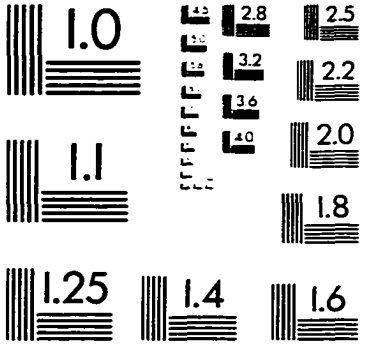

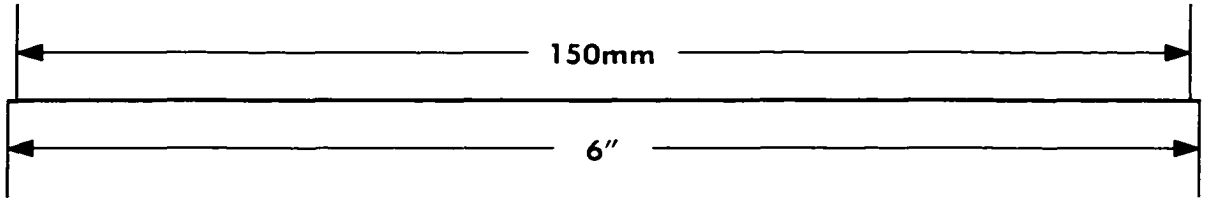

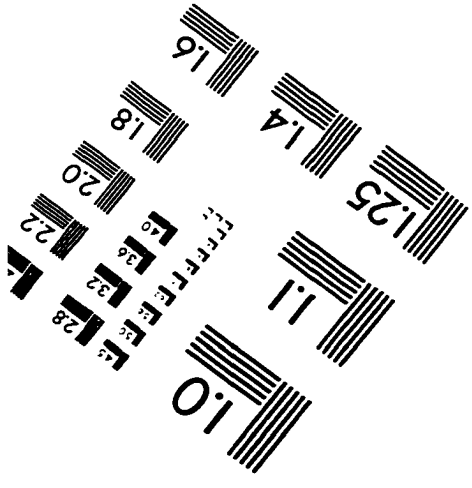

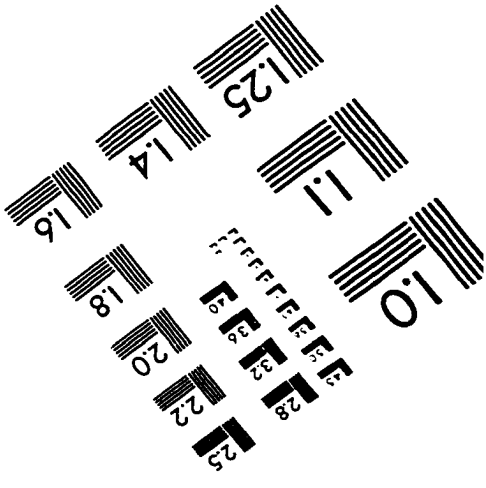

APPLIED IMAGE, Inc
1653 East Main Street
Rochester, NY 14609 USA
Phone: 716/482-0300
Fax: 716/288-5989